SISSA
Scuola
Internazionale
Superiore di
Studi Avanzati

Physics Area - PhD course in
Statistical Physics

Quantum simulations of gauge theories and topological phases

Candidate:
Pierpaolo Fontana

Advisor:
Prof. Andrea Trombettoni

Academic Year 2021-22

List of publications

Papers appearing in this thesis

Chapter 2 - [1] P. Fontana, J.C. Pinto Barros, A. Trombettoni, "Reformulation of gauge theories in terms of gauge invariants", Annals of Physics 436 (2022) 168683.

Chapter 4 - [2] P. Fontana, J.C. Pinto Barros, A. Trombettoni, "Quantum simulator of link models using spinor dipolar ultracold atoms", arXiv:2210.14836.

Chapter 6 - [3] P. Fontana, M. Burrello, A. Trombettoni, "Topological van Hove singularities at phase transitions in Weyl metals", Phys. Rev. B 104 (2021) 195127.

Other journal papers

[4] P. Fontana, "Scaling behavior of Ising systems at first-order phase transitions", J. Stat. Mech. (2019) 063206.

Introduction

Gauge theories and topological phases play a fundamental role in different areas of physics. The first ones are at the basis of the Standard Model in the field of particle physics, describing the electroweak and strong interactions through a non-Abelian gauge theory [5–7]. In condensed matter and statistical physics, gauge theories arise as low-energy effective descriptions of strongly correlated phenomena, such as quantum spin liquids and quantum Hall effect [8]. In this realm there is a strong connection with topological phases and order, as emergent gauge fermions and bosons often describe collective excitations of new exotic states of matter of spin models [9].

The discretization on a lattice is a possible way of dealing with the strongly coupled nature of these theories [10, 11], due to the fact that this formulation at finite volume provides natural regularizing cut-offs, i.e. the lattice size and spacing. This allows for the investigation of different non-perturbative properties both numerically and analytically [12, 13]. Despite the success of these methods, there are various aspects which remain intractable due to the sign or complex action problems, like the out of equilibrium real time evolution or the analysis of quantum chromodynamics with finite chemical potential [14, 15].

In this respect, quantum simulators of many-body systems to simulate high energy physics arise as promising alternatives to face these problems in the near future. They are quantum systems that can be controlled and used to simulate more complicated systems, whose properties could not be analysed with classical computational, experimental or theoretical tools. In the last decades, there has been a huge development in the fields of quantum optics and atomic physics, allowing for the realization highly precise and controllable platforms [16–18] by means of trapped ions [19], superconducting circuits [20], Rydberg atoms [21] and ultracold atoms in optical lattices [22].

This work of Thesis is part of these fields and has different purposes, all of them connected with the study of gauge theories and topological phases. Firstly, we want to develop a reformulation of lattice gauge theories in terms of gauge invariant fields, in a way to deal solely with physical variables directly in the action. Among several possible advantages, a crucial point is that this can be particularly helpful for the construction of consistent approximation schemes, such as mean-field theories, in order to understand and capture some of the physical features of the theory and make the mean-field approximation consistent with the Elitzur theorem, stating that a local gauge symmetry can not be spontaneously broken [23].

As a second point, we face the problem of simulating higher dimensional gauge theories with ultracold atoms. One of the challenges in more than one dimension is indeed the realization of plaquette interaction terms in the Hamiltonian of lattice gauge theories: these can be engineered through four correlated hoppings in perturbation theory, or by means of constrained hoppings in the dual formulation [21]. In this respect, our main target is to set up an ultracold atomic platform generating the plaquette term in two dimensions using only two correlated hoppings, and

protecting gauge invariance through angular momentum conservation [24].

The last point we address in the Thesis is related to the analysis of particles moving in static background gauge potentials, i.e. when the considered gauge field has no dynamical term in the action of the system. Indeed, the dynamics of quantum particles in the presence of static gauge fields gives rise to intriguing physical phenomena. In particular, using ultracold atom setups, the realization of artificial gauge potentials can be used to investigate the physics of topological semimetals, such as Weyl or Dirac type [25]. In the last ten years, a lot of attention has been paid to their characterization, due to the appearence of clear theoretical predictions and very well-controlled experimental techniques [26]. We investigate here the relation between topological phase transitions and van Hove singularities, i.e. the discontinuities in the energy derivative of the density of states, in three-dimensional gapless systems. In such materials, topological phase transitions can be defined by changes of the topological invariants of the Fermi sheets, happening at specific singular points. Moreover, Fermi surface singularities result in the presence of the so-called van Hove points. We then present a general argument to relate topological phase transitions and van Hove singularities, and show observable consequences that are related to the transport properties of the system. We exemplify our argument in Weyl systems by analyzing the three-dimensional Hofstadter model for various commensurate fluxes, which offers the opportunity to consider different kinds of Weyl metals and to understand the features of their density of states.

The structure of the Thesis is divided into three parts, each one referred to the previous points. Each part contains two chapters, i.e. a first opening Chapter, as a reminder of known results necessary for the topics we are going to treat, and a second Chapter containing the original results of our research.

In particular, Part I is devoted to reformulations of lattice gauge theories. Chapter 1 contains a brief introduction about gauge theories in the continuum and on the lattice, alongside a brief summary of the different reformulations present in literature and the application of analytical methods to analyze them. Chapter 2 presents our gauge invariant reformulation of Abelian gauge theories, and is based on Ref. [1].

The Part II is about the quantum simulators of lattice gauge theories: in Chapter 3 we give a short summary about quantum simulators with ultracold atoms, paying particular attention to the discussion of the higher dimensional proposals present in literature so far. Chapter 4 contains our proposal for bosonic and fermionic link models in two dimensions,and is based on Ref. [2].

The last part of the thesis, Part III, discusses topological phases of lattice models. In Chapter 5 we discuss the role of topology in condensed matter systems, presenting the topological invariants that characterize the three-dimensional topological metals we are interested in. Chapter 6 is entirely based on Ref. [3], and shows the connection between topological phase transitions and van Hove singularities in Weyl metals.

Part IV contains the Appendices relative to the results presented in the Chapters 2, 4 and 6, respectively.

Contents

Part I

Reformulations of lattice gauge theories

Chapter 1

Gauge theories: review of formulations and mean-field methods

Due to their broad applicability, gauge theories have a key importance in physics that can be hardly overstated [5–7]. In the field of particle physics they are at the basis of the Standard Model, a non-Abelian gauge theory with gauge symmetry group $U(1) \times SU(2) \times SU(3)$, where the first two groups refer to the electroweak sector and the last to quantum chromodynamics (QCD). They also play an important role in condensed matter physics, where gauge fields may emerge from the effective description of strongly correlated phenomena at low energies, like quantum Hall systems and quantum spin liquids [8].

In the first Chapter of this Thesis we define the mathematical structure of gauge theories in quantum field theory (QFT), summarizing their main features firstly in the continuum and then on the lattice, where we present both the Lagrangian and the Hamiltonian formulations. The last two Sections constitute the most important parts of this Chapter, where respectively we are going to:

- review the reformulations of gauge theories in terms of gauge invariant fields;
- show how the mean-field method is applied to gauge theories.

In both cases we explore and summarize, to our best knowledge, the state of the art present in the scientific literature. This has a double purpose, i.e. to highlight the main difficulties encountered so far in the various attempts and to set the background for our proposal, that we are going to present in Chapter 2.

1.1 Gauge symmetry in quantum field theory

To define what are gauge theories, we consider as a starting point a multicomponent scalar field $\phi = (\phi_1, \ldots, \phi_n)^T$ with values in the vector space $V = \mathbb{C}^n$, whose Lagrangian and Lorentz invariant action are

$$\mathcal{L}[\phi, \partial_\mu \phi] = \partial_\mu \phi^* \cdot \partial^\mu \phi - m^2 \phi^* \cdot \phi, \qquad S = \int d^d x \; \mathcal{L}[\phi, \partial_\mu \phi]. \tag{1.1}$$

The Lagrangian is invariant under global $U(n)$ transformations of the scalar field

$$\phi(x) \;\longrightarrow\; \phi'(x) = \Omega \; \phi(x), \qquad \Omega \in U(n), \tag{1.2}$$

where Ω does not depend on the space-time point coordinates. At the same time, the scalar product is invariant under simultaneous $U(n)$ transformations, since $\phi^* \cdot \chi = (\phi')^* \cdot \chi'$. Despite these properties, the Lagrangian is not invariant under the corresponding *local* transformation

$$\phi(x) \;\longrightarrow\; \phi'(x) = \Omega(x) \; \phi(x), \qquad \Omega(x) \in U(n). \tag{1.3}$$

It is however possible to extend the above global symmetry to a local one, by coupling the charged scalar field ϕ to a *gauge potential* A_μ [5–7, 27]. In the so-called *minimal coupling* procedure, the rule is to replace the space-time derivative with the *covariant derivative*

$$\partial_\mu \;\longrightarrow\; D_\mu(A) = \partial_\mu - igA_\mu, \tag{1.4}$$

where g is the coupling constant of the matter-gauge interaction. By requiring that the covariant derivative locally transforms as

$$D_\mu(A')\phi'(x) = \Omega(x) D_\mu(A) \phi(x) \tag{1.5}$$

we find that, using Eq. (1.3), this reduces to the condition

$$D_\mu(A')\phi'(x) = \Omega(x) D_\mu(A) \Omega(x)^{-1}. \tag{1.6}$$

This last equation is satisfied if the gauge potential transforms as

$$A'_\mu(x) = \Omega(x) A_\mu(x) \Omega(x)^{-1} - \frac{i}{g} [\partial_\mu \Omega(x)] \Omega(x)^{-1}. \tag{1.7}$$

If we assume that $\Omega(x) \in \mathcal{G}$, where $\mathcal{G}$ is a Lie group, then all the other elements appearing in Eq. (1.7) are Lie-algebra valued.

Out of the gauge potential we can construct the *field strength tensor* as the commutator

$$F_{\mu\nu}(A) = \frac{i}{g}[D_\mu, D_\nu] = \partial_\mu A_\nu - \partial_\nu A_\mu - ig[A_\mu, A_\nu], \qquad F_{\mu\nu} \;\longrightarrow\; \Omega(x) F_{\mu\nu} \Omega(x)^{-1}. \tag{1.8}$$

In analogy to quantum electrodynamics (QED), we could take the square of $F_{\mu\nu}$ to obtain the dynamical term of the gauge field. However, if the gauge symmetry group is non-Abelian, the quantity $F_{\mu\nu}F^{\mu\nu}$ is not gauge invariant. If we consider its trace, i.e. $\mathrm{tr}(F_{\mu\nu}F^{\mu\nu})$, we generalize the QED term to the *Yang-Mills term*.

With this in mind, the full, gauge invariant, Lagrangian is then

$$\mathcal{L}_G[\phi, A_\mu] = -\frac{1}{4}\mathrm{tr}(F_{\mu\nu}F^{\mu\nu}) + \mathcal{L}[\phi, D_\mu\phi]. \tag{1.9}$$

We notice that, apart from the Yang-Mills term for the gauge part, we have the original Lagrangian in Eq. (1.1) with the substitution $\partial_\mu \to D_\mu(A)$.

From now on we will consider the specific case of Abelian groups, referring to the *Abelian gauge theories*. Formally, the previous local transformations can be written as

$$\phi(x) \to \Omega(x)\phi(x), \qquad A_\mu \to A_\mu - \frac{i}{g}[\partial_\mu\Omega(x)]\Omega^{-1}(x) \tag{1.10}$$

for the matter and gauge fields, respectively. The field strength tensor $F_{\mu\nu}$ takes the form

$$F_{\mu\nu} \equiv \partial_\mu A_\nu - \partial_\nu A_\mu. \tag{1.11}$$

Under a gauge transformation, this quantity is left unchanged, i.e. $F_{\mu\nu} \to F_{\mu\nu}$, therefore it represents a *gauge invariant* of the theory. A prominent example of an Abelian gauge theory is QED. Its Lagrangian reads

$$\mathcal{L}_{\mathrm{QED}} = \bar{\psi}(i\not{D} - m)\psi - \frac{1}{4}F_{\mu\nu}F^{\mu\nu} = \bar{\psi}(i\not{\partial} - m)\psi - eA_\mu\bar{\psi}\gamma^\mu\psi - \frac{1}{4}F_{\mu\nu}F^{\mu\nu}. \tag{1.12}$$

where ψ and $\bar{\psi}$ are the fermionic degrees of freedom and m and e are, respectively, the fermionic mass and charge parameters. The gauge group is $\mathcal{G} = U(1)$ and a generic local transformation can be written as a phase factor $\Omega(x) = \exp(ie\Lambda(x))$.

1.1.1 Parallel transport

A key object in the passage to the lattice formulation of a gauge theory is the *parallel transport*. This can be defined in the continuum, and on the lattice its discretized version will be the fundamental constituent of the theory, as we are going to see in the next Section.

We start with the definition of a *covariantly constant field*, i.e. a field ϕ that satisfies

$$D_\mu\phi = 0 \qquad \Rightarrow \qquad [D_\mu, D_\nu]\phi = 0. \tag{1.13}$$

This equation can be studied along a path $\mathcal{C}_{xy}$ joining two space-time points $x,\ y$. We can parametrize this path by $z(s)$, with $s \in [0,1]$ and $z(0) = x,\ z(1) = y$. The field ϕ is said covariantly constant along the path $\mathcal{C}_{xy}$ if

$$\dot{z}^\mu D_\mu \phi = 0 \qquad \Rightarrow \qquad \dot{\phi}(s) - igA_\mu(z(s))\dot{z}^\mu(s)\phi(s) = 0, \tag{1.14}$$

where $\phi(s) \equiv \phi(z(s))$. The solution to this equation can be obtained by direct integration

$$\phi(s) = \mathcal{P}\left(e^{ig\int_0^s du\ A_\mu(z(u))\dot{z}^\mu(u)}\right)\phi(x), \tag{1.15}$$

where $\mathcal{P}$ stands for the path-ordering operation. This symbol is necessary in the non-Abelian case, while is superfluous for Abelian theories, due to the commutativity of the symmetry group. The definition of parallel transporter can be obtained by putting $s = 1$ in the previous equation

$$\phi(y) = U_{\mathcal{C}_{xy}}(A)\phi(x), \qquad U_{\mathcal{C}_{xy}}(A) = \mathcal{P}\left(e^{ig\int_0^1 ds\ A_\mu \dot{z}^\mu}\right). \tag{1.16}$$

The parallel transport is, by definition, a path-dependent quantity, as it is a function of $\mathcal{C}_{xy}$. It has the following properties:

- if $\mathcal{C}_1 :\ x \to y$ and $\mathcal{C}_2 :\ y \to z$ are two space-time paths, it satisfies the composition rule

$$U_{\mathcal{C}_1 \circ \mathcal{C}_2} = U_{\mathcal{C}_1} U_{\mathcal{C}_2}; \tag{1.17}$$

- under a gauge transformation

$$U_{\mathcal{C}_{xy}}(A') = \Omega(y) U_{\mathcal{C}_{xy}}(A) \Omega(x)^{-1}. \tag{1.18}$$

From the last property, it follows immediately that the trace of the parallel transporter associated to an arbitrary closed loop is a gauge invariant quantity, called *Wilson loop*, and is defined as

$$W_{\mathcal{C}_{xy}}(A) \equiv \mathrm{tr}[U_{\mathcal{C}_{xy}}(A)]. \tag{1.19}$$

As anticipated, this is a gauge invariant quantity since $\mathrm{tr}[U_{\mathcal{C}_{xy}}(A')] = \mathrm{tr}[U_{\mathcal{C}_{xy}}(A)]$.

1.2 Lattice gauge theories

The analysis of gauge theories in the strong coupling regime is an arduous problem where perturbative approaches typically fail. One way to deal with this problem is to work under the framework of *lattice gauge theories* (LGT) [10–12, 28]. The lattice formulation at finite volume provides natural infrared and ultraviolet cut-offs that regularize the theory. Moreover, within this formulation,

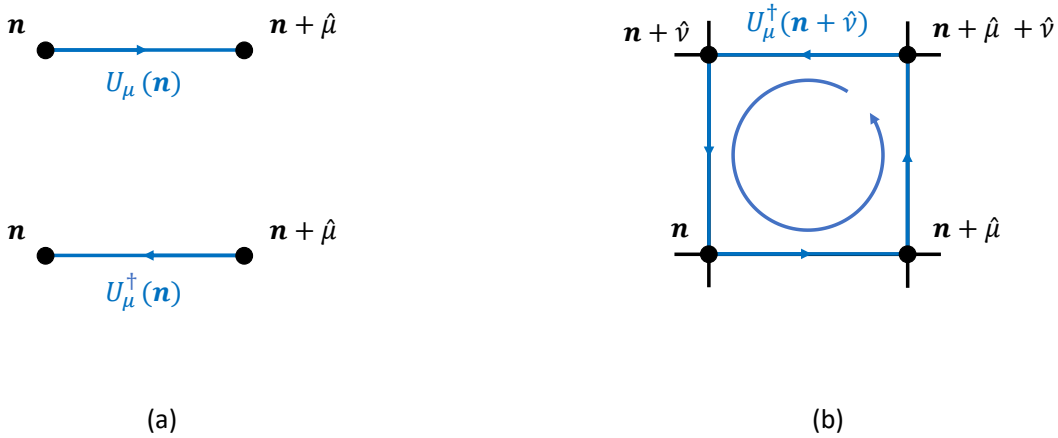

Figure 1.1: (a) Graphical representations of link variables $U_\mu(\mathbf{n})$, $U_\mu^\dagger(\mathbf{n})$. (b) The contribution $U_{\mu\nu}$(n) of an elementary plaquette with base site $\mathbf{n}$, in the $\mu - \nu$ plane.

numerical approaches to the problem are possible using Monte Carlo methods [12, 28] and crucial results have been obtained, e.g. for lattice QCD in its strongly coupled low-energy regime. Among the various points that have been addressed, we mention here the studies regarding string tension and quark potentials in pure gauge theories and full QCD [29–32], chiral symmetry breaking [33], mass spectrum of bound states in pure QCD [34], hadron mass spectrum [35, 36], deconfinement phase transition and high-temperature phases of QCD [37].

The lattice discretization of gauge theories can be performed following essentially two paths. The first one entails the discretization of the continuum theory Lagrangian. This constitutes the *Lagrangian formalism* of LGT. There is also the possibility of considering the *Hamiltonian formalism*, in which space dimensions are discretized but time is not. In this formulation the theory is projected only on its physical states $|\Psi\rangle$, i.e. the ones satisfying Gauss's law [11, 38]. In these discretization schemes involving fermions, it is well known that particular attention must be paid to address the fermion doubling problem[1] [12].

1.2.1 Lagrangian formulation

We denote a generic site, on a $(d+1)$ dimensional lattice, by $(d+1)$ integers $\mathbf{n} = (n_0, \ldots, n_d)$, where each component takes values between 1 and N. According to the original picture of Wilson [10], the gauge field A_μ is defined on the links of the lattice, while the field strength tensor $F_{\mu\nu}$

[1]This can be done by considering different discretizations of the fermionic field (e.g. Wilson fermions, staggered fermions or domain wall fermions). As these schemes preserve gauge invariance, our following discussion about the reformulations in terms of gauge invariants is largely independent on the type of employed lattice fermions.

lives on the plaquettes. It is useful to define [12]

$$U_\mu(\mathbf{n}) = e^{ieaA_\mu(\mathbf{n})}, \qquad U_{\mu\nu}(\mathbf{n}) = e^{iea^2F_{\mu\nu}(\mathbf{n})}, \tag{1.20}$$

where $U_\mu \in \mathcal{G}$ are the link variables connecting the site $\mathbf{n}$ to the site $\mathbf{n}+\hat{\mu}$, for $\mu \in \{0,\dots,N\}$, and $U_{\mu\nu}(\mathbf{n})$ are the plaquette variables (see Fig. 1.1 for their graphical representations). We observe that the U_μ are nothing but the discretized version of Eq. (1.16) along the path $\mathbf{n} \to \mathbf{n}+\hat{\mu}$. The discretized version of the field strength tensor is written as

$$aF_{\mu\nu}(\mathbf{n}) \equiv A_\nu(\mathbf{n}+\hat{\mu}) - A_\nu(\mathbf{n}) - A_\mu(\mathbf{n}+\hat{\nu}) + A_\mu(\mathbf{n}). \tag{1.21}$$

The quantities e and a are respectively the charge and the lattice spacing. We set $a = 1$ and we will only recover it once we take the continuum limit.

Referring explicitly to the $\mathcal{G} = U(1)$ gauge group, the action is given by

$$S = S_G[U_{\mu\nu}] + S_{\text{fermions}}[\psi, \bar{\psi}, U_\mu], \tag{1.22}$$

where

$$S_G = \frac{1}{g^2}\sum_P \left[1 - \frac{1}{2}(U_{\mu\nu} + U_{\mu\nu}^\dagger)\right] \tag{1.23}$$

is the pure gauge contribution, with the sum extended over all the plaquettes P, and S_{fermions} represents the interaction with matter, whose explicit form depends on the discretization scheme used to treat the fermions.

1.2.2 Hamiltonian formulation

With respect to the Lagrangian formulation presented in the previous Subsection, the electric and magnetic fields are now operators acting in a given Hilbert space [16]. The electric field operator, acting on the link connecting the site $\mathbf{n}$ to the site $\mathbf{n}+\hat{\mu}$, is represented by $E_\mu(\mathbf{n})$ and commutes non-trivially with the Wilson operator $U_\mu(\mathbf{n})$ on the same link, according to

$$[U_\mu(\mathbf{n}), E_\nu(\mathbf{n}')] = -\delta_{\mu,\nu}\delta_{\mathbf{n},\mathbf{n}'}U_\mu(\mathbf{n}), \qquad [U_\mu^\dagger(\mathbf{n}), E_\nu(\mathbf{n}')] = \delta_{\mu,\nu}\delta_{\mathbf{n},\mathbf{n}'}U_\mu^\dagger(\mathbf{n}), \tag{1.24}$$

with all remaining commutation relations set to zero. Along with the definitions in Eq. (1.20), we can write down the Hamiltonian of the system in terms of spatial plaquettes $U_{\mu\nu}$ and electric fields E_μ, which is called the Kogut-Susskind (KS) Hamiltonian [11]. Mathematically its structure is $H = H_g + H_m$, where

$$H_g = \frac{e^2}{2}\sum_{\mathbf{n},\mu} E_\mu^2(\mathbf{n}) - \frac{1}{4a^2e^2}\sum_P (U_{\mu\nu} + U_{\mu\nu}^\dagger) \tag{1.25}$$

is the pure gauge field contribution, while H_m is the matter contribution, that depends again on the employed discretization scheme for the lattice fermions. When matter is absent, Eq. (1.25)

represents the KS Hamiltonian of a pure Abelian $U(1)$ LGTs. The KS Hamiltonian is gauge invariant, i.e. it commutes with the set of local operators

$$G(\mathbf{n}) = \sum_{\mu}[E_{\mu}(\mathbf{n}) - E_{\mu}(\mathbf{n} - \hat{\mu})], \qquad [H, G(\mathbf{n})] = 0. \tag{1.26}$$

Among the eigenstates of H, The physical states $|\psi\rangle$ of the system are the ones satisfying Gauss' law $G(\mathbf{n})|\psi\rangle = 0$, $\forall \mathbf{n}$. We point out that possible gauge invariant extensions, i.e. terms preserving the above commutation relations, can be added to the Hamiltonian[2].

The condition in Eq. (1.26) identifies the gauge invariant Hilbert space of the model. We note, however, that the physical Hilbert space is infinite-dimensional, because of the continuous nature of the $U(1)$ gauge group. A possible way of dealing with this infinite dimensionality is to introduce *quantum link models* (QLMs), i.e. to replace the Wilson operators U_{μ} by discrete quantum degrees of freedom, still living on the links of the lattice, that are called *quantum links* [40–42]. In the remaining part of this Section, we briefly review the bosonic and fermionic versions of the QLMs.

Bosonic quantum link models

QLMs realize the commutation relations in Eq. (1.24) using quantum spin operators as

$$U_{\mu}(\mathbf{n}) = S^{+}_{\mu}(\mathbf{n}), \qquad U^{\dagger}_{\mu}(\mathbf{n}) = S^{-}_{\mu}(\mathbf{n}), \qquad E_{\mu}(\mathbf{n}) = S^{z}_{\mu}(\mathbf{n}). \tag{1.27}$$

The local Hilbert space is now finite-dimensional: for a spin S, on each link of the lattice the Hilbert space is $(2S+1)$-dimensional [16]. When compared with the Wilson formulation, the Wilson operators of different links are not commuting anymore, as they satisfy

$$[U_{\mu}(\mathbf{n}), U^{\dagger}_{\nu}(\mathbf{n}')] = 2E_{\mu}(\mathbf{n})\delta_{\mu,\nu}\delta_{\mathbf{n},\mathbf{n}'}. \tag{1.28}$$

This difference gives rise to interesting physical phenomena [43–45], while still providing a route to recover the Wilson discretization as one takes the spin representation S to be large.

In the particular case of $S = 1/2$ there are only two states per link, associated with the values $E_{\mu}(\mathbf{n}) = \pm 1/2$ of the electric field. The Hamiltonian gets simplified because $(S^{z}_{\mu})^2 = 1/4$: the electric part is trivial and we are left with magnetic interactions only. The physics of the described Hamiltonian (1.25) can be enriched by introducing the Rokhsar-Kivelson (RK) term, with coupling λ, giving rise to the Hamiltonian [39]

$$H_{RK} = H_g + \lambda \sum_{P} (U_{\mu\nu} + U^{\dagger}_{\mu\nu})^2. \tag{1.29}$$

[2]In the electric basis, the sum of plaquette operators can be seen as a kinetic term acting on electric configurations, by interchanging them. Potential terms that are diagonal in the electric basis can be added without modifying the gauge invariance of the Hamiltonian. An important example is given by the Roksha-Kivelson (RK) Hamiltonian [39].

We point out that in the particular case of $d = 2$, only six states satisfy the Gauss law in Eq. (1.26). Despite the apparent simplicity of the model, its physics is very rich [16], being closely related to the quantum dimer model [46].

An alternative way to view the spin-1/2 QLM is provided by mapping spins to hardcore bosons. There, the + or − signs of $E_\mu(\mathbf{n})$ label, respectively, the presence or absence of an hardcore boson in the link $\mathbf{n} \to \mathbf{n} + \hat{\mu}$ [47]. In terms of bosons, the gauge operators are written as

$$U_\mu(\mathbf{n}) = b^\dagger_\mu(\mathbf{n}), \qquad U^\dagger_\mu(\mathbf{n}) = b_\mu(\mathbf{n}), \qquad E_\mu(\mathbf{n}) = n_\mu(\mathbf{n}) - \frac{1}{2}. \tag{1.30}$$

The plaquette term can be written as

$$U_{\mu\nu}(\mathbf{n}) = b_\mu(\mathbf{n}) b_\nu(\mathbf{n} + \hat{\nu}) b^\dagger_\mu(\mathbf{n} + \hat{\nu}) b^\dagger_\nu(\mathbf{n}) \tag{1.31}$$

and can be interpreted as a correlated hopping of two bosons. The RK term can be written in this language as a sum of two-, three- and four-particles interactions. While this is simple to write, it does not arise as easily in an ultracold atomic setting. In this language, the generators in Eq. (1.26) take the form

$$G(\mathbf{n}) = \sum_\mu [n_\mu(\mathbf{n}) - n_\mu(\mathbf{n} - \hat{\mu})]. \tag{1.32}$$

and commute with the Hamiltonian by construction.

Fermionic quantum link models

The particle representation opens the door to the construction of an alternative gauge theory, constructed with fermionic links [47, 48]. By replacing the bosonic creation and annihilation operators in Eq. (1.30) by fermionic ones we obtain a new theory. This is still gauge theory, as there is still a set of local symmetries, but possibly hosting different physics due to the different commutation relations between the Wilson operators U_μ and $U^\dagger_\mu$. It turns out that in $d = 2$ the theories are equivalent, while for $d = 3$ they represent effectively different models [47, 48].

For concreteness, in the fermionic case, we can choose, as a basis for the two-dimensional local Hilbert space the states $|0\rangle$ and $|1\rangle = c^\dagger_\mu(\mathbf{n})|0\rangle$, and identify the Wilson and electric field through

$$U_\mu(\mathbf{n}) = c^\dagger_\mu(\mathbf{n}), \qquad U^\dagger_\mu(\mathbf{n}) = c_\mu(\mathbf{n}), \qquad E_\mu(\mathbf{n}) = n_\mu(\mathbf{n}) - \frac{1}{2}, \tag{1.33}$$

where $n_\mu(\mathbf{n}) \equiv c^\dagger_\mu(\mathbf{n}) c_\mu(\mathbf{n})$ is the number operator. It is straightforward to verify that Eq.s (1.24), (1.28) are satisfied with these definitions. As anticipated, the Wilson operators anticommute.

Fermionic QLMs have been subjected to much less intense research when compared to their bosonic counterparts. Their analysis can lead, in principle, to the characterization of new phases of matter for LGTs. At the same time, quantum simulators of LGTs in $d = 2$ with ultracold atoms may profit from the fermionic interpretation of the plaquette interactions, as they provide an alternative equivalent way of realizing the same physics.

1.3 Reformulations in terms of gauge invariants

The gauge symmetry is not properly physical, since it has no observable consequences to look at, as happens in the case of global symmetries. Mathematically speaking, it represents a *redundancy* in our description of the system, in a way to describe the theory in terms of a local and causal Lagrangian. This is particularly important in the spirit of QFT, as non-local theories may have poles in the scattering matrix that are not associated with physical[3] particles, meaning that the theory is non-unitary. Therefore, from the usual field theoretical point of view, working with a redundancy is easier, since it simplifies the computations, and it is consistent with the properties that we want to preserve in the realm of QFT [5–7].

Besides the usual writing in terms of the gauge potential there is another way to study gauge theories, relying on their formulation directly in terms of gauge invariant variables. In the pure gauge case, this happens if we try to quantize the theory directly in terms of the field strength tensor $F_{\mu\nu}$, instead than the gauge potential A_μ. In that procedure, we usually encounter two difficulties: the Lagrangian will contain non-local terms and the dynamics of the variables is moved to the interaction terms [6]. However, a crucial point is that this can be particularly helpful for the construction of consistent analytical approximation schemes, such as strong coupling expansions or mean-field methods [49].

In this Section we provide a summary of the main approaches present in the scientific literature to reformulate gauge theories in terms of gauge invariant degrees of freedom, pointing out the possible pros and cons of the various attempts. We distinguish three principal paths developed over the past years: the first one relies on the recombination of matter and gauge fields to rewrite the theory in terms of gauge invariant variables; the second one regards the so-called *field strength reformulations*, entirely based on the above mentioned substitution $A_\mu \to F[A_\mu]$, while the third one is about the *Wilson loop reformulations*, where the fundamental blocks are the Wilson lines introduced in Eq. (1.19).

1.3.1 Recombinations of degrees of freedom

Historically, Dirac was the first one to think about gauge invariant reformulations of Abelian gauge theories [50]. He firstly proposed to use the field

$$\Psi(x) \equiv e^{iC(x)}\psi(x), \qquad C(x) \equiv \frac{e\partial_i A^i}{\nabla^2} \tag{1.34}$$

as the gauge invariant redefinition of fermions in QED. The object $\Psi(x)$ represents the electron dressed with its Coulomb field: the reformulated theory has gauge invariant operators associated

[3]With physical we mean here that they do not belong to the Hilbert space of the underlying field theory.

to these dressed particles. Physically, we could interpret these particles as electrons with a photon cloud around them, being the field $\Psi(x)$ in Eq. (1.34) non-local (and even non-covariant).

A second attempt was done few years later by Mandelstam, who proposed a reformulation of QED without gauge potentials [51]. His purpose was to use directly the electromagnetic field $F_{\mu\nu}$, without introducing A_μ, to show that the usual schemes to quantize QED could be derived from a gauge-independent formalism. The set of gauge invariant fundamental variables is

$$\{F_{\mu\nu}, \Psi, \Psi^*\}, \qquad \Psi(x) \equiv \psi(x) e^{-ie\int_{-\infty}^{x} d\xi_\mu A^\mu(\xi)}, \tag{1.35}$$

and we observe that $\Psi(x)$ is again non-local, and path-dependent. This last property is a deep seated phenomenon, as it is related to the arbitrariness in the choice of the phase factors in the field operators. Moreover, as the $F_{\mu\nu}$ is now a fundamental variable, the inhomogeneous Maxwell equations must be imposed as consistency condition, as they are not automatically satisfied[4].

From the early 1980s on, a series of papers came out with the aim to realize a precise quantization program, i.e. to reformulate the physical action of QED and find the generating functional of the quantum theory in terms of solely gauge invariant variables [52–57]. Specifically, scalar QED and $SU(2)$ LGTs in presence of bosonic matter fields were investigated in [52]. The main idea consists in introducing the gauge invariants of the corresponding continuum theories to rewrite the Lagrangians and derive the associated dynamics. In the continuum, this change of variables was applied to bosonic matter fields [53] and later to classical [54] and quantum [55, 57] electrodynamics. In particular, the matter fields are combined into new bosonic fields. In the case of $1+1$ dimensions, the Schwinger model, it was shown [56] that the construction is related to the bosonization of the original theory [58, 59].

More recently, in [60] non-Abelian $SU(N)$ QLMs were reformulated in terms of *rishons*, i.e. variables encoding the fermionic constituents of the non-Abelian gauge fields. Despite these variables are not explicitly gauge invariant, they can be recombined with the color index of the fermions (or that of the neighbouring links, in the pure gauge cause) to give rise to gauge invariants with which reformulate the theory [61, 62].

In the last decade, $SU(2)$ LGTs with fundamental fermions were studied and reformulated via the so-called *loop-string-hadron formulation* [63]: this allows for a description of the dynamics of the theory in terms of local and physical observables, using strictly $SU(2)$ gauge invariant variables at the cost of introducing extra lattice links and an Abelian Gauss law. In [64–66] the problem is addressed making use of dual formulations for the case of $U(1)$ gauge symmetry and having as a particular motivation the implementation of gauge theories in quantum devices.

[4]This is because $F_{\mu\nu}$ has no memory of its structure in terms of the gauge potential in this formulation. This is an important non-trivial point, and will be important in the context of the field strength reformulations.

1.3.2 Field strength reformulations

The purpose of this class of reformulations is to obtain, even in the case of pure gauge theories, a theory entirely written using $F_{\mu\nu}$. However, since not all the components of this tensor are independent, the reformulated model will be *constrained*. In this spirit, Mandelstam was the first to think about using $F_{\mu\nu}$ to quantize QED, but we inserted his proposal in the previous discussion, as he recombines gauge and matter degrees of freedom to obtain the set of variables in Eq. (1.35).

In the late 1970s Halpern obtained the inversion $A_\mu \to F_{\mu\nu}(A_\mu)$ for QED in $d = 3$, using a completely fixed axial gauge [67]. The change of variables can be schematically summarized in the following equations for the generating functional

$$Z_A = \int \mathcal{D}A\, \delta[\mathcal{F}(A)] e^{-\frac{1}{4}\int F^2(A)} \qquad \Longrightarrow \qquad Z_F = \int \mathcal{D}F\, \delta[\mathcal{I}(F)] e^{-\frac{1}{4}\int F^2}. \tag{1.36}$$

Respectively, Z_A is the starting generating functional in terms of the gauge potential, constrained with the gauge fixing condition $\mathcal{F}(A) = 0$. On the other side, we have the reformulated functional Z_F using the field strength, that is now constrained with the Bianchi identities $\mathcal{I}(F) = 0$. The main advantages of this formulation involve the absence of constraints on the state of the theory and the fact that confining states are easier to construct in the reformulated theory.

Later in the 1980s other attempts were done on the same lines in the coordinate gauge, both in the Lagrangian and Hamiltonian formulations [68, 69]. The resulting theory has still a non-local action in terms of $F_{\mu\nu}$, constrained with a set of restricted Bianchi identities, similarly to Eq. (1.36). In the Hamiltonian approach, the constraints coming from the Lagrangian formulation need to be complemented by extra conditions, to properly construct the quantization of the theory [69]. In these papers it appears firstly, to our best knowledge, the *reconstruction theorem*, i.e. the set of conditions that A_μ and $F_{\mu\nu}[A_\mu]$ must satisfy in a way to be in one-to-one correspondence[5].

1.3.3 Wilson loop reformulations

The last class of reformulations employs the Wilson loops as fundamental variables of the gauge theories. The first attempt in this direction, both for the Abelian and non-Abelian cases, was done in the 1980s by Giles, with the aim to reconstruct the gauge potentials from a complete set of Wilson loops [70]. Here it is proved that the Wilson loops along with a specific class of kinematical constraints, called *Mandelstam constraints*, provide sufficient conditions to reproduce the underlying local gauge theory. The presence of constraints is necessary because the Wilson variables are non-local, and form an overcomplete set with respect to the gauge potential A_μ.

[5]This is also present in the series of papers [52–57], generalized to the one-to-one correspondence between classes of generic gauge equivalent configurations and sets of gauge invariant degrees of freedom.

Moreover, it is showed that a reconstruction theorem holds also in this case: the gauge fields indeed can be reconstructed uniquely from the Wilson lines, up to gauge transformations. This equivalence theorem can be stated as

$$\mathcal{A}/\mathcal{G} \simeq \{W(\gamma)\}/\mathcal{M}, \tag{1.37}$$

where the left-hand side gives the usual description in terms of gauge potentials and gauge transformations ($\mathcal{A}$ is the space of gauge orbits, $\mathcal{G}$ the set of gauge transformations), and the right-hand side denotes the set of Wilson lines $W(\gamma)$ associated to the path γ, subjected to the Mandelstam constraints $\mathcal{M}$ [71].

The features of the space of all Wilson loops are well discussed in Ref. [72]: such a group is non-Abelian and non-locally compact, meaning that even at the local level is very large. The Mandelstam constraints represent non-linear algebraic equations to be solved for the Wilson lines, whose form depends the gauge group features. In Ref. [72] their explicit form in the $U(1)$, $SU(N)$ classical cases is discussed. In the lattice framework, the gauge invariant states can be labelled by closed paths of the lattice links. The main problem is to find an efficient way of isolating a set of independent loop states.

There are various reasons why, during the year, the development of a consistent loop reformulation for gauge theories failed to succeed [6, 71, 72]. In addition to the difficulties due to quantization procedures and the Mandelstam constraints, we mention that, due to the complicated structure of the loop space, it is hard to argue which part is the most physically relevant. In spite of these considerations, the formulation in terms of independent loop variables opens new possibilities in the analysis of LGTs. First of all, for the fact that the theory is reformulated using gauge invariants; secondly, it could lead to the construction of meaningful, intrinsically gauge invariant analytical approaches, such as analytical loop perturbation theory, strong coupling and mean-field expansions [49, 72].

1.4 Analytical methods for gauge theories

LGTs may be considered, in all respects, as statistical mechanics lattice models. Therefore, tools coming from statistical mechanics like series expansions and mean-field methods offer powerful analytical methods to extract approximate results [13, 49]. When applying these methods to LGTs, a particular attention to the intrinsic local nature of gauge symmetry must be paid, and how this is reflected in the variables formulating the theory. This issue has been already addressed in literature, leading to different conclusions depending on the formulation of the underlying theory.

In this Thesis we focus on the mean-field theoretical approach to the analysis of gauge theories. In the remaining part of this Section we briefly remind what is mean-field theory in statistical

mechanics, and then show its application to pure LGTs with generic compact gauge group. In the final part we discuss how this method has been applied in literature, discussing the results obtained so far and how they depend on the formulation of the theory.

1.4.1 Mean-field theory

We present the mean-field technique in its variational formulation, which is more suitable for the application to LGTs in the Lagrangian formulation [13, 49]. Given a statistical system with action $S[\phi]$, its partition function is written as

$$Z = \int \mathcal{D}\phi \; e^{-\beta S[\phi]}, \tag{1.38}$$

where $\beta = T^{-1}$ is the inverse temperature. The general idea behind the mean-field approximation is to replace the dynamics of the theory by that of independent degrees of freedom in a given external source, which must me chosen carefully in a way to simulate the real dynamics in the best possible way. For this reason, we add and subtract a source term $S_h[\phi]$ in the action

$$S[\phi] \;\rightarrow\; S[\phi] + S_h[\phi] - S_h[\phi] \equiv \tilde{S}_h[\phi] - S_h[\phi], \tag{1.39}$$

where h is a variational parameter; the partition function becomes

$$Z = \int \mathcal{D}\phi \; e^{-\beta \tilde{S}_h[\phi] + \beta S_h[\phi]}. \tag{1.40}$$

At this point we can use the convexity inequality

$$\langle e^f \rangle \geq e^{\langle f \rangle}, \qquad\qquad \langle f \rangle \equiv \int f(x)\rho(x)\, dx, \tag{1.41}$$

where $\rho(x)$ is a normalized measure, to bound the exact free energy of the model from below. Mathematically, the application of Eq. (1.41) to the free energy gives

$$F \geq F_h + \langle \tilde{S}_h[\phi] \rangle_h, \tag{1.42}$$

and the optimal estimate in terms of the variational parameter h leads us to the formula

$$F_{\text{var}} = \max_h \left[F_h + \langle \tilde{S}_h[\phi] \rangle_h \right], \tag{1.43}$$

which gives a self-consistent equation for the external field h.

1.4.2 Application to gauge theories

We apply the previous variational argument to the pure gauge action in Eq. (1.23), in generic dimensions d, with a source term of the form

$$S_h[U] = h \sum_{\mu} (U_\mu + U_\mu^\dagger) \tag{1.44}$$

for all the links of the lattice. The equation for the mean-field free energy is

$$F_{\rm MF} = -\frac{d(d-1)}{2}\, t(h)^4 + \frac{d}{\beta} h\, t(h) - d \log c(h), \tag{1.45}$$

where

$$c(h) \equiv \int e^{h(U+U^\dagger)}\, dU\ , \qquad\qquad t(h) \equiv c^{-1}(h) \int (U+U^\dagger) e^{h(U+U^\dagger)}\, dU \tag{1.46}$$

are the hyperbolic functions for the $U(1)$ gauge group[6]. The self-consistent equation for h is obtained through the differentiation

$$\frac{dF_{\rm MF}}{dh} = 0 \qquad \Rightarrow \qquad h = 2(d-1)\beta\, t^3(h). \tag{1.47}$$

We observe that, since $t(h=0) = 0$, the trivial solution $h = 0$ is always present, and it is the only one for high temperatures. Moreover, this is always a local minimum for the mean-field free energy in Eq. (1.45). The mean-field solutions of Eq. (1.47) predict a first-order transition, and this results is true also for other gauge groups, and, as usual in mean-field theory, should be trusted only for large dimensions.

The most important observation, however, is the following one: in this form, the mean-field solution violates an important theorem by Elitzur, which states that, in gauge theories with compact gauge groups, the only operators that can have non-trivial expectation values are invariant under local gauge transformations [23]. This is in contrast with Eq. (1.44): a non-trivial solution to the mean-field equation would imply $\langle U_\mu \rangle \neq 0$, but we know that $\langle U_\mu \rangle = 0$ because the link variable is not gauge invariant.

This problem may be faced in three different ways:

1. perform the computation in a given gauge. This, of course, will give a different result for any possible gauge choice. For example, in the axial gauge, where the temporal links are fixed to the identity and are no more dynamical, this restores the Elitzur theorem, but the price to pay is to have long-range correlated spatial links along the temporal direction [73];

[6]The generalization to arbitrary continuous gauge groups gives a redefinition of the hyperbolic functions, while the form of the variational equation is the same [13].

2. use a generalized mean-field procedure [49], where the source term is chosen as

$$S_h[U] \sim \sum_{\mu,\nu} h_{\mu\nu}(U_{\mu\nu} + U^\dagger_{\mu\nu}), \tag{1.48}$$

with $h_{\mu\nu}$ being a square matrix for each link variable. However, the general solutions with this method are basically impossible to be found. With a guided ansatz of the form $h_{\mu\nu} = h g_i g_j^{-1},\ g_i \in \mathcal{G}$, we recover the original mean-field picture of Eq. (1.47), but without the violation of the Elitzur theorem in the intermediate steps [74];

3. reformulate the theory in terms of gauge invariant variables. This allows for the choice of any possible type of order parameter, without violation of the Elitzur theorem. However, depending on the reformulation, we have different pros and cons that we are going to comment.

Field strength reformulations

On the lattice, the first step is to change from links U_μ to plaquette variables $U_{\mu\nu}$, and was firstly accomplished by Batrouni [75]. When performing this change of variables, we get a Jacobian enforcing the Bianchi identity as a constraint for the new variables. Once the plaquettes are introduced, they are gauge invariant objects by construction, and can be taken as order parameters for consistent mean-field expansions. More recently, it was shown that the mean-field approximation can be further improved by determining the self-consistent mean distributions for the plaquette variables [76]. This approach works again at zero temperature, and has some disadvantages, even if it solves the inconsistency with gauge invariance. First of all, it does not allow straightforwardly the computation of non-local quantities at the mean-field level. Secondly, it is practically difficult to extend to the case of non-Abelian gauge theories.

Loop reformulations

The reformulation in terms of Wilson loops, despite being consistent with the Elitzur theorem, would be particularly hard to analyze with mean-field theory, and we are not aware of any attempt in the scientific literature towards this direction. This is because of the presence of Mandelstam constraints, discussed in Sec. 1.3.3, that are more complicated to be handled with respect to the Bianchi identity.

At last, we mention that LGTs can be reformulated also in terms of Polyakov loops, to obtain a description in terms of effective line actions. Once reformulated, consistent mean-field procedures can be developed for the effective theory at any temperature [77].

Chapter 2

A gauge invariant reformulation and applications to mean-field computations

In this Chapter we set up a formalism allowing to reformulate Abelian gauge theories in terms of gauge invariant fields (GIF). In particular, we look for a reformulation satisfying three requirements:

1. it should allow to investigate the dependence on the particular construction used to eliminate the gauge covariant quantities;
2. it would be suitably extendable to continuum gauge theories;
3. in presence of matter fields ψ, it should allow to straightforwardly determine a gauge invariant combination ψ' of the original matter and gauge variables.

Regarding the second point, we present two different constructions to split the gauge field into its gauge invariant and gauge covariant part. The gauge invariant part is taken as a new variable, while the gauge covariant part can be combined with matter to obtain, as mentioned, a new GIF. These constructions are presented – keeping the size of the system finite – both on the lattice and in the continuum for arbitrary dimension and for two kinds of boundary conditions: periodic and open.

Fulfilling the last requirement is the key point of the presented formalism, since once the GIF ψ' has been identified it can be used as a new gauge invariant degree of freedom of the theory. While generic expectation values of ψ are not gauge invariant, the corresponding expectation values of ψ' are fully physical. This is particularly relevant for finding suitable order parameters in light of Elitzur's theorem, stating that local symmetries cannot be spontaneously broken [23]. For this reason, the presented reformulation could be useful to analyze the phase diagrams of gauge theories using approximate analytical methods, such as the mean-field one, since it gives information about possible – gauge invariant – order parameters of the theory.

We finally observe that the choice of the GIF is not unique: other combinations of the initial gauge and matter covariant fields can be gauge invariant, and a choice for the definition of ψ' should emerge from the procedure. Our reformulation leads to a simple expression for ψ' in the form $\psi' \sim \mathcal{E}\psi$, where $\mathcal{E}$ is an operator depending only on the gauge field. Once this choice has been done, we can perform the elimination of the initial matter and gauge fields with different geometrical constructions, whose role is explicitly discussed in the following Sections. This structure of the GIF is analogous to the one already introduced by Dirac in [50], where the proper gauge invariant operator creates the electron along with a "photon cloud" around it. A similar structure is also present in [78], where gauge invariance is traded by a path-dependent choice of gauge invariant variables.

This Chapter is structured as follows: we firstly present the idea of our reformulation, to elucidate the logic behind the change of variables. In the Sections 2.2, 2.3 and 2.4 we discuss the details of the reformulation in various dimensions, starting from the simplest case of $d = 1$ and then generalizing to arbitrary $d > 1$, investigating the constraints that come out in the various constructions. We then show how to rewrite the lattice action for pure Abelian gauge theories on the lattice, focusing on the particular example of gauge theories in $(2 + 1)$ dimensions (Sec. 2.5), the Hamiltonian of a single particle in a magnetic field and the Lagrangian of QED (Sec. 2.6). In Section 2.7 we consider the Hofstadter Hamiltonian in $d = 2$ and $d = 3$, showing how they are written in terms of the new gauge invariant variables. In Section 2.8 we comment about the applications of the reformulation. In Section 2.9 we summarize our results and present our conclusions.

2.1 Introduction of the new variables: main idea

The main idea behind our formalism is to use the lattice definition of the Maxwell tensor given in Eq. (1.21) to express the gauge field A_μ as a function of $F_{\mu\nu}$. Clearly, this operation is not uniquely defined, since $F_{\mu\nu}$ is gauge invariant while A_μ is not. Stated differently, the Maxwell tensor does not carry the gauge covariant part of A_μ, which, instead, will be carried by a new scalar field ϕ. This will amount to replace A_μ by a combination of $F_{\mu\nu}$ and ϕ. In turn, not all the components of $F_{\mu\nu}$ are independent. The idea is then to define independent sums of $F_{\mu\nu}$ over various strips on the lattice, which will be denoted by $\bar{F}_{\mu\nu}$. The presented formalism allows finally to perform the change of variables

$$A_\mu \to \{\bar{F}_{\mu\nu}, \phi\}. \tag{2.1}$$

We will show how to reformulate the Lagrangian with the new variables in two ways, referred in the following as *asymmetric* and *symmetric* constructions. One has to check, for each construction, whether the new fields $\bar{F}_{\mu\nu}$ are independent, and, if not, what are the constraints between them. Our procedure bears some similarities with the path-dependent choice of gauge invariant fields in

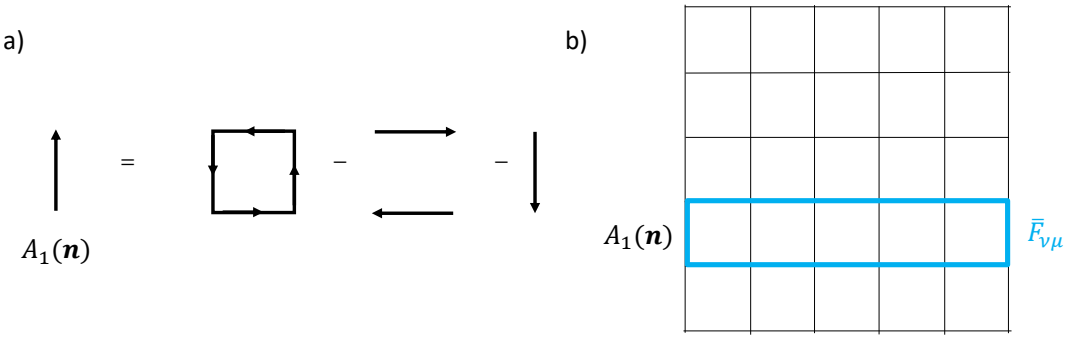

Figure 2.1: (a) Graphical representation of $A_1(\mathbf{n})$ after the first iteration of our procedure. (b) Iterative isolation of the link $A_1(\mathbf{n})$, the leftmost in the blue column, in terms of plaquettes. The highlighted strip is the sum of F_{10} present in Eq. (2.3). The temporal and spatial directions are, respectively, the horizontal and vertical ones.

[78]. In contrast to that approach, all of our gauge invariant variables are independent and do not have to satisfy any constraint.

We emphasize that ϕ is a field and it is not fixed by our procedure: in the computation of the generating functional of the theory, we must sum over all the possible configurations of $\bar{F}_{\mu\nu}$. On the other hand, we can fix ϕ, corresponding to choosing a specific gauge, or sum over it. The result will be the same. Contrary to standard gauge fixing, this will not alter the form of the Lagrangian, as the non-physical degrees of freedom were decoupled. This description holds both for open boundary conditions (OBC) and periodic boundary conditions (PBC). However, in order to correctly reproduce all the degrees of freedom, some extra care is needed for the latter. To this end, a further new set of variables, associated with Wilson loops piercing the lattice, will be introduced for PBC.

We finally anticipate that when the matter fields ψ are present, an advantage of our reformulation with respect to other possible ones is that the introduction of ϕ naturally indicates how to rewrite ψ in terms of a new gauge invariant matter field ψ', combining both ψ and ϕ. Once the integration over ϕ is performed, part of the contribution of the gauge field remains through $\bar{F}_{\mu\nu}$ and – as will be clarified in the following – the theory will be expressed in terms of the fields ψ' and $\bar{F}_{\mu\nu}$.

2.2 The $(1+1)-d$ case: asymmetric construction

In $(1+1)$ dimensions there is only one independent component of the strength tensor, i.e. F_{10}. Since we want to express the gauge fields A_0 and A_1 in terms of F_{10}, we use Eq. (1.21) to isolate

A_1 for a generic site $\mathbf{n}$

$$A_1(\mathbf{n}) = F_{10}(\mathbf{n}) - A_0(\mathbf{n}+\hat{1}) + A_0(\mathbf{n}) + A_1(\mathbf{n}+\hat{0}). \tag{2.2}$$

Graphically, this has a simple interpretation: it can be thought of as a plaquette with all the edges being removed except for $A_1(\mathbf{n})$. The next step is to use Eq. (2.2), iteratively, to express all the A_1 links appearing on the right-hand side. This is done until the boundary $n_0 = N$ is reached, as illustrated in Fig. 2.1. In the end, we are left with the following expression for the gauge field:

$$A_1(\mathbf{n}) = \sum_{k=0}^{N-n_0-1} \Big[F_{10}(\mathbf{n}+k\cdot\hat{0}) - A_0(\mathbf{n}+\hat{1}+k\cdot\hat{0}) + A_0(\mathbf{n}+k\cdot\hat{0}) \Big] + A_1(\mathbf{n}+(N-n_0)\cdot\hat{0}). \tag{2.3}$$

We now introduce the *vertex variables* $\phi(\mathbf{n})$, defined on the vertices of the lattice, as shown in Fig. 2.2, and encoding the gauge covariant part of $A_\mu(\mathbf{n})$. Due to the nature of the considered gauge group $\mathcal{G} = U(1)$, these are scalar fields. The variables ϕ are related to A_0 through a finite derivative along the $\hat{0}$ direction, that is

$$A_0(\mathbf{n}) \equiv \phi(\mathbf{n}+\hat{0}) - \phi(\mathbf{n}). \tag{2.4}$$

Note that this can always be done. In turn, the choices for the values of ϕ are not unique, as we can always shift them by a function with arbitrary dependence on n_1 without changing the value of any $A_0\,(\mathbf{n})$. This freedom will be explored in what follows. Inserting this into Eq. (2.3) we obtain a telescopic sum, resolving the part associated to the horizontal links

$$\begin{aligned} A_1(\mathbf{n}) = {} & A_1(\mathbf{n}+(N-n_0)\cdot\hat{0}) - [\phi(\mathbf{n}+(N-n_0)\cdot\hat{0}+\hat{1}) - \phi(\mathbf{n}+(N-n_0)\cdot\hat{0})] \\ & + \phi(\mathbf{n}+\hat{1}) - \phi(\mathbf{n}) + \sum_{k=0}^{N-n_0-1} F_{10}(\mathbf{n}+k\cdot\hat{0}). \end{aligned} \tag{2.5}$$

By exploiting the aforementioned freedom for choosing the field ϕ, we can set

$$A_1(\mathbf{n}_B) = \phi(\mathbf{n}_B+\hat{1}) - \phi(\mathbf{n}_B) \tag{2.6}$$

at the boundary points $\mathbf{n}_B \equiv (N, n_1)$. For the OBC case this essentially completes the map, while for PBC further considerations are necessary.

2.2.1 Open boundary conditions

The OBC case is depicted in Fig. 2.2(a). By plugging Eq. (2.6) into (2.5) we can write

$$A_1(\mathbf{n}) = \sum_{k=0}^{N-n_0-1} F_{10}(\mathbf{n}+k\cdot\hat{0}) + \phi(\mathbf{n}+\hat{1}) - \phi(\mathbf{n}) \tag{2.7}$$

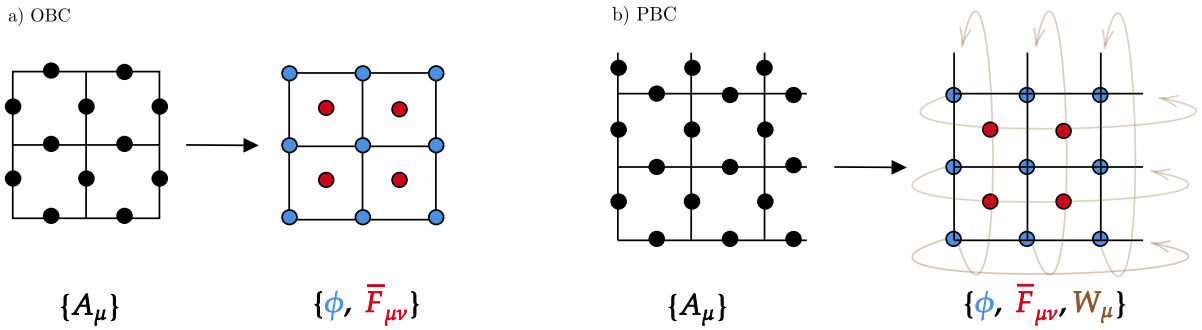

Figure 2.2: Plot of a lattice with linear size $N = 3$. In black the original gauge field components A_μ living on the links. In color the representation of the new set of variables. a) For OBC the new degrees of freedom are represented in blue (the ϕ's that live on the vertices) and in red (the $\bar{F}_{\mu\nu}$'s defined on the plaquettes). b) For PBC the same new degrees of freedom are present plus extra ones corresponding to the loops (the f_μ in brown).

which, with (2.6), concludes the rewriting of the vertical links. By defining the *plaquette strip*

$$\bar{F}_{10}(\mathbf{n}) \equiv \sum_{k=0}^{N-n_0-1} F_{10}(\mathbf{n} + k \cdot \hat{0}), \tag{2.8}$$

the vertical links can be written as

$$A_1(\mathbf{n}) = \bar{F}_{10}(\mathbf{n}) + \phi(\mathbf{n} + \hat{1}) - \phi(\mathbf{n}). \tag{2.9}$$

We can characterize OBC by imposing $A_0(N, n_1) = 0$ and $A_1(n_0, N) = 0$. Consequently, Eqs. (2.4) and (2.9) summarize the mapping of Eq. (2.1) for the OBC case, by adopting the boundary conditions $\bar{F}_{10}(N, n_1) = \bar{F}_{10}(n_0, N) = 0$. There is yet the residual freedom on the choice of the field ϕ. This is reflected by the fact that shifting all $\phi(\mathbf{n})$ by a constant will leave the initial $A_\mu(\mathbf{n})$ invariant. This ambiguity can be resolved by simply imposing $\phi(N, N) = 0$, for example. We can now verify that the number of degrees of freedom matches the original one. There is a total of $N^2 - 1$ non-trivial values for ϕ and $(N-1)^2$ for $\bar{F}_{10}$, which sum to the original $2N(N-1)$ degrees of freedom associated with the links of open boundaries.

2.2.2 Periodic boundary conditions

The PBC case is depicted in Fig. 2.2(b). In comparison to OBC, we need to map an extra set of degrees of freedom. These correspond to links emanating from the boundary, i.e. $A_0(N, n_1)$ and $A_1(n_0, N)$, as well as to specify how the fields transform under a full lattice translation, i.e. $A_\mu(\mathbf{n} + N\hat{\nu})$. Regarding the first set of variables, we introduce the Wilson loops $W_{\mathcal{C}_0}$ and $W_{\mathcal{C}_1}$, which are associated to paths that wrap around the lattice along the $\hat{0}$ and $\hat{1}$ directions. We may

formally write these loops as [12]

$$W_{\mathcal{C}_0} = \prod_{n_i=1}^{N} e^{ieA_0(n_i,n_1)} \equiv e^{ief_0(n_1)}, \qquad W_{\mathcal{C}_1} = \prod_{n_i=1}^{N} e^{ieA_1(n_0,n_i)} \equiv e^{ief_1(n_0)}, \tag{2.10}$$

where $f_\mu(n_\nu)$ corresponds to the sum of all A_μ along a straight line of constant n_ν ($\mu \neq \nu$). Using the definitions in Eqs. (2.4), (2.7) to rewrite the gauge fields for the remaining links, we can isolate the boundary fields as functions of the introduced loops as

$$\begin{aligned} A_0(N,n_1) &= f_0(n_1) - \phi(N,n_1) + \phi(1,n_1), \\ A_1(n_0,N) &= f_1(n_0) - \phi(n_0,N) + \phi(n_0,1) - \sum_{n_j=1}^{N-1} \bar{F}_{10}(n_0,n_j). \end{aligned} \tag{2.11}$$

By complementing Eqs. (2.4), (2.6) and (2.9) with the above expression we can see that the mapping $\{A_0, A_1\} \to \{\phi, \bar{F}_{10}, f_0, f_1\}$ is one-to-one. In particular, the number of degrees of freedom correctly match. In fact, the link variables A_μ form a total of $2N^2$ degrees of freedom. At the same time, the set $\{\phi, \bar{F}_{10}\}$ introduced in the OBC case has $2N(N-1)$ non-trivial values and the remaining $2N$ degrees of freedom are precisely given by the set of $2N$ loops $\{f_0, f_1\}$. It remains to specify how the fields $A_\mu(\mathbf{n} + N\hat{\nu})$ are expressed in terms of the gauge invariant degrees of freedom. As PBC should only be imposed on physical fields, the most general form of PBC on a gauge theory amounts to imposing periodicity on A_μ up to a gauge transformation [79–82]. Explicitly this means that

$$A_\mu(\mathbf{n} + N\hat{\nu}) = A_\mu(\mathbf{n}) + \varphi_\nu(\mathbf{n} + \hat{\mu}) - \varphi_\nu(\mathbf{n}), \tag{2.12}$$

where φ_ν are called *transition functions* and are crucial to study non-trivial topological sectors of the theory [82, 83]. They have to satisfy a consistency condition, called the *cocycle condition*, guaranteeing that certain quantities, such as $A_\mu(\mathbf{n} + N\hat{0} + N\hat{1})$, are single valued. Such a condition reads

$$\varphi_\nu(\mathbf{n} + N\hat{\mu}) + \varphi_\mu(\mathbf{n}) = \varphi_\mu(\mathbf{n} + N\hat{\nu}) + \varphi_\nu(\mathbf{n}) + \varphi_{\nu\mu}, \tag{2.13}$$

where $\varphi_{\mu\nu}$ is the *twist tensor*, which is antisymmetric and gauge invariant [82]. Moreover, the φ_ν's have to be considered as a set of new dynamical variables, i.e. physical degrees of freedom to be integrated in the functional integrals of the theory [79].

We can show that these boundary conditions can be incorporated within our reformulation. In fact, it follows from Eqs. (2.4), (2.9) and (2.11) that the twisted boundary conditions in Eq. (2.12) are exactly implemented by the following boundary conditions on ϕ

$$\phi(\mathbf{n} + N\hat{\nu}) = \phi(\mathbf{n}) + \varphi_\nu(\mathbf{n}). \tag{2.14}$$

The transition functions are the same in our reformulation and, consequently, the degrees of freedom that they carry are trivially translated to our construction. Concerning the strip variables $\bar{F}_{10}$, they

are subject to PBC, i.e. $\bar{F}_{10}(\mathbf{n}+N\hat{\mu}) = \bar{F}_{10}(\mathbf{n})$. This can be taken into account by appropriately redefining the strips as

$$\bar{F}_{10}(\mathbf{n}) = \sum_{k=0}^{(N-n_0-1) \bmod N} F_{10}(\mathbf{n}+k\cdot\hat{0}). \tag{2.15}$$

We finally observe that the loops f_0, f_1 obey PBC as long as periodic gauge transformations are considered. Indeed, the Wilson loops (2.10) acquire non-trivial phases under the application of topologically non-trivial gauge transformations, i.e. transition functions that are periodic up to integer multiples of $2\pi/e$ (sometimes such gauge transformations are called *large* topologically non-trivial gauge transformations [82]). This gauge redundancy can further be lifted by suitably combining the transition functions φ_ν with the loops f_ν. Accordingly, we define

$$\bar{f}_0(n_1) = f_0(n_1) - \varphi_0(1,n_1), \qquad \bar{f}_1(n_0) = f_1(n_0) - \varphi_1(n_0,1). \tag{2.16}$$

The non-trivial phases acquired by the Wilson loops in Eq. (2.10) under large gauge transformations, corresponding to translations of the f_μ, are canceled by the respective gauge transformations of the transition functions and we obtain quantities that are invariant under general gauge transformations. Under a full lattice translation, these loops are transformed by the twist tensor: $\bar{f}_0(n_1+N) = \bar{f}_0(n_1) + \varphi_{01}$ and $\bar{f}_1(n_0+N) = \bar{f}_1(n_0) + \varphi_{10}$.

2.2.3 Comments about gauge fixing

We showed that the mapping presented is defined in a consistent way, as any gauge field $A_\mu(\mathbf{n})$ can be expressed as a function of the new, independent, variables $\{\phi, \bar{F}_{10}\}$ through Eqs. (2.4), (2.6) and (2.9) for OBC – or as a function of $\{\phi, \bar{F}_{10}, f_0, f_1\}$ through Eqs. (2.4), (2.9), (2.6) and (2.11) for PBC. The price to pay is hidden in locality and translational invariance. The reformulation, as anticipated, shifts the effect of gauge transformations G to the vertex variables, since $A_\mu \sim A_\mu + \Lambda(\mathbf{n}+\hat{\mu}) - \Lambda(\mathbf{n})$, which is the lattice version of Eq. (1.7), implies $\phi(\mathbf{n}) \sim \phi(\mathbf{n}) + \Lambda(\mathbf{n})$.

We observe that fixing a particular configuration of the vertex variables, e.g. $\phi = \tilde{\phi}$, would be equivalent to some gauge fixing $\mathcal{F}$, where one sums only over configurations that satisfy the constraint $\mathcal{F}(A_\mu) = 0$. As an example one could choose $\tilde{\phi} = 0$, which corresponds to a maximal tree gauge [84].

A careful reader could object that there is no real difference between our reformulation and other approaches corresponding to particular choices of ϕ. However, the substantial difference is *not* that in these approaches ϕ is fixed and in ours is not, since the ϕ at the end will be anyway integrated out. At variance, the main difference will be clear when the matter field ψ will be introduced: we will show that our reformulation allows for the definition of new matter variables ψ' expressed in terms of the original variables ψ and the to-be-integrated variables ϕ. So the

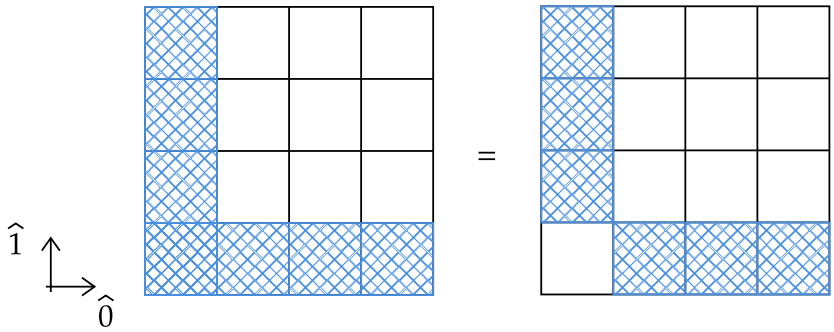

Figure 2.3: Graphical representation of the constraint in Eq. (2.26), equivalent to the Mandelstam constraint for crossing Wilson loops on the square lattice showed in fig. 2.5(a).

initial fields are $\{\psi, A_\mu\}$, which are separately gauge variants, while at the end of our reformulation procedure the theory is expressed in terms of the variables $\{\psi', \bar{F}_{\mu\nu}\}$:

$$\{\psi, A_\mu\} \to \{\psi', \bar{F}_{\mu\nu}\}, \tag{2.17}$$

where the fields $\{\psi', \bar{F}_{\mu\nu}\}$ are gauge invariant. In the case of PBC, new degrees of freedom are present through transition functions. Analogously, a reformulation in terms of purely gauge invariant fields can be achieved through $(\psi, A_\mu, \varphi_\mu) \to (\psi', \bar{F}_{\mu\nu}, \bar{f}_\mu)$.

2.3 The $(1+1)-d$ case: symmetric construction

Here we present an alternative construction starting from the set $\{\phi, F_{\mu\nu}\}$. As previously mentioned, if we choose to isolate the temporal component in Eq. (2.2) rather than the spatial one, we get vertical strips instead of the horizontal ones of the previous setup. The idea of the symmetric constructions is to remove such arbitrariness in the procedure and to combine both these asymmetric constructions, to obtain a more symmetric result.

We proceed following the same structure of Sec. 2.2. For the OBC case, the gauge fields in the asymmetric construction are written in Eqs. (2.4) and (2.9) in terms of $\bar{F}_{10}$. However, if we had chosen F_{01}, the final formulas would have been

$$A_1(\mathbf{n}) \equiv \phi'(\mathbf{n} + \hat{1}) - \phi'(\mathbf{n}), \tag{2.18}$$

$$A_0(\mathbf{n}) = \sum_{k=0}^{N-n_1-1} F_{01}(\mathbf{n} + k \cdot \hat{1}) + \phi'(\mathbf{n} + \hat{0}) - \phi'(\mathbf{n}) \equiv \bar{F}_{01} + \phi'(\mathbf{n} + \hat{0}) - \phi'(\mathbf{n}). \tag{2.19}$$

Here the fundamental variables are $\{\phi', \bar{F}_{01}\}$. To obtain a symmetric construction, we can define

$$\tilde{\phi} = \frac{\phi + \phi'}{2} \tag{2.20}$$

and sum the previous relations with Eqs. (2.4), (2.7). The symmetrized gauge fields are

$$A_0(\mathbf{n}) = \tilde{\phi}(\mathbf{n}+\hat{0}) - \tilde{\phi}(\mathbf{n}) + \frac{1}{2}\sum_{k=0}^{N-n_1-1} F_{01}(\mathbf{n}+k\cdot\hat{1}), \tag{2.21}$$

$$A_1(\mathbf{n}) = \tilde{\phi}(\mathbf{n}+\hat{1}) - \tilde{\phi}(\mathbf{n}) + \frac{1}{2}\sum_{k=0}^{N-n_0-1} F_{10}(\mathbf{n}+k\cdot\hat{0}). \tag{2.22}$$

This result can be obtained from the asymmetric construction, as in Eqs. (2.18) and (2.19), by means of the gauge transformation

$$\phi \;\longrightarrow\; \tilde{\phi} - \frac{1}{2}\sum_{k=0}^{N-n_0-1}\sum_{\ell=0}^{N-n_1-1} F_{01}(\mathbf{n}+k\cdot\hat{0}+\ell\cdot\hat{1}). \tag{2.23}$$

The specific details pertaining to PBC trivially extend to the symmetric construction. In particular, the boundary condition in Eq. (2.14) of the periodic case still holds with $\tilde{\phi}$ in place of ϕ and the boundary links in Eq. (2.11) are symmetrized with respect to the strips $\bar{F}_{10}$ and $\bar{F}_{01}$, i.e.

$$A_0(N,n_1) = f_0(n_1) - \tilde{\phi}(N,n_1) + \tilde{\phi}(1,n_1) - \frac{1}{2}\sum_{n_j=1}^{N-1}\bar{F}_{01}(n_j,n_1), \tag{2.24}$$

$$A_1(n_0,N) = f_1(n_0) - \tilde{\phi}(n_0,N) + \tilde{\phi}(n_0,1) - \frac{1}{2}\sum_{n_j=1}^{N-1}\bar{F}_{10}(n_0,n_j). \tag{2.25}$$

where the loops f_μ are introduced according to the definition in Eq. (2.10). Finally we notice that, within this particular construction, the strips $\bar{F}_{10}$ and $\bar{F}_{01}$ satisfy the relation

$$\bar{F}_{01}(\mathbf{n}) + \bar{F}_{10}(\mathbf{n}+\hat{0}) - \bar{F}_{10}(\mathbf{n}) - \bar{F}_{10}(\mathbf{n}+\hat{1}) = 0, \tag{2.26}$$

which shows explicitly that they are not all independent variables (see Fig. 2.3 for the graphical representation). This is a particular case of more general constraints that are present in higher dimensions, as we are going to discuss, called *Mandelstam constraints*.

2.4 Higher dimensions

We now consider $(d+1)$ dimensions, generalizing the previous construction to a hypercubic lattice of size N^{d+1}. We choose a reference plane to which we apply the procedure described in Sec. 2.2. Then, given an arbitrary link, we can repeatedly apply identities of the form of Eq. (2.2) until we arrive at the reference plane.

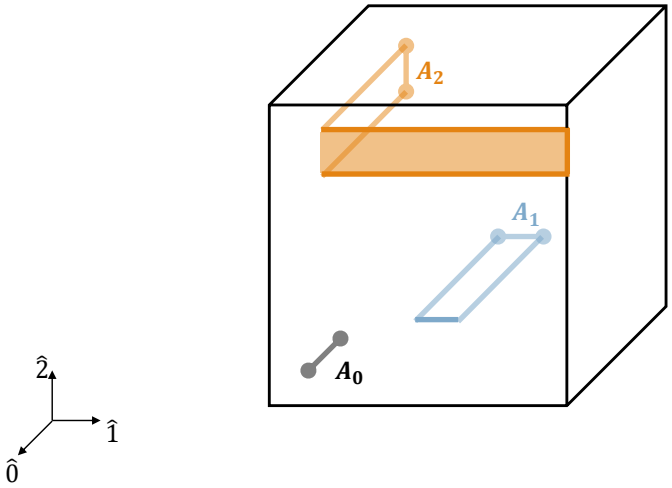

Figure 2.4: Graphical representation of the $(2+1)-d$ case: the link $A_0(\mathbf{n})$ (light black line) is a difference of vertex variables (light black dots), while the others, $A_1(\mathbf{n})$ and $A_2(\mathbf{n})$, involves plaquette strips (light blue and orange lines, respectively). The surface links and strips are in blue (and orange) for the links $A_1(\mathbf{n})$ (and $A_2(\mathbf{n})$) respectively.

2.4.1 Asymmetric construction

We choose the reference plane to be the $d=2$ surface defined by $n_i = N$ for $i = 2, \ldots, d$. To lighten the notation, we will denote a boundary site by

$$\mathbf{n}^{(\mu)} \equiv (\underbrace{N, \ldots, N}_{\mu+1-\text{times}}, n_{\mu+1}, \ldots, n_d). \tag{2.27}$$

Accordingly, $\mathbf{n}^{(0)}$ represents a point at the boundary 0, $\mathbf{n}^{(1)}$ a point at boundaries 0 and 1, and so on. Moreover, we generalize the plaquette strip on the lattice as

$$\bar{F}_{\mu\nu}(\mathbf{n}^{(\nu-1)}) \equiv \sum_{\ell=0}^{N-n_\nu-1} F_{\mu\nu}(\mathbf{n}^{(\nu-1)} + \ell \cdot \hat{\nu}). \tag{2.28}$$

In this compact notation the rewriting of a generic component $A_\mu(\mathbf{n})$ of the gauge field is

$$A_\mu(\mathbf{n}) = \sum_{\nu<\mu} \bar{F}_{\mu\nu}(\mathbf{n}^{(\nu-1)}) + \phi(\mathbf{n}+\hat{\mu}) - \phi(\mathbf{n}). \tag{2.29}$$

As before, there is a component written solely in terms of vertex variables, i.e. $A_0(\mathbf{n})$, and all the others are built by filling the lattice with the plaquette strips. Now $A_0(\mathbf{n})$ fixes ϕ up to arbitrary translations by functions dependent on $n_1, \ldots, n_d$ (but not n_0), a freedom that is explored to fix the remaining A_i at the boundaries. In agreement with (2.29), we can take $\bar{F}_{\mu\nu}(\mathbf{n}^{(j-1)})$, with $\mu > \nu$, as the new set of independent variables.

Open boundary conditions

As in the $(1+1)$ dimensional case, the considerations above are enough to establish the transformation to the new variables for OBC. Once again, the values of the field ϕ is completely fixed up to an overall shift by a constant which is used to set $\phi(N,\dots,N)=0$. Furthermore the plaquette strips, at the proper boundary, are put to zero as well

$$\bar{F}_{\mu\nu}(\mathbf{n}^{(\nu-1)})=0, \quad n_\mu = N \text{ or } n_\nu = N. \tag{2.30}$$

Here, we also observe that the degrees of freedom are properly matched. There is a total of $N^{d+1}-1$ vertex variables ϕ. The strips $\bar{F}_{ij}$ entail $N^{d-1-j}(N-1)^2$ for any $0\leq j<i\leq d$, giving a total of $dN^{d+1}-(d+1)N^d+1$ strip variables. Summing these together we find the required $(d+1)N^d(N-1)$ link variables of the initial formulation.

Periodic boundary conditions

For the periodic case, the rewriting of $(1+1)$ dimensions also extends to higher dimensions, including the introduction of the loops f_μ defined in Eq. (2.10) and the corresponding gauge invariant $\bar{f}_\mu$. In particular, a generic boundary link $A_\mu(n_0,\dots,n_\mu=N,\dots,n_d)$ is expressed as

$$\begin{aligned} A_\mu(n_0,\dots,n_\mu=N,\dots,n_d) = f_\mu(n_0,\dots,n_{\mu-1},n_{\mu+1},\dots,n_d) - \sum_{\nu<\mu}\sum_{n_\mu=1}^{N-1}\bar{F}_{\mu\nu}(\mathbf{n}^{(\nu-1)}) \\ - \phi(n_0,\dots,n_\mu=N,\dots,n_d)+\phi(n_0,\dots,n_\mu=1,\dots,n_d). \end{aligned} \tag{2.31}$$

The transformation in Eq. (2.14) implements the periodicity on the gauge field of Eq. (2.29), up to a gauge transformation in exactly the same way. Once again the $\bar{F}_{\mu\nu}$ are periodic and $\bar{f}_\mu$ transform with the twist tensor, i.e. $\bar{F}_{\mu\nu}(\mathbf{n}+N\hat{\delta})=\bar{F}_{\mu\nu}(\mathbf{n})$ and $\bar{f}_\mu(\mathbf{n}+N\hat{\delta})=\bar{f}_\mu(\mathbf{n})+\varphi_{\mu\delta}$. The number of degrees of freedom can be computed by summing the ones from OBC, i.e. $(d+1)N^d(N-1)$, with the number of loops f_μ introduced, i.e. $(d+1)N^d$. This gives $(d+1)N^{d+1}$, which matches exactly the number of starting links A_μ.

2.4.2 Symmetric construction

We repeat here the procedure done in $(1+1)-d$ for the symmetrization of the gauge field. The first step towards this is to allow for the presence of strips $\bar{F}_{\mu\nu}$ with $\nu\neq\mu$, with $\mu\in\mathcal{U}=\{0,1,\dots,d\}$. Given these variables, the idea is to consider the possible asymmetric constructions along the different directions and then take their average. The final result will be a gauge field written as

$$A_\mu(\mathbf{n})=\Delta_\mu\phi(\mathbf{n})+\sum_{\nu\neq\mu}\alpha^\nu\bar{F}_{\mu\nu}(\mathbf{n}^{(\nu-1)}), \tag{2.32}$$

where $\Delta_\mu\phi(\mathbf{n}) \equiv \phi(\mathbf{n}+\hat{\mu})-\phi(\mathbf{n})$, the strips are defined in the usual way, and α^ν are real coefficients, that must be chosen in a way to reproduce consistently the Maxwell tensor. The simplest way to realize our proposal in general dimensions is to start from cyclically permuted asymmetric constructions, and then average over them. This procedure defines the new vertex variables as the average of the cyclically permuted ones and automatically gives the correct strips to be included in the gauge field's component.

We consider the cyclic permutations defined by the map $\sigma = (0\ 1\ \ldots\ d)$, written in the cycle notation. This means that every time σ acts on $\mu_i \in \mathcal{U}$ it returns $\sigma(\mu_i) = \mu_{i+1}$, with the condition $\sigma(d) = 0.$ of the set of indices μ. For example:

$$\sigma_1(\mathcal{U}) = \mathcal{U}' = \begin{pmatrix} 0 & 1 & \ldots & d-1 & d \\ 1 & 2 & \ldots & d & 0 \end{pmatrix} = \{1, 2, \ldots, d, 0\}, \tag{2.33}$$

and so on. This defines a set of reshuffled indices $\Gamma = \{\mathcal{U}, \sigma(\mathcal{U}), \sigma(\sigma(\mathcal{U})), \ldots\} \equiv \{\mathcal{U}_0, \mathcal{U}_1, \ldots, \mathcal{U}_d\}$ that contains exactly $d+1$ elements.

The starting point is the asymmetric construction with $\mu \in \mathcal{U}_0$:

$$A_\mu(\mathbf{n}) = \Delta_\mu\phi(\mathbf{n}) + \sum_{\nu<\mu} \bar{F}_{\mu\nu}(\mathbf{n}^{(\nu-1)}), \tag{2.34}$$

and the procedure is the following one: we do $d+1$ asymmetric constructions with $\mu \in \mathcal{U}_i,\ \forall i \in \mathcal{U}$, and sum over them. This is equivalent to sum cyclically over the permutations of the indices μ. The important remark in the i-th construction is the *order of the indices in* $\mathcal{U}_i$: this has to be taken as the right order in the sum of the strips, and also for their definition. Indeed, it can be recast in the form

$$\bar{F}_{\mu\nu}(\mathbf{n}^{(\nu-1)}) \equiv \int_{x_\nu}^{L} F_{\mu\nu}(\mathbf{y}_\nu)\, dy_\nu, \qquad \mu,\ \nu \in \mathcal{U} \text{ within its internal order.} \tag{2.35}$$

With these definitions, we can formally combine the asymmetric constructions $A_{\sigma(\mu)}$ as a cyclic sum:

$$A_\mu(\mathbf{n}) \equiv \frac{1}{d+1} \sum_\sigma A_{\sigma(\mu)}(\mathbf{n}). \tag{2.36}$$

This will automatically define a mapping $A_\mu \ \rightarrow\ \{\phi', \bar{F}_{\mu\nu}\}$, where again the vertex variables ϕ' are encoding the gauge covariant part of A_μ, while the $\bar{F}$ are gauge invariant. Out of this last equation, the coefficients α^ν can be determined by direct comparison.

To present a concrete example, let us consider the symmetrization of the $d = 2$ case. In the asymmetric construction we have (we omit the vertex variables, for simplicity)

$$A_0 \sim 0, \qquad A_1 \sim \bar{F}_{10}(\mathbf{n}), \qquad A_2 \sim \bar{F}_{20}(\mathbf{n}) + \bar{F}_{21}(\mathbf{n}^{(0)}). \tag{2.37}$$

We now consider the new frame $\sigma(\mu) = \{1, 2, 0\} = \{0', 1', 2'\}$, with coordinates $\mathbf{n}' = (n_1, n_2, n_0)$. In terms of the primed indices, the expressions of $A_{\mu'}$ are the same as in the previous equation. We have however to read the strips in the original frame, that is

$$\bar{F}_{1'0'}(\mathbf{n}') = \int_{n'_0}^{L} F_{1'0'}(y_0, n'_1, n'_2)\, dy_0 = \int_{n_1}^{L} F_{21}(n_0, y_0, n_2)\, dy_0 \equiv \bar{F}_{21}(\mathbf{n}), \tag{2.38}$$

$$\bar{F}_{2'0'}(\mathbf{n}') \equiv \bar{F}_{01}(\mathbf{n}), \qquad \bar{F}_{2'1'}(\mathbf{n}^{(0)}) \equiv \bar{F}_{02}(\mathbf{n}'^{(0)}) = \bar{F}_{02}(n_1 = L). \tag{2.39}$$

The last line clarify the notation for $\mathbf{n}'^{(0)}$: we have to take the rotated $\mathbf{n}'$ and use the compact notation $\mathbf{n}^{(\nu-1)}$ introduced for the asymmetric construction. There is however a different order in this set of indices; the 0-th component of $\mathbf{n}'$ is now n_1, then it is this that we have to set to $n_1 = L$. In general it is easier to write $\mathbf{n}'^{(\nu-1)}$, to make it compatible with our previous notation: this denotes $\mathbf{n}'^{(\nu-1)} = (L, \ldots, L, n'_\nu, \ldots, n'_{d'})$. When doing the cyclic sum, however, we have to read everything in the original frame $\mu \in \mathcal{U}$.

With these prescriptions, at the end of the computation we will have

$$A_0 = \frac{\Delta_0\tilde{\phi} + \bar{F}_{02}(\mathbf{n}) + \bar{F}_{02}(\mathbf{n}'^{(0)}) + \bar{F}_{01}(\mathbf{n})}{3}, \tag{2.40}$$

$$A_1 = \frac{\Delta_1\tilde{\phi} + \bar{F}_{10}(\mathbf{n}) + \bar{F}_{10}(\mathbf{n}''^{(0)}) + \bar{F}_{12}(\mathbf{n})}{3}, \tag{2.41}$$

$$A_2 = \frac{\Delta_2\tilde{\phi} + \bar{F}_{20}(\mathbf{n}) + \bar{F}_{21}(\mathbf{n}^{(0)}) + \bar{F}_{21}(\mathbf{n})}{3}, \tag{2.42}$$

and this correctly reproduces the components of $F_{\mu\nu}$.

Despite the more symmetric form of the gauge fields rewritings, here the disadvantage with respect to the asymmetric construction is that the $\{\bar{F}_{\mu\nu}\}_{\mu\neq\nu}$ are not all independent: they satisfy the so-called *Mandelstam constraints*, which will be examinated in the next Sections.

The Mandelstam constraints

Our reformulation corresponds to change variables from gauge fields to specific elementary lattice Wilson loops, i.e. $\bar{F}_{\mu\nu}(\mathbf{n}^{(\nu-1)})$. In the case of $\mu > \nu$, they are independent, as we showed in the previous Sections. If however we pass to the symmetric construction, they must satisfy the so-called Mandelstam constraints, as introduced in Chapter 1, Section 1.3.3.

In our case, where we have elementary loops corresponding to $\bar{F}_{\mu\nu}$ with $\mu \neq \nu$ in the most general case, we have to look at the case of *crossing Wilson loops*, as showed for example in Fig. 2.5(a) for two generic space-time directions μ, ν. In the continuum, the Mandelstam constraints for an Abelian gauge group read

$$W(C_1)W(C_2) - W(C_1 \circ C_2) = 0, \tag{2.43}$$

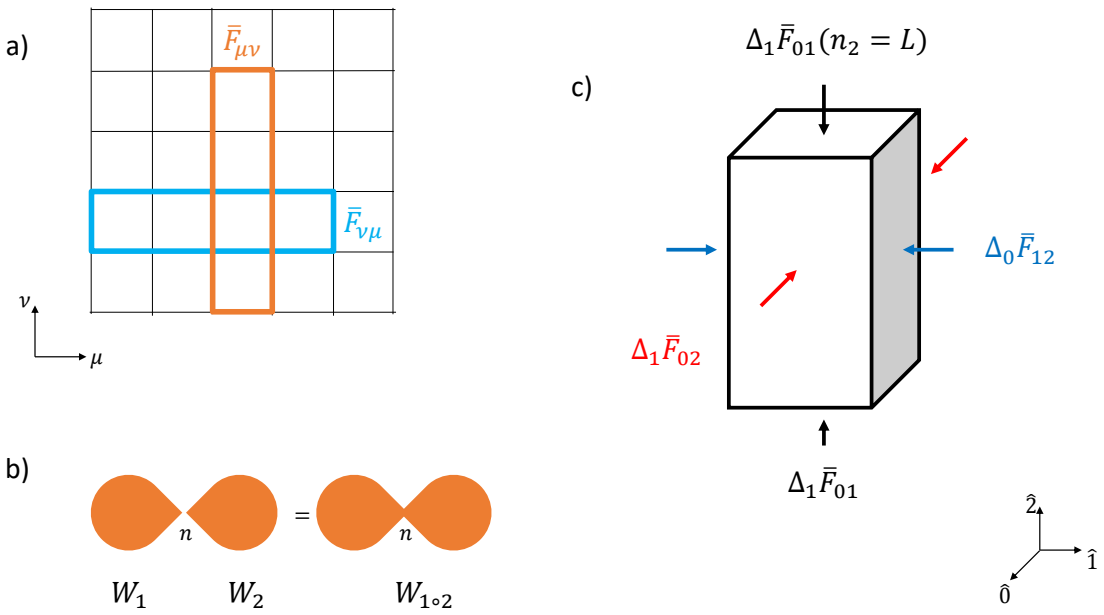

Figure 2.5: (a) Graphical representation of crossing loops (blue and orange) along the (μ, ν) space-time directions. (b) Graphical representation of the Abelian Mandelstam constraints for the loops W_1, W_2 and the composite loop $W_{1\circ 2}$, in the continuum. (c) Representation of the tubes that are obtained moving out from the planar Mandelstam constraints in the case $d = 2$. The colored arrows are associated to the corresponding differences of plaquette strips along the different space-time directions.

where C_1 and C_2 are two paths joining at $x = \mathbf{n}$, and $C_1 \circ C_2$ is their composition. Such a constraint, in the continuum, is pictorially showed in Fig. 2.5(b). For our variables on the lattice, the identification should be

$$W(C_1) = \bar{F}_{\nu\mu}(\mathbf{n_2}^{(\mu-1)}), \qquad W(C_2) = \bar{F}_{\mu\nu}(\mathbf{n_1}^{(\nu-1)}), \tag{2.44}$$

for the horizontal and vertical strips in Fig. 2.5(a), with $\mathbf{n}_{\{1,2\}}^{(\{\nu,\mu\}-1)}$ the corresponding boundary sites. By imposing the Mandelstam constraints on these planes, and calling $\mathbf{n}_{int}$ the site at which the two strips touch, they result in

$$\bar{F}_{\mu\nu}[(\mathbf{n}_{int} + \hat{\nu})^{(\nu-1)}] + \bar{F}_{\nu\mu}[(\mathbf{n}_{int} + \hat{\mu})^{(\mu-1)}] - \bar{F}_{\mu\nu}[(\mathbf{n}_{int})^{(\nu-1)}] - \bar{F}_{\nu\mu}[(\mathbf{n}_{int})^{(\mu-1)}] = 0. \tag{2.45}$$

This enforces the Mandelstam constraints for crossing loops on a given plane.

However, the plaquette strips can intersect also when we move out from the above planar situation. This case is depicted in Fig. 2.5(c): graphically this situation reminds the lattice Bianchi identity, where if we sum all the plaquettes forming a cube on the lattice we must get zero. Here, the situation is the same, but our variables are the strips: instead of getting a sum over cubes, we

get sums over rectangular parallelepipeds. We make again reference to the $d = 2$ case, since it is the only non-trivial visual example, and refer to Fig. 2.5 (c).

To derive the relative constraint analytically, we start from the expression of the Maxwell tensor written in terms of the plaquette strips. In the case of Fig. 2.5(c), we consider

$$F_{01}(\mathbf{n}) = \frac{1}{3}[\Delta_0 \bar{F}_{10}(\mathbf{n}) + \Delta_0 \bar{F}_{10}(\mathbf{n}''^{(0)}) + \Delta_0 \bar{F}_{12}(\mathbf{n}) - \Delta_1 \bar{F}_{02}(\mathbf{n}) - \Delta_1 \bar{F}_{01}(\mathbf{n})] \tag{2.46}$$

and use the fact that $F_{01} = \Delta_1 \bar{F}_{01}$, from the definition in Eq. (2.28). By inserting this in the previous equation, we end up in the constraint

$$\Delta_1 \bar{F}_{10}(\mathbf{n}) + \Delta_0 \bar{F}_{10}(\mathbf{n}''^{(0)}) + \Delta_0 \bar{F}_{12}(\mathbf{n}) - \Delta_1 \bar{F}_{02}(\mathbf{n}) = 0, \tag{2.47}$$

i.e. exactly the tube represented in Fig. 2.5(c). For the other components of the Maxwell tensor the logic is the same, and the final result is similar to Eq. (2.47).

In generic dimensions, the explicit form of the non-planar Mandelstam constraints is in principle difficult to write, because of the symmetric definition of the gauge field in Eq. (2.36). What is important, however, is that the sets of planar and non-planar Mandelstam constraints give the right number of degrees of freedom to match the asymmetric construction.

2.4.3 Continuum limit

So far we developed the formalism on the lattice. It is straightforward to take the continuum limit of Eq. (2.29). We recover the lattice spacing a and take the limit $a \to 0$ and $N \to \infty$ while keeping $Na \equiv L$ fixed. We obtain

$$\bar{F}_{\mu\nu}(\mathbf{x}^{(\nu-1)}) = \int_{x_\nu}^{L} dy_\nu \; F_{\mu\nu}(\mathbf{y}_\nu) \tag{2.48}$$

as the continuum counterpart of the plaquette strip, while the gauge field is written as

$$A_\mu(\mathbf{x}) = \partial_\mu \phi(\mathbf{x}) + \sum_{\nu<\mu} \bar{F}_{\mu\nu}(\mathbf{x}^{(\nu-1)}). \tag{2.49}$$

In the previous expressions we have introduced

$$\mathbf{x}^{(\nu)} \equiv (\underbrace{L, \ldots, L}_{\nu+1-\text{times}}, x_{\nu+1}, \ldots, x_d), \tag{2.50}$$

$$\mathbf{y}_\nu \equiv (\underbrace{L, \ldots, L}_{\nu-\text{times}}, y_\nu, x_{\nu+1}, \ldots, x_d), \tag{2.51}$$

as a shorthand notation for the real space vectors, being $\nu \in \{0, \ldots, d\}$. We remark that this completely characterizes the case of open but not of periodic boundaries, since the lattice description

of the latter relied on the special mapping of a single link, which does not generalize straightforwardly in the continuum limit at finite size L. We do not see conceptual problems in doing it, and we leave the explicit implementation of PBC at finite L in the continuum limit as a subject for a future work.

2.5 Pure abelian gauge theories on the lattice

Before discussing systems with matter fields present, we provide a more concrete example. We consider the standard action for non-compact gauge fields, in imaginary time and in $(d+1)$ dimensions

$$S = \frac{\beta}{2} \sum_{\mathbf{n}} F_{\mu\nu}(\mathbf{n})^2 \tag{2.52}$$

where the sum is taken over the N^{d+1} lattice points. The present discussion holds for any action depending solely on $F_{\mu\nu}$. The main premise of the present Chapter is to rewrite the model purely in terms of gauge invariant quantities. This is already done in Eq. (2.52) where the action only depends on $F_{\mu\nu}(\mathbf{n})$: however, *they are not all independent*. They satisfy the Bianchi identity in the continuum, and, on the lattice, a discretized version that in this case can be written as

$$F_{\mu\nu}(\mathbf{n}+\hat{\alpha}) - F_{\mu\nu}(\mathbf{n}) + F_{\alpha\mu}(\mathbf{n}+\hat{\nu}) - F_{\alpha\mu}(\mathbf{n}) + F_{\nu\alpha}(\mathbf{n}+\hat{\mu}) - F_{\nu\alpha}(\mathbf{n}) = 0. \tag{2.53}$$

This identity is trivially satisfied when the $F_{\mu\nu}$ are written in terms of the A_α. In other words, while $F_{\mu\nu}$ are gauge invariant but not all independent, A_α are gauge covariant but independent. With our construction we are able to achieve both gauge invariance and independence on the new variables. In fact, since the description of the theory in terms of A_α satisfies the Bianchi identity and Eq. (2.29) is a rewriting of them in terms of independent quantities, the Bianchi identity will be automatically satisfied for this case.

In order to make the discussion more specific, let us focus on the non-trivial case of the $(2+1)-d$ gauge theory. Following Eq. (2.29) we write

$$A_0(\mathbf{n}) = \phi(\mathbf{n}+\hat{0}) - \phi(\mathbf{n}), \qquad A_1(\mathbf{n}) = \bar{F}_{10}(\mathbf{n}) + \phi(\mathbf{n}+\hat{1}) - \phi(\mathbf{n}), \tag{2.54}$$

$$A_2(\mathbf{n}) = \bar{F}_{20}(\mathbf{n}) + \bar{F}_{21}(\mathbf{n^{(0)}}) + \phi(\mathbf{n}+\hat{2}) - \phi(\mathbf{n}). \tag{2.55}$$

In these formulas $\bar{F}_{10}$ and $\bar{F}_{20}$ are defined in all lattice points. At variance, $\bar{F}_{21}$ is only defined for boundary points where $n_0 = N$. The plaquettes $F_{\mu\nu}(\mathbf{n})$ in terms of these fields are given by

$$F_{10}(\mathbf{n}) = \bar{F}_{10}(\mathbf{n}) - \bar{F}_{10}(\mathbf{n}+\hat{0}), \qquad F_{20}(\mathbf{n}) = \bar{F}_{20}(\mathbf{n}) - \bar{F}_{20}(\mathbf{n}+\hat{0}) \tag{2.56}$$

$$F_{21}(\mathbf{n}) = \bar{F}_{10}(\mathbf{n}+\hat{2}) - \bar{F}_{10}(\mathbf{n}) + \bar{F}_{20}(\mathbf{n}) - \bar{F}_{20}(\mathbf{n}+\hat{1}) + \bar{F}_{21}(\mathbf{n^{(0)}}) - \bar{F}_{21}(\mathbf{n^{(0)}}+\hat{1}). \tag{2.57}$$

where we define any $\bar{F}_{10}$ to be zero outside of any point on the lattice.

As a further check, one can see that the Bianchi identity is trivially satisfied once the $F_{\mu\nu}$ are written in this way. To emphasize the differences with the new description of the theory, let us denote $a_{\mathbf{n}} \equiv \bar{F}_{10}(\mathbf{n})$, $c_{\mathbf{n}} \equiv \bar{F}_{20}(\mathbf{n})$ and $b_{\mathbf{n}^{(0)}} \equiv \bar{F}_{21}(\mathbf{n}^{(\mathbf{0})})$ as a boundary field. We have, for a general lattice point, $\mathbf{n} = (n_0, n_1, n_2)$ and $(n_0, n_1, n_2)^{(0)} = (N, n_1, n_2)$. The action takes the form

$$\begin{aligned} S =& \beta \sum_{\mathbf{n}} \left[\left(a_{\mathbf{n}+\hat{0}} - a_{\mathbf{n}}\right)^2 + \left(c_{\mathbf{n}+\hat{0}} - c_{\mathbf{n}}\right)^2 + \left(a_{\mathbf{n}+\hat{2}} - a_{\mathbf{n}}\right)^2 + \left(c_{\mathbf{n}+\hat{1}} - c_{\mathbf{n}}\right)^2 \right] \\ &+ \beta N \sum_{\mathbf{n}, n_0 = N} \left[\left(b_{\mathbf{n}+\hat{1}} - b_{\mathbf{n}}\right)^2 \right] + 2\beta \sum_{\mathbf{n}} \left[\left(b_{\mathbf{n}^{(0)}+\hat{1}} - b_{\mathbf{n}^{(0)}}\right) \left(a_{\mathbf{n}+\hat{2}} - a_{\mathbf{n}} - c_{\mathbf{n}+\hat{1}} + c_{\mathbf{n}}\right) \right]. \end{aligned} \tag{2.58}$$

This is a non-isotropic, non-local model. The first two terms are purely local. The second term is a boundary term that, nonetheless, is not predicted to be negligible in the infinite volume limit since it has a prefactor N. The last term is non-local and couples fields in the bulk to the boundary fields (at the boundary $n_0 = N$). The resulting non-locality can be regarded as the integration of the gauge covariant part of the gauge fields. Other examples of the integration of gauge fields lead naturally to non-local interactions [85–87]. In contrast to the cited results, here the full gauge degrees of freedom are not totally integrated out but only their non-physical part.

Despite the apparent complication of this model, it is described by fewer degrees of freedom, all of them physical. As an example, for the case of OBC where we counted the degrees of freedom, all the $N^3 - 1$ vertex variables ϕ have decoupled from the system.

2.6 Quantum electrodynamics

In this Section we rewrite the Lagrangian of QED in terms of gauge invariant quantities, using the asymmetric construction in $(3+1)$ dimensions. We refer to the next Section, where we discuss the Hofstadter model, for a discussion of the effects produced by the choice of the asymmetric *vs* symmetric construction. In that example, the differences are particularly clear. Before dealing with QED case, we investigate the simple and instructive case of the Hamiltonian of a particle in the presence of an external magnetic field, in $d = 3$.

2.6.1 Single particle in a magnetic field

We consider a quantum particle in a static background magnetic field. As it is usually done in quantum mechanics textbooks, the particle is charged (with charge $-e$) and we denote the size of the system by L, taking then the thermodynamic limit $L \to \infty$. The Hamiltonian reads

$$\mathcal{H} = \frac{(\mathbf{p} + e\mathbf{A})^2}{2m}, \tag{2.59}$$

where $\mathbf{p} = -i\nabla$ and we make use of natural units $\hbar = c = 1$. The only non-trivial component of the field strength tensor is $F_{21} = B$, therefore we only have the strip $\bar{F}_{21}$ in the asymmetric construction. This results in

$$A_i = \partial_i \phi, \quad i \neq 2, \tag{2.60}$$

$$A_2 = \partial_2 \phi + \bar{F}_{21} = \partial_2 \phi + B(L - x) \tag{2.61}$$

where $i = 1, 2, 3$. The crucial point consists in transforming the wavefunction, $|\psi\rangle$, and observables in such a way that we deal only with gauge invariant quantities, independent of ϕ. This is achived by the unitary transformation $|\psi'\rangle = \exp(-ie\phi)|\psi\rangle \equiv S|\psi\rangle$ and $\mathcal{H}' = S\mathcal{H}S^{-1}$. A closer look into the new momenta

$$p_i' = Sp_iS^{-1} = p_i + e\partial_i\phi \tag{2.62}$$

confirms that the vertex variables are reabsorbed . It is easy to verify that both $|\psi'\rangle$ and p_i' are gauge invariant. We conclude that

$$\mathcal{H}' = \frac{1}{2m}\sum_{i=1}^{3}\left(p_i' + \sum_{j<i}\bar{F}_{ij}\right)^2. \tag{2.63}$$

is the correct rewriting for the Hamiltonian. Since the transformation S is unitary, the spectra of $\mathcal{H}'$ and $\mathcal{H}$ coincide, reproducing the well-known Landau levels as expected [88].

2.6.2 The QED Lagrangian

Let us now consider the QED Lagrangian of Eq. (1.12), defined in a cubic volume with OBC, for simplicity. It can be transformed into

$$\mathcal{L} = \bar{\psi}\left[i\partial\!\!\!/ - m - e(\partial_\mu\phi)\gamma^\mu - e\sum_{\nu<\mu}\bar{F}_{\mu\nu}\gamma^\mu\right]\psi - \frac{1}{4}\left[\sum_{\alpha<\nu}\partial_\mu\bar{F}_{\nu\alpha} - \sum_{\alpha<\mu}\partial_\nu\bar{F}_{\mu\alpha}\right]\left[\sum_{\alpha<\nu}\partial^\mu\bar{F}^{\nu\alpha} - \sum_{\alpha<\mu}\partial^\nu\bar{F}^{\mu\alpha}\right]. \tag{2.64}$$

using the continuum rewriting of the gauge field of Eq. (2.49). Due to the presence of matter, this is not yet written in terms of gauge invariant fields alone. Consequently, we define

$$\psi' = \exp(ie\phi)\,\psi. \tag{2.65}$$

The equation above is the most important result of this Section, since it provides an expression of the GIF expressed in the form of the field operator ψ of the initial fermionic operator, which is not gauge invariant, multiplied by an operator depending on the gauge degrees of freedom. Overall, ψ' is gauge invariant. The term with the vertex variables is canceled from the Lagrangian, which finally reads

$$\mathcal{L} = \bar{\psi}'\left[i\partial\!\!\!/ - m - e\sum_{\nu<\mu}\bar{F}_{\mu\nu}\gamma^\mu\right]\psi' - \frac{1}{4}\left[\sum_{\alpha<\nu}\partial_\mu\bar{F}_{\nu\alpha} - \sum_{\alpha<\mu}\partial_\nu\bar{F}_{\mu\alpha}\right]\left[\sum_{\alpha<\nu}\partial^\mu\bar{F}^{\nu\alpha} - \sum_{\alpha<\mu}\partial^\nu\bar{F}^{\mu\alpha}\right]. \tag{2.66}$$

This completes the rewriting of the QED Lagrangian in terms of $\bar{F}_{\mu\nu}$ and the new fields ψ', $\bar{\psi}'$, which are combinations of the vertex variables and the original fermionic fields. When written explicitly we find a non-local structure of the Lagrangian both in the gauge kinetic part as well as in the coupling to the matter fields. In principle, it is possible to derive a Hamiltonian through canonical quantization. In practice, due to the non-locality of the kinetic term, this may be highly non-trivial[1].

2.7 Hofstadter model

We present now the reformulation of the Hofstadter model in $d = 2$ and $d = 3$, in terms of the new variables. We perform it by using the asymmetric and symmetric constructions, in order to discuss their differences and to show how they reproduce the correct results for the energy spectrum.

For a complete discussion of the importance and analytical properties of the Hofstadter model we refer to Section 5.3.3. Here we remind its Hamiltonian, assuming the Peierls substitution to take into account the effects of the external field [89]

$$\mathcal{H} = -t \sum_{\mathbf{r},\hat{j}} c^{\dagger}_{\mathbf{r}+\hat{j}} e^{i\theta_{\mathbf{r}+\hat{j},\mathbf{r}}} c_{\mathbf{r}} + \text{h.c.}, \tag{2.67}$$

where $\hat{j}$ are unit vectors along the spatial directions of the lattice ($\hat{j} = \hat{x},\ \hat{y}$ in $d = 2$ and $\hat{j} = \hat{x},\ \hat{y},\ \hat{z}$ in $d = 3$) , $c^{\dagger}_{\mathbf{r}},\ c_{\mathbf{r}}$ are the fermionic creation and annihilation operators and $\theta_{\mathbf{r}+\hat{j},\mathbf{r}}$ is the Peierls phase. The vector potential $\mathbf{A}(\mathbf{x})$ is associated with the external field. In order to have an isotropic magnetic flux on each plaquette of the lattice, we consider a magnetic field whose magnitude is

$$\Phi = \frac{2\pi m}{n} \tag{2.68}$$

where $m,\ n$ are coprime integer numbers. Its direction will be specified below. In the following, we consider cubic lattices with $V = N^d$ sites, d being the dimension, and sizes $N = \kappa n$, with $\kappa \in \mathbb{N}$.

In the next two Subsections we consider the $2d$ and $3d$ models, in both cases assuming PBC. Our aim is to explicitly show how the formal constructions presented in Sections 2.2.2, 2.3 and 2.4.1 work and reproduce the known results.

[1]More precisely, writing explicitly the terms involving the strips in Eq. (2.66) we get that the only non-trivial conjugate momenta are associated to $\bar{F}_{i0},\ i = 1, 2, 3$, the electric field components. The right way to proceed should be to introduce a set of Lagrange multipliers, associated to the vanishing conjugate momenta of the theory, i.e. $\bar{F}_{21,31,32}$. Once done that, it should be quantized as a constrained theory.

2.7.1 The $2d$ model

We consider a square lattice with $V = N^2$ sites and a perpendicular commensurate magnetic field $\mathbf{B} = \Phi(0, 0, 1)$. We change notation with respect to Sec. 2.2, denoting a generic lattice site by $\mathbf{r} = (r_1, r_2)$, in order to avoid confusion with the integer n appearing in Eq. (2.68).

Asymmetric construction

The only non-trivial component of the field strength tensor is F_{21}. We use then Eqs. (2.28) and (2.29) to rewrite the gauge field. The only non-zero plaquette strip is $\bar{F}_{21} = \Phi(N - r_1)$, with $r_1 < N$. We have still to specify the gauge invariant loops $\bar{f}_i$: they can be determined by imposing that the flux on the plaquettes of the boundary sites $\mathbf{r}_{B,1} = (N, r_2)$, $\mathbf{r}_{B,2} = (r_1, N)$ is equal to Φ, so we have a uniform magnetic field through the whole lattice. Using the definitions in Eq. (2.11) we get

$$\bar{f}_1(r_2) = \Phi N r_2 + \vartheta_1, \qquad \bar{f}_2(r_1) = -\Phi N r_1 + \vartheta_2. \tag{2.69}$$

The constants ϑ_1, ϑ_2 account for twists of the fermionic operators at the boundaries. They are gauge invariant physical quantities that should be specified along with the magnetic field. In order to compare our construction with the known results in the literature for PBC, we choose these parameter to be $\vartheta_1 = \vartheta_2 = 0$, and for further discussion on these parameters we refer to [90]. The Hamiltonian (2.67) is rewritten as

$$\mathcal{H} = -t \sum_{\mathbf{r} \neq \mathbf{r}_{B,i}} (c^\dagger_{\mathbf{r}+\hat{1}} e^{i[\phi(\mathbf{r}+\hat{1}) - \phi(\mathbf{r})]} c_{\mathbf{r}} + c^\dagger_{\mathbf{r}+\hat{2}} e^{i[\phi(\mathbf{r}+\hat{2}) - \phi(\mathbf{r}) + \bar{F}_{21}]} c_{\mathbf{r}} + \text{h.c.}) + \mathcal{H}_B,$$

where the boundary terms are

$$\mathcal{H}_B = -t(c^\dagger_{\mathbf{r}_{B,1}+\hat{1}} e^{i(f_1(r_2) - \phi(N,r_2) + \phi(1,r_2))} c_{\mathbf{r}_{B,1}} + c^\dagger_{\mathbf{r}_{B,2}+\hat{2}} e^{i(f_2(r_1) - \phi(r_1,N) + \phi(r_1,1) - (N-1)\bar{F}_{21}(r_1))} c_{\mathbf{r}_{B,2}} + \text{h.c.}). \tag{2.70}$$

The fermionic operators at the boundaries transform as

$$c^\dagger_{\mathbf{r}_{B,1}+\hat{1}} = e^{-i\varphi_1(1,r_2)} c^\dagger_{(1,r_2)}, \qquad c^\dagger_{\mathbf{r}_{B,2}+\hat{2}} = e^{-i\varphi_2(r_1,1)} c^\dagger_{(r_1,1)}, \tag{2.71}$$

which allow us to suitably identify gauge invariant loops $\bar{f}_i$ in the hopping phases of $\mathcal{H}_B$ and replace them with their values (2.69). Analogously to the QED case, we define new fermionic gauge invariant operators

$$d_{\mathbf{r}} \equiv e^{-i\phi(\mathbf{r})} c_{\mathbf{r}}, \qquad d^\dagger_{\mathbf{r}} \equiv c^\dagger_{\mathbf{r}} e^{i\phi(\mathbf{r})}. \tag{2.72}$$

The operator $d_{\mathbf{r}}$ is the equivalent of the GIF ψ' introduced for QED in Eq. (2.65). The gauge invariance of the operator $d_{\mathbf{r}}$, as well as its fermionic nature, is explicit. A gauge transformation of function $\Lambda(\mathbf{r})$ modifies the vertex variables through the shift $\phi(\mathbf{r}) \sim \phi(\mathbf{r}) + \Lambda(\mathbf{r})$, exactly canceled by the phases of the gauge transformed operators $c_{\mathbf{r}}$, $c^\dagger_{\mathbf{r}}$, see Eq. (1.10).

It is now immediate to check that the boundary terms in $\mathcal{H}_B$ have the same structure of the bulk terms. This is due to the definitions of Φ, N (since ΦN is an integer multiple of 2π) and the chosen values of $\vartheta_1 = \vartheta_2 = 0$. Indeed we have

$$e^{i\bar{f}_1(r_2)} = e^{i\Phi N r_2} = 1, \qquad e^{i\bar{f}_2(r_1)} = e^{i(\Phi(N-N^2)-\Phi r_1)} = e^{-i\Phi r_1} \tag{2.73}$$

As a consequence, the Hamiltonian in terms of the new gauge invariant variables is

$$\mathcal{H} = -t \sum_{\mathbf{r}} (d^\dagger_{\mathbf{r}+\hat{2}} e^{-i\Phi r_1} d_{\mathbf{r}} + d^\dagger_{\mathbf{r}+\hat{1}} d_{\mathbf{r}} + \text{h.c.}). \tag{2.74}$$

We remark that the above description of the physical system, which does not reference gauge covariant operators, was achieved without ever fixing a gauge.

We now move to the momentum space, introducing the Fourier transformed operators

$$d_{\mathbf{r}} = \frac{1}{\sqrt{V}} \sum_{\mathbf{k}} d_{\mathbf{k}} e^{i\mathbf{k}\cdot\mathbf{r}}, \quad d^\dagger_{\mathbf{r}} = \frac{1}{\sqrt{V}} \sum_{\mathbf{k}} d^\dagger_{\mathbf{k}} e^{-i\mathbf{k}\cdot\mathbf{r}}. \tag{2.75}$$

The full Hamiltonian then becomes

$$\mathcal{H} = -t \sum_{\mathbf{k}} (2\cos k_1 d^\dagger_{\mathbf{k}} d_{\mathbf{k}} + e^{-ik_2} d^\dagger_{\mathbf{k}+\Phi\hat{1}} d_{\mathbf{k}} + \text{h.c.}) \tag{2.76}$$

where the momenta are chosen in the first Brillouin zone (1BZ), i.e. the square $[-\pi, \pi) \times [-\pi, \pi)$.

The interplay between gauge and translational invariance in presence of a commensurate background magnetic field allows us to introduce the concept of magnetic Brillouin zone [91]. In this case, it is given by

$$\text{MBZ}: \quad k_1 \in \left[-\frac{\pi}{n}, \frac{\pi}{n} \right), \; k_2 \in \Big[-\pi, \pi \Big). \tag{2.77}$$

This enables us to split the structure of the Hamiltonian in terms of the so-called magnetic bands, labeled by an index $\tau \in \{0, 1, \ldots, n-1\}$:

$$\mathcal{H} = -t \sum_{\mathbf{k}\in\text{MBZ}} \sum_{\tau} [2\cos(k_1 + \tau\Phi) d^\dagger_{\mathbf{k}+\tau\Phi\hat{1}} d_{\mathbf{k}+\tau\Phi\hat{1}} + e^{-ik_2} d^\dagger_{\mathbf{k}+(\tau+1)\Phi\hat{1}} d_{\mathbf{k}+\tau\Phi\hat{1}} + \text{h.c.}]. \tag{2.78}$$

In matrix form, it can be written compactly as

$$\mathcal{H} = -t \sum_{\mathbf{k}\in\text{MBZ}} (d^\dagger_{\mathbf{k}}, \ldots, d^\dagger_{\mathbf{k}+(n-1)\Phi\hat{1}}) \, \mathcal{G}_n \begin{pmatrix} d_{\mathbf{k}} \\ \vdots \\ d_{\mathbf{k}+(n-1)\Phi\hat{1}} \end{pmatrix}, \tag{2.79}$$

where

$$\mathcal{G}_n = \begin{pmatrix} 2\cos(k_1) & e^{-ik_2} & 0 & \ldots & e^{ik_2} \\ e^{ik_2} & 2\cos(k_1+\Phi) & e^{-ik_2} & 0 & \ldots \\ 0 & e^{ik_2} & \ddots & \ddots & \ddots \\ \vdots & 0 & \ddots & \ddots & e^{-ik_2} \\ e^{-ik_2} & \vdots & \ddots & e^{ik_2} & 2\cos(k_1+(n-1)\Phi) \end{pmatrix}. \tag{2.80}$$

This matrix depends on the flux, it has size $n \times n$, and its eigenvalues, for each value of $\mathbf{k}$, provide the energy spectrum of the model. It is immediate to check that the result coincides with the one obtained using directly a gauge, such as the Landau gauge. A simple check can be done in the so-called $\pi-$flux case, where $(m, n) = (1, 2)$. Here the matrix is

$$\frac{\mathcal{G}_2}{2} = \begin{pmatrix} \cos k_1 & -\cos k_2 \\ -\cos k_2 & -\cos k_1 \end{pmatrix} \tag{2.81}$$

and the associated spectrum

$$E_{\mathbf{k}} = \pm 2t\sqrt{\cos^2 k_1 + \cos^2 k_2}, \tag{2.82}$$

recovering the known $2d$ analytical result [92, 93]. For general values of the magnetic fields, i.e. for generic n and m, we checked that the spectrum of $\mathcal{G}_n$ is the correct one, e.g. by comparison with the exact diagonalization of Eq. (2.67).

Symmetric construction

We present here the rewriting of Eq. (2.67) using the symmetric construction of Sec. 2.3. The symmetry considerations leading to the definition of the MBZ still hold, the only difference is that now the size of the lattice has to be $N = 2\kappa n$, with $\kappa \in \mathbb{N}$. The gauge field for the sites $\mathbf{r} \neq \mathbf{r}_{B,i}$ is now rewritten using Eqs. (2.21) and (2.22) , with

$$\bar{F}_{12} = -\Phi(N - r_2), \qquad \bar{F}_{21} = \Phi(N - r_1), \qquad r_i < N. \tag{2.83}$$

For the links at the boundary sites $\mathbf{r}_{B,i}$ we use the Eqs. (2.24), (2.25) with the gauge invariant loops $\bar{f}_i$ of Eq. (2.69). As in the asymmetric case, the boundary terms have the same functional form of the bulk ones, because of the assumption on the size N. Going into momentum space, the MBZ is

$$\text{MBZ}: \quad \left[-\frac{\pi}{2n}, \frac{\pi}{2n}\right) \times \left[-\frac{\pi}{2n}, \frac{\pi}{2n}\right). \tag{2.84}$$

Introducing the gauge invariant operators $d^\dagger_{\mathbf{r}}$, $d_{\mathbf{r}}$ as in Eq. (2.72) and the reduced magnetic field $\tilde{\Phi} \equiv \Phi/2$, the Hamiltonian can be rewritten as

$$\mathcal{H} = -t \sum_{\mathbf{k}\in \text{MBZ}} \sum_{\lambda,\tau} [e^{-i(k_1+\tau\tilde{\Phi})} d^\dagger_{\mathbf{k}+\tau\tilde{\Phi}\hat{1}+(\lambda+1)\tilde{\Phi}\hat{2}} d_{\mathbf{k}+\tau\tilde{\Phi}\hat{1}+\lambda\tilde{\Phi}\hat{2}} + e^{-i(k_2+\lambda\tilde{\Phi})} d^\dagger_{\mathbf{k}+\tau\tilde{\Phi}\hat{1}+\lambda\tilde{\Phi}\hat{2}} d_{\mathbf{k}+(\tau+1)\tilde{\Phi}\hat{1}+\lambda\tilde{\Phi}\hat{2}} + \text{h.c.}]. \tag{2.85}$$

using the two magnetic band indices $\tau, \lambda = \{0, \ldots, 2n-1\}$. The associated matrix turns out to be of size $(2n)^2 \times (2n)^2$, which has to be compared with the $\mathcal{G}_n$, of size $n \times n$, obtained with the asymmetric construction. Besides the energy spectrum being the same, the main difference is in the definition of the MBZ, as we are going to discuss at the end of the Section.

2.7.2 The $3d$ model

The analysis done in $2d$ can be extended to the $3d$ model. We consider a cubic lattice of size $V = N^3$, with an isotropic magnetic field $\mathbf{B} = \Phi(1,1,1)$. Different orientations of the magnetic field, such as $\mathbf{B} = \Phi(1,0,0)$, produce different results, but the method is the same and for convenience of exposition we limit ourselves to the isotropic case. In the following we will show how to retrieve the spectrum of the model within our formalism.

Asymmetric construction

The non-trivial components of the field strength tensor are $F_{21} = F_{32} = \Phi$ and $F_{31} = -\Phi$. We use Eq. (2.29) to express the vector potential $\mathbf{A}(\mathbf{x})$. The relevant strip variables are

$$\bar{F}_{21} = -\bar{F}_{31} = \Phi(N - r_1), \qquad \bar{F}_{32} = \Phi(N - r_2), \qquad r_i < N. \tag{2.86}$$

The functional form of the loops $\bar{f}_i$ can be determined by imposing the constraints on the proper flux per plaquette at the boundary sites, as for the $2d$ case. By using the definition in Eq. (2.31), we obtain the loops

$$\bar{f}_1(r_2, r_3) = \Phi N(r_2 - r_3) + \vartheta_1, \qquad \bar{f}_2(r_1, r_3) = N\Phi(r_3 - r_1) + \vartheta_2, \qquad \bar{f}_3(r_1, r_2) = N\Phi(r_1 - r_2) + \vartheta_3. \tag{2.87}$$

As before, we consider the case $\vartheta_1 = \vartheta_2 = \vartheta_3 = 0$. Introducing directly the operators in Eq. (2.72) and the MBZ

$$\text{MBZ}: \ \left[-\frac{\pi}{n}, \frac{\pi}{n}\right) \times \left[-\frac{\pi}{n}, \frac{\pi}{n}\right) \times \Big[-\pi, \pi\Big), \tag{2.88}$$

we split the structure of the Hamiltonian in magnetic bands, labeled by two indices $\lambda,\ \tau \in \{0, 1, \ldots, n-1\}$:

$$\mathcal{H} = -t \sum_{\mathbf{k}\in \text{MBZ}} \sum_{\lambda,\tau} \Big[2\cos(k_1 + \lambda\Phi) d^\dagger_{\mathbf{k}+\lambda\Phi\hat{1}+\tau\Phi\hat{2}} d_{\mathbf{k}+\lambda\Phi\hat{1}+\tau\Phi\hat{2}} + e^{-i(k_2+\tau\Phi)} d^\dagger_{\mathbf{k}+\lambda\Phi\hat{1}+\tau\Phi\hat{2}} d_{\mathbf{k}+(\lambda+1)\Phi\hat{1}+\tau\Phi\hat{2}} \tag{2.89}$$

$$+ e^{-ik_3} d^\dagger_{\mathbf{k}+\lambda\Phi\hat{1}+\tau\Phi\hat{2}} d_{\mathbf{k}+(\lambda-1)\Phi\hat{1}+(\tau+1)\Phi\hat{2}} + \text{h.c.} \Big].$$

The associated matrix has size $n^2 \times n^2$. We verified that the spectrum of this Hamiltonian coincides with the known one in literature [94]. A simple analytical check can be done in the $\pi-$flux case, where $(m, n) = (1, 2)$. Here the matrix is (factorizing an overall factor of 2)

$$\mathcal{G}_2 = \begin{pmatrix} \cos k_1 & 0 & \cos k_2 & \cos k_3 \\ 0 & \cos k_1 & \cos k_3 & -\cos k_2 \\ \cos k_2 & \cos k_3 & -\cos k_1 & 0 \\ \cos k_3 & -\cos k_2 & 0 & -\cos k_1 \end{pmatrix} = \cos k_1\ \sigma_z \otimes \mathbb{1}_2 + \cos k_2\ \sigma_x \otimes \sigma_z + \cos k_3\ \sigma_x \otimes \sigma_x \tag{2.90}$$

whose eigenvalues are

$$\lambda_{1,2}(\mathbf{k}) = \pm\sqrt{\cos^2 k_1 + \cos^2 k_2 + \cos^2 k_3}. \tag{2.91}$$

The full spectrum is related to them via

$$\frac{E(\mathbf{k})}{2t} = \lambda_{1,2}(\mathbf{k}), \tag{2.92}$$

reproducing exactly the dispersion relation in [94].

Symmetric construction

One can proceed as in the $2d$ case, the only computational difference being represented by the size of the lattice, which now has to be $N = 3\kappa n$, with $\kappa \in \mathbb{N}$. The gauge field components are

$$A_1 = \phi(\mathbf{r}+\hat{1}) - \phi(\mathbf{r}) + \frac{2\bar{F}_{13} + \bar{F}_{12}}{3}, \tag{2.93}$$

$$A_2 = \phi(\mathbf{r}+\hat{2}) - \phi(\mathbf{r}) + \frac{2\bar{F}_{21} + \bar{F}_{23}}{3}, \tag{2.94}$$

$$A_3 = \phi(\mathbf{r}+\hat{3}) - \phi(\mathbf{r}) + \frac{2\bar{F}_{32} + \bar{F}_{31}}{3}, \tag{2.95}$$

with the boundary links that can be immediately obtained through the proper symmetrization of Eq. (2.31). Going into momentum space, the resulting MBZ is

$$\text{MBZ}: \quad \left[-\frac{\pi}{3n}, \frac{\pi}{3n}\right) \times \left[-\frac{\pi}{3n}, \frac{\pi}{3n}\right) \times \left[-\frac{\pi}{3n}, \frac{\pi}{3n}\right). \tag{2.96}$$

Introducing the gauge invariant operators $d^\dagger_{\mathbf{r}}$, $d_{\mathbf{r}}$ as in Eq. (2.72) and the reduced magnetic field $\tilde{\Phi} \equiv \Phi/3$, the Hamiltonian can be rewritten as

$$\begin{aligned}\mathcal{H} = -t \sum_{\tau,\epsilon,\lambda} \sum_{\mathbf{k}\in\text{MBZ}} \Big[& d^\dagger_{\mathbf{k}+\tau\tilde{\Phi}\hat{1}+(\epsilon+1)\tilde{\Phi}\hat{2}+(\lambda-2)\tilde{\Phi}\hat{3}} d_{\mathbf{k}+\tau\tilde{\Phi}\hat{1}+\epsilon\tilde{\Phi}\hat{2}+\lambda\tilde{\Phi}\hat{3}} e^{-i(k_1+\tau\tilde{\Phi})} \\ & + d^\dagger_{\mathbf{k}+(\tau-2)\tilde{\Phi}\hat{1}+\epsilon\tilde{\Phi}\hat{2}+(\lambda+1)\tilde{\Phi}\hat{3}} d_{\mathbf{k}+\tau\tilde{\Phi}\hat{1}+\epsilon\tilde{\Phi}\hat{2}+\lambda\tilde{\Phi}\hat{3}} e^{-i(k_2+\epsilon\tilde{\Phi})} \\ & + d^\dagger_{\mathbf{k}+(\tau+1)\tilde{\Phi}\hat{1}+(\epsilon-2)\tilde{\Phi}\hat{2}+\lambda\tilde{\Phi}\hat{3}} d_{\mathbf{k}+\tau\tilde{\Phi}\hat{1}+\epsilon\tilde{\Phi}\hat{2}+\lambda\tilde{\Phi}\hat{3}} e^{-i(k_3+\lambda\tilde{\Phi})} + \text{h.c.}\Big],\end{aligned} \tag{2.97}$$

with the help of three magnetic band indices $\tau, \epsilon, \lambda = \{0, \ldots, 3n-1\}$. The size of the associated matrix is $(3n)^3 \times (3n)^3$, much larger than the one obtained with the asymmetric construction. Obviously, the spectra associated to the same pair (m, n) are found to coincide.

Comparison between constructions

We are now ready to compare the two constructions applied to the Hofstadter model. First, we remind that using the Hasegawa gauge [95] in $3d$ (or the Landau gauge [88] in $2d$) one has to diagonalize, for each $\mathbf{k}$ belonging to the MBZ, a matrix $n \times n$. If one uses a different gauge, the matrix to be diagonalized may be of larger size, and, at the same time, the MBZ also changes. What does not change is the energy spectrum.

Let us now discuss the results obtained using our formalism in which a choice of the gauge is not done. In $2d$, with the asymmetric construction we obtained a matrix in momentum space of size $n \times n$, where the MBZ is Eq. (2.77). With the symmetric construction we symmetrized the MBZ, as showed in Eq. (2.84), and the band structure of the Hamiltonian, but the price to pay is in the dimensionality of the matrix, of size $(2n)^2 \times (2n)^2$, larger than the asymmetric one. The same considerations hold for the $3d$ case, with different dimensions of the matrix, respectively $n^2 \times n^2$ and $(3n)^3 \times (3n)^3$, and the definitions of MBZ, given by Eqs. (2.88) and (2.96). One concludes that the MBZ depends, in our formalism, on the chosen construction. Furthermore the most symmetric MBZ, in which the x, y, z axis enter equally – as one would expect since the magnetic field is isotropic – is given by the symmetric construction[2]. Therefore, if the symmetry in momentum space has to be preserved, it is more convenient to use the symmetric construction. If, at variance, one wants to reduce the dimension of the matrix to be diagonalized, e.g. for numerical purposes, then the asymmetric construction is more suitable.

2.8 Gauge invariant mean-field theory

In the previous Sections, after having introduced the main ideas of the reformulation, we applied it to different cases: a single particle in a static magnetic field, the pure lattice gauge theory (without dynamical matter), the Hofstadter model (where the magnetic field is static) and QED (where there are both dynamical matter and gauge fields). The reformulation can be applied as well to other models, such as the Schwinger-Thirring model, where the matter is interacting with a term $\mathcal{L}_{int} \propto (\bar{\psi}\gamma^\mu\psi)^2$, the Gross-Neveau model or bosonic QED [96]. For example, in the case of the Thirring interaction, the Lagrangian would be

$$\mathcal{L}[\bar{F}_{\mu\nu}, \psi', \bar{\psi}'] = \mathcal{L}_{\text{QED}}[\bar{F}_{\mu\nu}, \psi', \bar{\psi}'] + g(\bar{\psi}'\gamma^\mu\psi')^2, \tag{2.98}$$

[2]We remark that from the textbook definition of MBZ one can see that its volume is unique for each dimensionality [91]. Focusing on the $2d$ case, this is because, denoting with $\hat{T}_{\hat{j}}$ the generators of the magnetic translational group, the minimal integer doublet (a, b) such that $[\hat{T}_{a\hat{0}}, \hat{T}_{b\hat{1}}] = 0$ defines the magnetic unit cell in real space. For the asymmetric construction we have $(a, b) = (2, 1)$, while in the symmetric one $(a, b) = (4, 4)$, therefore the minimal one is the first one.

where $\mathcal{L}_{\rm QED}[\bar{F}_{\mu\nu}, \psi', \bar{\psi}']$ is the reformulated Lagrangian in Eq. (2.66). Moreover, the reformulation could be applied to models in ladder geometries, which are nowadays subject of considerable attention [97–100].

The most interesting theories are the ones in which the matter is interacting in presence of a magnetic field, or, even more, lattice and continuum gauge theories where the gauge fields are dynamical. Here we discuss how the present formalism may be advantageous in both cases.

For fermions in a static magnetic field, interactions give rise to the so-called Hubbard-Hofstadter model, which is considerably more difficult to analyze. Our reformulation provides an alternative path, arguably more suitable as it preserves gauge invariance exactly, to study these models within certain approximation schemes, like mean-field. Indeed, the order parameters that one may introduce in the (non-magnetic) Hubbard model are clearly not gauge invariant. At variance, using the fermionic operators d, $d^\dagger$ one can construct gauge invariant order parameters, whose self-consistency has to be checked. In a similar way the correlation functions of the Hubbard model, when an approximation is used, are expected to be gauge dependent. However, if one determines, even in an approximate way, correlation functions of the $d\, d^\dagger$ operators, they will be gauge invariant.

The situation is even more relevant for standard gauge theories, which have dynamical gauge fields. The application of a naive mean-field approximation leads to a self-consistent equation for a non gauge-invariant quantity, which is in tension with Elitzur theorem [10, 23]. On the lattice, subsequent efforts were able to fix these drawbacks by introducing a generalized mean-field procedure, where several "mean-fields" for each gauge degree of freedom are introduced [49]. In general, this procedure appears rather cumbersome to be implemented and not easily extendable to the continuum. The present reformulation provides an alternative starting point for a mean-field approximation where a self-consistent equation for the targeted order parameter can be written in agreement with Elitzur theorem. The main challenges consist in identifying suitable order parameters in terms of $\bar{F}_{\mu\nu}$, ψ' and subsequently solving their related self-consistent equations (see Appendix A.1 for more details about Abelian LGTs).

2.9 Conclusions

In this Chapter we gave a reformulation of Abelian gauge theories in terms of gauge invariant fields (GIF). In particular, we discussed how to split the gauge field A_μ into its gauge invariant part, represented by $F_{\mu\nu}$, and its gauge covariant one, enclosed in the vertex variables ϕ. From the field stress tensor, we have introduced the plaquette strips $\bar{F}_{\mu\nu}$ in order to define a set of independent field variables $\{\bar{F}_{\mu\nu}, \phi\}$, whose determination is the main goal of our reformulation. For periodic boundary conditions, these variables are supplemented by loops $\bar{f}_\mu$ that wrap around the different

directions of space-time.

The construction was first developed on the lattice and in $(1+1)-d$, which provides the basic building block for the generalization to arbitrary dimensions and to the continuum limit. The choice of how to make these constructions is not unique and here we explored two of them, that we called asymmetric and symmetric constructions. All possible constructions are related by gauge transformations and, therefore, are physically equivalent. We stress, however, that a gauge is not fixed and we deal only with fields that are independent of any possible chosen gauge. The procedure is performed at finite volume and we have used open (OBC) and periodic (PBC) boundary conditions, which fit well within the formalism.

This kind of constructions arises naturally, as a change of variables, in the Lagrangian formalism. However, performing their canonical quantization is predicted to be an arduous task due to the presence of non-local kinetic terms. Despite that, we emphasize that the non-locality of the Lagrangian formalism does not break unitarity nor Lorentz invariance. Furthermore, we showed through two examples, i.e. charged particle in an external magnetic field and in the Hofstadter model, that the same kind of construction can be applied in the Hamiltonian formalism.

From the example provided by the Hofstadter model it becomes clear that different choices on the constructions have practical implications. The Hamiltonian diagonalization can be reduced to the diagonalization of matrices of finite size for every value of the momentum. The asymmetric construction leads to smaller matrices but an asymmetric magnetic Brillouin zone (MBZ). At variance, the symmetric constructions implies the diagonalization of larger matrices but produces a symmetric MBZ.

In the literature, there are similar efforts of describing gauge theories solely in terms of gauge invariant fields. The method presented in [54–57] recombines properly the matter and gauge fields in order to rewrite quantum electrodynamics (QED) in terms of gauge invariants, and quantize the theory in terms of them. Difficulties arise due to the presence of non-local quantities in the quantization procedure [55, 57]. In this aspect this is analogous to our rewriting, as the plaquette strips interact non-locally. Moreover, the authors underline that, within their approach, the fermions and the photons are no longer fundamental fields [55]. The new degrees of freedom are the currents of the theory, regarding the matter, and a couple of covector and complex scalar fields, regarding the gauge part. In our rewriting the new degrees of freedom are different: we combined the vertex variables with the matter fields to obtain degrees of freedom that remain fermionic but are also now gauge invariant. Some aspects of our reformulation are also shared with [64–66] where the plaquettes terms, on the lattice, are used to replace the links associated to the gauge field A_μ. The main difference lies, again, in the definition of the matter variables, in Eqs. (2.65) and (2.72) as just described. In our procedure, this leads to non-local interactions between gauge and matter fields. The removal of non-locality, of a similar form, was solved in [66], thanks to the introduction of new variables. A future interesting step would be to understand if it is possible to

introduce further variables, in a similar way, in order to make the matter-gauge interacting term of our theory local as well.

The reformulation presented here has been applied to gauge theories with an Abelian symmetry group. We expect that the generalization to non-Abelian gauge theories is possible by following the same lines presented here, and we do not anticipate specific problems related to the non-Abelian nature of the symmetry group. At variance, we think that the generalization to LGTs on non-bipartite lattices would not be straightforward. Moreover, in view of possible developments, we observe that this formalism could be useful to investigate phase diagrams of gauge theories within a mean-field framework, both in the continuum and on the lattice.

Finally, we would like to stress that both classical and quantum simulations of gauge theories may considerably profit from the reformulation presented here. Clearly, reducing the number of degrees of freedom is potentially interesting in both cases. For the case of quantum simulators there is no longer a local symmetry to be implemented, as it was used to decouple the non-physical fields. From the point of view of the reduction of the number of degrees of freedom, this formalism is on a similar footing with maximal gauge fixings [84]. The difference lies in the fact that our reformulation allows for the identification of a new matter field ψ', expressed in terms of the variables ϕ which are integrated out, and new fields $\bar{F}_{\mu\nu}$. Both ψ' and $\bar{F}_{\mu\nu}$ are gauge invariant and the reformulated theory is expressed in terms of them: $\mathcal{L} = \mathcal{L}(\psi', \bar{F}_{\mu\nu})$. In this, which is for all practical purposes a trading of difficulties, the final Lagrangian has non-local terms and the construction of the Hamiltonian could be a non-trivial step. Depending on the form of the final theory, this may provide the starting point of approximate methods, in which correlation functions and order parameters are gauge invariant by construction. Ultimately, it will be the success of performing sensible approximations of interacting lattice field theories that will show whether the reformulation presented here is useful.

Part II

Quantum simulators of lattice gauge theories

Chapter 3

Quantum simulators with ultracold atoms

In this second Part of the Thesis we focus directly on quantum simulations of Abelian gauge theories, employing the Hamiltonian formulation introduced in Section 1.2.2. Among the various platforms that have been developed during the last year, we make use of ultracold atoms loaded in optical lattice to simulate the gauge degrees of freedom. The following Chapter has then a dual purpose, i.e. to introduce the basic concepts about ultracold atoms loaded in optical lattice and to show how they can be employed as quantum simulators of lattice gauge theories. Its structure is divided into three blocks.

In the first and second parts, we discuss how to generate optical potentials to trap neutral atoms in periodic lattices, and present the Hamiltonians describing the resulting systems in the tight-binding approximation. After a general discussion, we focus in particular on the features of the extended Hubbard models, allowing for the description of trapped ultracold Bose gases with internal degrees of freedom.

In the third part, we show what is the state of the art regarding quantum simulators of gauge theories with ultracold atoms, discussing the general features of the proposals that are present in the scientific literature. We finally point out what are the open problems and challenges in higher dimensions.

3.1 Ultracold atoms in optical lattices

Ultracold dilute atomic gases are made of neutral atoms that can have bosonic or fermionic features, depending on their statistics, cooled down to temperatures of the order $T \simeq 10 - 100$ nK by means of techniques such as the laser or evaporative coolings [101]. The typical length scales and number of atoms are $L \simeq 10 - 100$ μm and $N = 10^2 - 10^6$ atoms, giving rise to densities $\rho \simeq 10^{13} - 10^{15}$ cm^{-3}.

The presence of interfering counter-propagating laser beams leads to the generation of spatially periodic optical potential, i.e. to the presence of an *optical lattice*. Ultracold atoms that experience this potential are confined into periodic spatial structures, resembling crystalline lattices, whose parameters and effective Hamiltonians can be controlled and tuned through the ultracold atomic parameters.

Historically, there has been a huge progress starting from the 1980s, both theoretically and experimentally, thanks to the development of optical control and imaging techniques for atoms and molecules. In particular, ultracold atoms in optical lattices acquired a huge importance during the last ten years in the realm of quantum many-body physics and quantum simulators, since they allow for the study of various physical phenomena with a lot of flexibility in the design, analysis and control of experimental set-ups and optical lattice parameters.

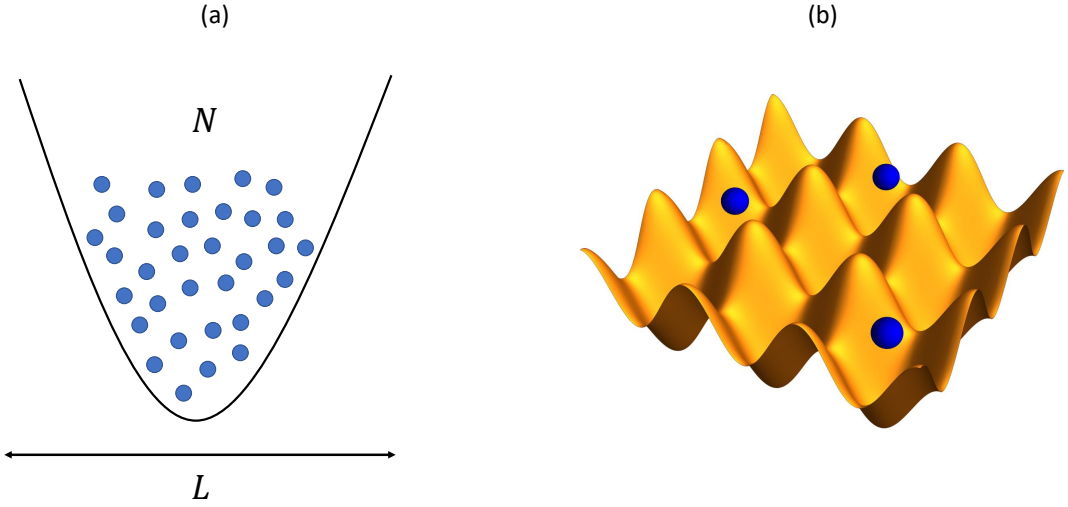

Figure 3.1: (a) Ultracold atoms in a parabolic optical trap. N and L are respectively the number of atoms and the size of the atomic cloud within the trap. (b) Three atoms loaded in the minima of an optical lattice.

3.1.1 Optical potentials and control parameters

The basic tools for the generation of ultracold lattice gases are the optical potentials. They essentially come from the interaction of the laser field with the induced dipole moment of the atom, causing a shift in the potential energy, an effect that is usually called the AC Stark shift [102]. Mathematically this can be understood by considering a two-level atom, with ground state $|g\rangle$ and excited state $|e\rangle$, in the presence of an external laser field of the form $\mathbf{E}(\mathbf{x},t) = E(\mathbf{x})e^{-i\omega t}\hat{\xi} + \text{h.c.}$. By defining the detuning $\delta \equiv \omega_e - \omega$ and moving to the rotating frame of frequency ω, the atomic Hamiltonian is written as

$$H_{\text{atom}} = \frac{\mathbf{p}^2}{2m} + \delta|e\rangle\langle e|. \tag{3.1}$$

If we assume that the amplitude of the electric field varies slowly with respect to the atomic size[1], we can consider the light-matter interaction in the dipolar approximation, i.e.

$$H_{\text{dip}} = -\mathbf{d} \cdot \mathbf{E}(\mathbf{x}, t), \tag{3.2}$$

being $\mathbf{d}$ the induced atomic dipole moment. In principle, there is also the coupling with the magnetic dipole moment of the atom, but usually it can be neglected in the study of optical lattices. The Hamiltonian term H_{dip} can be written in the rotating frame too, with the action of the unitary transformation $U(t) = e^{-i\omega t|e\rangle\langle e|}$, and neglecting the fast rotating terms $\propto e^{2i\omega t}$, i.e. performing the *rotating wave approximation*, it reduces to

$$H_{\text{dip}} = \frac{\Omega(\mathbf{x})}{2}|e\rangle\langle g| + \text{h.c.} \tag{3.3}$$

with Rabi frequency $\Omega(\mathbf{x}) = -2E(\mathbf{x})d_{eg}$. By further assuming the far-detuned condition, i.e. $|\delta| \gg \Omega$, the transitions between the ground and excited states are largely suppressed. The dipole term can be treated in perturbation theory, and the non-trivial virtual processes are associated to back and forth transitions from the ground to the excited levels. The effective Hamiltonian is

$$H = \frac{\mathbf{p}^2}{2m} + V_{\text{op}}(\mathbf{x}), \qquad V_{\text{op}} = -\frac{|\Omega(\mathbf{x})|^2}{4\delta}, \tag{3.4}$$

where $V_{\text{op}}(\mathbf{x})$ is the *optical trapping potential*. This is an effective potential felt by the atom in the ground state of this two-level picture, and can be attractive or repulsive depending on the sign of the detuning δ. For $\delta < 0$ the particles are trapped at the minima of V_{op}, and the lattice is said to be *blue-detuned*. In the opposite case, i.e. $\delta > 0$, the atoms sit at the maxima of the laser intensity and the lattice is said to be *red-detuned*.

The proper choice of the spatial dependence of the laser field can generate a periodic structure giving rise to the desired optical lattice, with the atoms filling the minima of the trapping potential. For example, the one-dimensional standing wave $E(x) = E_0 \cos(kx)$ results in the trapping potential $V_{\text{op}}(x) = V_0 \cos^2(kx)$, where $k = 2\pi/\lambda$, λ being the laser wavelength, and V_0 the depth of the optical lattice. In larger dimensions, pairs of counter-propagating lasers in orthogonal directions can be considered to generate the optical lattice. As a general comment, the lattice geometry and dimensionality of the optical lattice can be controlled by tuning the so called *control parameters*, i.e. the direction, polarization, intensity phase and frequency of the counter-propagating laser beams [103]. The optical lattices have a lot of interesting physical features: they are rigid and robust, not supporting phononic excitations; the tunneling of the atoms between the various potential wells can be controlled through various techniques, such as lattice tilting or laser assisted coherent transitions; the on-site interactions, as well as nearest neighbor or long range ones, governs the

[1]This is all what we need in this case, since the laser amplitude is assumed time-independent. If this is not the case, we must further assume that $E(\mathbf{x}, t)$ varies slowly with respect to ω^{-1}.

properties of the dilute atomic system. At last, we mention the possibility of having *spin-dependent* optical lattices, that can be created using counter-propagating laser beams with polarizations forming a given relative angle. In this way, atoms with different spin can experience different potentials.

3.1.2 Hubbard models

Due to the above mentioned physical features, optical lattices are ideal and rigid periodic potentials in which the ultracold atoms can move. For this reason, the moving particles resemble in many aspects electrons in solid state systems: in the free case, the single particle energy spectrum displays a band structure, where the Hamiltonian wave functions are the Bloch functions [104]. For deep lattices, i.e. for sufficiently strong lattice potentials, the bands are well separed in energy, and if the temperature is small enough only the lowest band of the system is occupied, constituting the well-known tight-binding approximation.

Mathematically, the atomic quantum field operators are projected into the lowest band. Instead of using the Bloch basis $u_{n\mathbf{k}}(\mathbf{x})$ we can write everything in the Wannier orthonormal basis $w_n(\mathbf{x}-\mathbf{x}_i)$, where n is the band index, $\mathbf{k}$ is the quasi-momentum in the first Brillouin zone (1BZ) and $\mathbf{x}_i$ are the lattice sites coordinates. Contrarily to the Bloch eigenfunctions, the Wannier ones are not eigenstates of the Hamiltonian, but they have the advantage of exponentially localized around the lattice sites $\mathbf{x}_i$: this choice of basis is particularly useful if one wishes to work with local single-particle wave functions [17]. The Wannier functions can be written as

$$w_n(\mathbf{x}-\mathbf{x}_i) \propto \sum_{\mathbf{k}} e^{-i\mathbf{k}\cdot\mathbf{x}_i} u_{n\mathbf{k}}(\mathbf{x}) \tag{3.5}$$

in terms of the Bloch waves. In the tight-binding approximation we need only the lowest Wannier orbital $w_0(\mathbf{x}-\mathbf{x}_i) \equiv \psi_{\mathbf{i}}(\mathbf{x})$, and we can perform a second-quantized expansion of the wave function $\Psi(\mathbf{x})$ in terms of the Wannier functions and single particle (bosonic or fermionic) annihilation operators $a_{\mathbf{i}}$ [105]

$$\Psi(\mathbf{x}) = \sum_{\mathbf{i}} \psi_{\mathbf{i}}(\mathbf{x}) a_{\mathbf{i}}. \tag{3.6}$$

The full quantum many-body Hamiltonian has the form

$$H_0 = \int d\mathbf{x} \left[\Psi^\dagger(\mathbf{x}) \left[-\frac{\nabla^2}{2m} + V_{\text{op}}(\mathbf{x}) \right] \Psi(\mathbf{x}) + \frac{g}{2} \Psi^\dagger(\mathbf{x}) \Psi^\dagger(\mathbf{x}) \Psi(\mathbf{x}) \Psi(\mathbf{x}) \right], \tag{3.7}$$

where we assumed that s-wave interactions are the most relevant in the ultracold regime, and the interactions between the atoms are given by the contact potential

$$V(\mathbf{x}-\mathbf{x}') = \frac{4\pi^2 a_0}{m} \delta(\mathbf{x}-\mathbf{x}') \equiv g\delta(\mathbf{x}-\mathbf{x}'), \tag{3.8}$$

where m is the atomic mass and a_0 is s-wave scattering length that characterizes the interactions by means of elastic binary collisions at low energies between neutral atoms. By inserting Eq. (3.6) into the last expression we get the *Hubbard Hamiltonian*

$$H_0 = -\sum_{\langle \mathbf{i},\mathbf{j}\rangle} t_{\mathbf{ij}} a_{\mathbf{i}}^\dagger a_{\mathbf{j}} + \text{h.c.} + \frac{1}{2}\sum_{\mathbf{i}} U_{\mathbf{i}} a_{\mathbf{i}}^\dagger a_{\mathbf{i}}^\dagger a_{\mathbf{i}} a_{\mathbf{i}} - \mu \sum_{\mathbf{i}} a_{\mathbf{i}}^\dagger a_{\mathbf{i}}, \tag{3.9}$$

with the parameters defined as

$$t_{\mathbf{ij}} \equiv -\int d\mathbf{x}\, w_0^*(\mathbf{x}-\mathbf{x}_i)\left[-\frac{\nabla^2}{2m} + V_{\text{op}}(\mathbf{x})\right] w_0(\mathbf{x}-\mathbf{x}_j), \qquad U_{\mathbf{i}} \equiv g\int d\mathbf{x}\, |w_0(\mathbf{x}-\mathbf{x}_i)|^4. \tag{3.10}$$

These parameters represent respectively the tunneling elements between nearest neighbors $\langle \mathbf{i}, \mathbf{j}\rangle$ in the optical lattice[2] and the on-site interaction $U_{\mathbf{i}}$ for the contact potential. Both of them can be tuned and controlled properly to achieve the target system when the Hubbard model is employed as a quantum simulator.

Indeed, the tunneling elements $t_{\mathbf{ij}}$ can be controlled through external laser beams, while the tuning of the on-site interaction $U_{\mathbf{i}}$ require some extra care because of the double dependence on the lattice laser beams and the Wannier orbitals. There are mainly two ways to tune the interaction term, and both of them require the presence of external fields: the first one is related to the Fano-Feshbach resonance, and makes use of a magnetic field B to change the effective scattering length of the system $a_s = a_s(B)$ [106–110]; the second one employs optical resonances to tune interactions using the Rabi frequency of an external laser. In both cases there are pros and cons, depending on the features of the external fields and on the atomic species loaded in the optical lattice.

As a last point, we write down the expression of the Hubbard Hamiltonian in presence of more than one atomic species with the same statistics [103, 110]. By denoting with Greek indices the atomic species, we have

$$H_0 = -\sum_{\substack{\langle \mathbf{i},\mathbf{j}\rangle \\ \alpha,\beta}} t_{\mathbf{ij}}^{\alpha\beta} a_{\mathbf{i}\alpha}^\dagger a_{\mathbf{j}\beta} + \text{h.c.} + \frac{1}{2}\sum_{\substack{\mathbf{i} \\ \alpha,\beta,\gamma,\delta}} U_{\mathbf{i}}^{\alpha\beta\gamma\delta} a_{\mathbf{i}\alpha}^\dagger a_{\mathbf{i}\beta}^\dagger a_{\mathbf{i}\gamma} a_{\mathbf{i}\delta} - \sum_{\mathbf{i},\alpha} \mu_\alpha a_{\mathbf{i}\alpha}^\dagger a_{\mathbf{i}\alpha}, \tag{3.11}$$

where in the most general case also the hopping and interaction parameters, as well as the chemical potential, depend on the given atomic species.

[2]This is true within the deep lattice condition, because the hopping energies are exponentially suppressed for all the sites that are not nearest neighbors.

3.2 Ultracold spinor atomic gases

In the previous Section we treated the theory of ultracold lattices and atoms without internal degrees of freedom, considering the spinless case. Here we include the possibility of having atoms with different internal states, considering the ultracold *spinor* atomic gases: the atoms can be either fermions or bosons with non-zero internal angular momentum whose spatial orientation is not externally constrained [103].

From now on, unless differently specified, we consider ultracold bosons loaded in optical lattice, and therefore we deal with the theory of *spinor Bose-Einstein condensates* (BECs), i.e. degenerate Bose gases with spin internal degrees of freedom. With respect to usual (scalar) BECs, they present multicomponent order parameters and display richer physical phenomena, due to the interplay between superfluidity and magnetic effects. As a consequence, they provide a useful platform for the study of different physical aspects, such as the role of symmetry breaking and long-range order in quantum-ordered materials, quantum phase transitions and non-equilibrium quantum dynamics [103, 111, 112].

The general atomic Hamiltonian of spinor BECs can be written on the basis of symmetry arguments, and, apart from the usual single-particle terms, it includes quantum number dependent interaction terms. For a spin-f BEC we denote with $\phi_m(\mathbf{r})$ the bosonic field operators, satisfying the canonical commutation relations $[\phi_m(\mathbf{r}), \phi^\dagger_{m'}(\mathbf{r}')] = \delta_{m,m'}\delta_{\mathbf{r},\mathbf{r}'}$, where $m = -f, -f+1, \ldots, f$ is the magnetic quantum number and f is the hyperfine spin of the given atomic species. The microscopic Hamiltonian is

$$H = H_0 + H^{(f)}_{int}, \qquad H_0 = \int d\mathbf{r} \sum_m \phi^\dagger_m(\mathbf{r}) \Big[-\frac{\hbar^2\nabla^2}{2M} + U_{\text{trap}}(\mathbf{r}) \Big] \phi_m(\mathbf{r}), \tag{3.12}$$

$$H^{(f)}_{int} = \frac{1}{2}\int d\mathbf{r} \sum_{m_1,m_2,m_1',m_2'} C^{m_1 m_2}_{m_1' m_2'}\, \phi^\dagger_{m_1}(\mathbf{r})\phi^\dagger_{m_2}(\mathbf{r})\phi_{m_1'}(\mathbf{r})\phi_{m_2'}(\mathbf{r}). \tag{3.13}$$

The single-particle term, H_0, includes the possibility of having a trapping potential $U_{\text{trap}}(\mathbf{r})$. $H^{(f)}_{int}$ is the most general on-site interaction term for hyperfine spin f. For our purposes, it is enough to consider the $f = 2$ case

$$H^{(2)}_{int} = \frac{1}{2}\int d\mathbf{r}\, [c_0 : n^2(\mathbf{r}) : + c_1 : \mathbf{F}^2(\mathbf{r}) : + c_2 A^\dagger_{00}(\mathbf{r}) A_{00}(\mathbf{r})], \tag{3.14}$$

where $: \mathcal{O} :$ represents the normal order for the operator $\mathcal{O}$, c_0, c_1 and c_2 are numerical coefficients related to the scattering lengths a_F in the various channels, and

$$n(\mathbf{r}) = \sum_{m=-2}^{2} \phi^\dagger_m \phi_m, \qquad A_{00}(\mathbf{r}) = \frac{2\phi_2\phi_{-2} - 2\phi_1\phi_{-1} + \phi_0^2}{\sqrt{5}}, \qquad F_i(\mathbf{r}) = \sum_{m,m'=-2}^{2} \phi^\dagger_m (f_i)_{mm'} \phi_{m'}. \tag{3.15}$$

The dependence on $\mathbf{r}$, on the right hand side, was ommitted for simplicity. The above defined quantities are $n(\mathbf{r})$ the total density operator, A_{00} the amplitude of the spin singlet pair, and F_i the spin density operators, with f_i representing the spin-2 rotation matrices.

3.2.1 Effective Hubbard Hamiltonians and dipolar interactions

Without further interactions, the spinor BECs in spin-independent optical lattices can be described by the Bose-Hubbard (BH) model [105, 113]. Expanding the field operators in terms of Wannier functions, and introducing the associated annihilation and creation operators $b_{\mathbf{i}m}$, $b^\dagger_{\mathbf{i}m}$, the BH Hamiltonian can be written as

$$H_{BH} = -t \sum_{\langle \mathbf{i},\mathbf{j}\rangle, m} (b^\dagger_{\mathbf{i}m} b_{\mathbf{j}m} + \text{h.c.}) + \frac{U_0}{2} \sum_{\mathbf{i}} n_{\mathbf{i}}(n_{\mathbf{i}}-1) + U_1 \sum_{\mathbf{i}} (A^\dagger_{00})_{\mathbf{i}} (A_{00})_{\mathbf{i}} + \frac{U_2}{2} \sum_{\mathbf{i}} \mathbf{F}^2_{\mathbf{i}} - \mu \sum_{\mathbf{i}} n_{\mathbf{i}}, \quad (3.16)$$

with $n_{\mathbf{i}} = \sum_m b^\dagger_{\mathbf{i}m} b_{\mathbf{i}m}$, $F_{\mathbf{i}\alpha} = \sum_{m,m'} b^\dagger_{\mathbf{i}m} (f_\alpha)_{mm'} b_{\mathbf{i}m'}$ and A_{00} is the spin singlet amplitude written in terms of $b_{\mathbf{i}m}$, $b^\dagger_{\mathbf{i}m}$. The single site interactions are not enough to generate the desired plaquette terms within our proposal. However, this can be accomplished by including magnetic dipole-dipole interaction (MDDI) terms, and considering *spinor dipolar BECs*. The MDDI couples the spin degrees of freedom with the orbital ones, conserving the total angular momentum. For spinor BECs, the MDDI can be relevant, as it is spin dependent and long-ranged. Its Hamiltonian in second quantization is given by

$$V_{dd} = \frac{c_{dd}}{2} \int d\mathbf{r} d\mathbf{r}' \sum_{\nu,\nu'} :F_\nu(\mathbf{r}) Q_{\nu\nu'}(\mathbf{r}-\mathbf{r}') F_\nu(\mathbf{r}'):, \qquad Q_{\nu\nu'}(\mathbf{r}) = \frac{\delta_{\nu\nu'} - 3\hat{r}_\nu \hat{r}_{\nu'}}{r^3}, \quad (3.17)$$

with the coefficient $c_{dd} \propto d^2$ related to the electric dipole moment. In the optical lattice Hamiltonian this generates a series of long-range terms

$$H_{dd} = \frac{1}{2} \sum_{\mathbf{i}\neq\mathbf{j}} U^{\mathbf{ij}}_{dd} n_{\mathbf{i}} n_{\mathbf{j}}, \qquad U^{\mathbf{ij}}_{dd} \equiv c_{dd} \int d\mathbf{r} d\mathbf{r}' \, |w(\mathbf{r}-\mathbf{r}_i)|^2 \frac{1-3\cos^2\theta}{|\mathbf{r}-\mathbf{r}'|^3} |w(\mathbf{r}'-\mathbf{r}_j)|^2, \quad (3.18)$$

where θ is the angle between the dipole moment and the vector $\mathbf{r}-\mathbf{r}_i$. The full Hamiltonian $H_{EBH} = H_{BH} + H_{dd}$ falls in the class of the so-called *extended Hubbard models*. Depending on the values of t, U_0, U_1 and U_{dd}, that can be tuned independently, the extended BH has different quantum transitions and phases, including Mott insulator, superfluid and even supersolid phases, provided that more than nearest neighbors interaction terms are considered in the extended Hamiltonian [114–116].

In principle, the dipolar interaction is dominant in gases of polar molecules when the application of a strong electric field is considered, due to their strong electric dipole moments. In this case, these are called spin-polarized dipolar BECs. The dipole-dipole interaction can be properly tuned

through a rotating field [117], allowing for the control of the interaction strength c_{dd}, that can be positive or negative according to the relative orientation of the dipoles. On the other hand, the MDDI can be neglected in several cold atomic systems, such as scalar alkali atoms, while they play an important role for other species, e.g. Cr and Dy [118, 119]. We refer to the reviews [111, 112], and the references therein, for more details on the various physical properties of spinor (dipolar) BECs.

3.3 Quantum simulators of lattice gauge theories

Due to their physical features, ultracold quantum gases in optical lattices are highly tunable systems, allowing for the investigation of strongly correlated quantum matter [120, 121] and proposing themselves as an optimal example of the original Feynman's idea about quantum simulators [122]. Indeed, they illustrate perfectly the modern definition of quantum simulator, i.e. a controllable system that mimics a family of physical models whose properties are otherwise inaccessible through the usual theoretical, experimental or numerical ways. In this respect, ultracold atoms can emulate the physics of different systems in various physical sectors, from correlated electronic systems, such as high-T_c superconductors [123, 124] to quantum phase transitions [125, 126].

Over the past years, particularly relevant has been the use of quantum simulators to study gauge theories, since the classical approaches to analyse them present various drawbacks, depending on the regimes and properties of interest. The most prominent example in high-energy physics is the analysis of quantum chromodynamics (QCD) through Monte Carlo simulations: due to the sign problem, this numerical method can not approach the out of equilibrium real time evolution or the analysis of the theory with finite chemical potential [14, 15]. Quantum simulators based on ultracold atomic platforms emerge here as a promising alternative to investigate such phenomena for lattice gauge theories (LGTs), being not affected by the intrinsic limitations of classical simulators [16, 17, 38]. Despite this, the quantum simulation of full QCD is still far from being realized, as there are challenging aspects to be faced [127–130].

As a consequence, various simpler models sharing the key physical features of the respective full models are analysed in the modern literature. In the case of pure Abelian gauge theories, quantum simulators of compact quantum electrodynamics (cQED) are studied in $(2+1)-d$ using both BECs [131] and single atoms [132] loaded in optical lattice. With the inclusion of dynamical matter, interesting features are observed both in $(1+1)-d$, with the simulation of the Schwinger model [40–42, 60], and in $(2+1)-d$, including dynamical fermions in the pure gauge case [133].

In all these cases, the gauge symmetry is obtained only at low-energies, manifesting itself as a property of the effective Hamiltonian of the model and not as a fundamental symmetry of the simulators. This is due mainly to the fact that the typical experimental platforms used as

quantum simulators of LGTs do not naturally encode any local symmetry. One has then to consider different strategies to enforce it, such as brute force Hamiltonian engineering [134–137], gauge or matter integration [63, 138–140], energy penalty [131, 132, 141–144] and Zeno dynamics [145]. For a detailed presentation of these methods we refer to the review [38]. Another possibility, that we are going to discuss in details in the next Section, is to enforce the gauge invariance in ultracold atomic platforms by means of many-body interaction symmetries [24]. With this method, the local invariance is directly built into the theory, and not obtained as an effective and emergent property of the quantum dynamics.

3.3.1 Higher dimensions: proposals and challenges

With respect to usual many-body quantum systems, there are additional features to be considered in the case of theories with gauge fields in dimensions $d > 1$. To be specific, the designed quantum platform should

- be properly consistent with the local symmetry, i.e. the *gauge invariance*, of the theory;
- involve complex many-body interaction terms to simulate the gauge fields dynamics.

In addition, the implementation of the Hilbert space of dynamical gauge fields in a quantum simulator is a complicated task, since it is infinite-dimensional for a single link in the Wilson formulation of LGTs [10]. A possible way to overcome this difficulty is to replace the link variables with discrete degrees of freedom, considering the quantum link formulation of gauge theories. Even if they possess a finite number of states, quantum link models (QLMs) preserve the gauge symmetry of the original model, paying the price of introducing non-unitary operators on the links of the lattice [40–42]. Due to the finiteness of the Hilbert space and the preservation of the local symmetry, they are suitable to be implemented and analysed as quantum simulators. In addition, being them different from standard LGTs, different new phases are expected to appear in the respective phase diagrams, and this is a further aspect that motivated the interest towards these model in the modern literature [43–45, 47, 146, 147].

Recently, concerning the features in $d > 1$ both in the Wilson and quantum link formulations, different proposals involving ultracold atoms in optical lattice ([24] and references therein) and Rydberg atoms [21] were presented in the literature. In the next Subsections we describe in details the techniques presented in [24], to highlight what are the strong points and limitations and show how the plaquette interactions arise. As a last point, we compare it with the proposal of Ref. [21].

Local gauge invariance from angular-momentum conservation

In the proposal of Ref. [24], the authors make use of a fundamental symmetry of the ultracold atomic system to enforce the gauge invariance of the target theory. The difference with respect to the above mentioned proposals is that the local symmetry is not emergent, but already built into the theory.

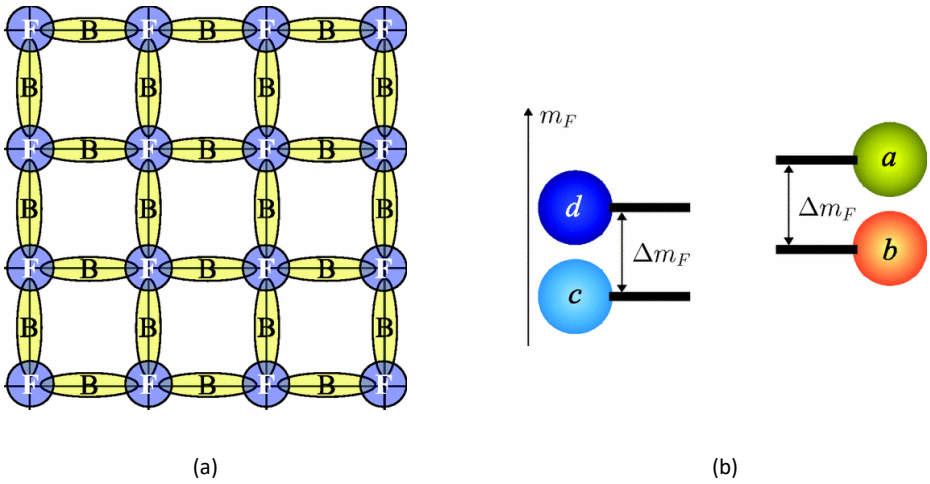

Figure 3.2: (a) Optical lattice structure with bosons (B) and fermions (F) respectively on the links and vertices. (b) Choice of the m_F values: the spacing between bosons (left) and fermions (right) is required to enforce gauge-invariant collisions. Both panels are adapted from Ref. [24].

The proposal under discussion includes both fermions and bosons, to simulate both matter and gauge fields. The gauge symmetry is generated by the atomic interactions between fermions and bosons loaded in the optical lattice, structured as in Fig. 3.2(a): in this scheme, the species are placed in order in order to have maximal interactions on the links.

Apart from the lattice structure, the internal states in the scattering processes between fermions and bosons are chosen in a way to respect the angular momentum conservation. Indeed, in the scatterings the z-component of the total hyperfine angular momentum, i.e. m_F, is conserved. The values of m_F for the employed atomic species can be chosen to keep only the gauge-invariant collisions, while others are automatically excluded since they violate a fundamental symmetry of the simulator. Said differently, the angular momentum conservation of the quantum simulator is equivalent to the gauge symmetry of the target theory.

With this setting, proposals for $(1+1)-d$ and $(2+1)-d$ cQED and $SU(N)$ theories are presented. For concreteness, let us discuss the $(1+1)-d$ case: here two bosonic species, i.e. (a, b) and two fermionic species, i.e. (c, d) are needed to simulate the theory. In the hypothesis that the number of bosons per link is a constant, i.e. N_0, we can represent each link with the Schwinger

algebra [148]

$$L_+ = a^\dagger b, \qquad L_- = b^\dagger a, \qquad L_z = \frac{a^\dagger a - b^\dagger b}{2}. \tag{3.19}$$

Concerning the fermions, the case in which the c-species populates the even vertices, while the d-species the odd ones, is considered, in a way to simulate staggered fermions [138, 149]. In this framework, the conservation of angular momentum reads

$$m_F(a) + m_F(c) = m_F(b) + m_F(d), \tag{3.20}$$

and the only allowed process[3] are scattering $a, c \to b, d$, associated to terms in the Hamiltonian like $c_i^\dagger a_i^\dagger b_i d_{i+1} + \text{h.c.}$. This ultimately means that the difference in angular momentum in the fermionic hoppings is exactly compensated by bosonic hoppings in the opposite directions, leading to *correlated hoppings* coming from the interactions between bosons and fermions.

Plaquette interactions and the loop method

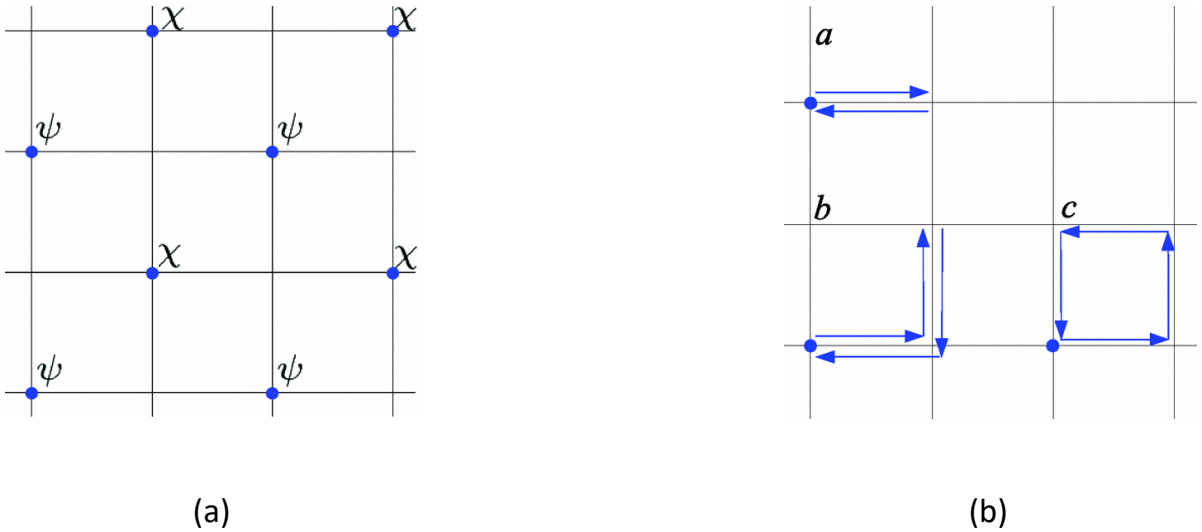

Figure 3.3: (a) Vertices associated to the auxiliary fermions ψ, χ: every plaquette in the lattice contains two vertices of different types. (b) Virtual processes arising in perturbation theory, respectively at second order (a) and fourth order (b and c), with c representing the plaquette interaction. Both panels are adapted from Ref. [24].

In addition to the gauge-invariant elementary interactions explained in the previous Subsection, we need the presence of plaquette terms in the Hamiltonian to generalize the discussion to higher

[3]The only other allowed scattering term is associated to density-density interactions. These are linear terms in the fermionic number operator, due to the conservation of the total number of bosons per link, fixed to N_0. When summed over all the lattice sites, this gives a simply a constant shift of the energy.

dimensions. In what follows we focus on the $(2+1)-d$ case, but the description of higher dimensional settings is the same.

The idea presented in Ref. [24] is to treat the two fermionic species ψ, χ present in the optical lattice as ancillary particles, by adding a constraint H_0 in the Hamiltonian that forces them to occupy only some lattice sites, according to the picture in Fig. 3.3(a). The logic is then to construct an effective theory in the ground sector of H_0 to get the plaquette interaction in perturbation theory. In this method the fermions are traced out at the end of the procedure, leaving us with a pure gauge theory. More species of fermions are needed if dynamical matter must be included in the proposal of the quantum simulator.

To consider a concrete example, we present here how the plaquette term arises in the $(2+1)-d$ cQED. The Hamiltonian of the system is

$$H = \frac{e^2}{2}\sum_{\mathbf{i},j} E^2_{\mathbf{i},j} + \epsilon \sum_{\mathbf{i},j} (\psi^\dagger_{\mathbf{i}} U_{\mathbf{i},j} \psi_{\mathbf{i}+\hat{j}} + \chi^\dagger_{\mathbf{i}} U_{\mathbf{i},j} \chi_{\mathbf{i}+\hat{j}} + \text{h.c.}) - \lambda \sum_{\mathbf{i}} (\mathcal{F}_{\psi,\mathbf{i}} \psi^\dagger_{\mathbf{i}} \psi_{\mathbf{i}} + \mathcal{F}_{\chi,\mathbf{i}} \chi^\dagger_{\mathbf{i}} \chi_{\mathbf{i}}) \tag{3.21}$$

$$\equiv H_E + H_{\text{int}} + H_0, \tag{3.22}$$

where H_E is the electric part, H_{int} is the interaction term between bosons and fermions and H_0 is the constraint on the fermions. The functions $\mathcal{F}_{\psi,\mathbf{i}}$, $\mathcal{F}_{\chi,\mathbf{i}}$ are defined as

$$\mathcal{F}_{\psi,\mathbf{i}} = \begin{cases} 0, & \text{if } (-1)^{i_1+i_2} = -1 \\ 1, & \text{if } (-1)^{i_1+i_2} = 1, \end{cases} \qquad \mathcal{F}_{\chi,\mathbf{i}} = \begin{cases} 0, & \text{if } (-1)^{i_1+i_2} = 1 \\ 1, & \text{if } (-1)^{i_1+i_2} = -1. \end{cases} \tag{3.23}$$

For large λ, H_0 represents an energy penalty term enforcing the configuration showed in Fig. 3.3(a). Then we can consider $\lambda \gg \epsilon$ and perform time-independent perturbation theory as in [150], having that[4]

- at first order we get only the electric part H_E, without fermionic terms;
- at second order we get the virtual process a in Fig. 3.3(b), associated to back and forth fermionic hoppings of both the species ψ and χ. These processes contribute only as constant energy shifts in the effective Hamiltonian;
- at third order we get a combination of first and second order terms, plus constant energy shifts;

[4]The following considerations in perturbation theory hold under the assumptions that the link operators $U_{\mathbf{i},j}$ are unitary, i.e. when the number of bosons per link $N_0 \to \infty$. If this is hypothesis is relaxed, non-constant terms appear from the second order on, due to the non-unitarity of the ladder operators appearing in the interaction term H_{int}.

- at fourth order we get a renormalization of the electric part, the back and forth processes on two consecutive links reported in the virtual process b in Fig. 3.3(b), and the plaquette term, with virtual process c in Fig. 3.3(b).

The final effective Hamiltonian is then

$$H_{\text{eff}} = H_E + \delta H_E + H_\square, \qquad \delta H_E \propto \frac{\epsilon^2}{\lambda^3}, \qquad H_\square \propto \frac{\epsilon^4}{\lambda^3}, \tag{3.24}$$

where δH_E and $H_\square$ are respectively the renormalization of the electric Hamiltonian and the plaquette term.

As a final consideration, we mention that all the terms coming out in the perturbative expansion have as energy scale ϵ^2, and not ϵ: it is then sufficient to require $\lambda^2 \gg \epsilon^2$. This means that the plaquette term is effectively of second order in ϵ^2, due to the vanishing of the odd orders in the expansion.

Before closing the Chapter and move on with the presentation of our proposal for the plaquette term using ultracold atomic platforms, we compare the perturbative approach present in Ref. [24] with the proposal of Ref. [21], that employs Rydberg atoms.

We just showed that in Ref. [24] the gauge invariance of the theory is obtained through angular momentum conservation in the scattering processes of the atoms in the optical lattice, while the dynamics of the gauge field emerges effectively in perturbation theory. At variance, using the dual formulation [151], in Ref. [21] the implementation of quantum simulators for $U(1)$ spin$-1/2$ models in $d = 2$ is treated, where plaquette interactions are mapped into single constrained hopping processes on the dual lattice. A concrete proposals in terms of Rydberg configurable arrays is presented, in which the physical states have a blockade character. As in Ref. [24], this proposal is intrinsically done in terms of bosons. However, while in [24] the specific terms of the link models are emerging at the fourth-order of a strong-coupling expansion, in this proposal the plaquette term is implemented directly, without the use of any perturbative expansion. At the same time, this approach relies on the two-dimensional nature of the system, and does not seem to be easily generalizable to higher dimensions. In this respect, it would be desirable to have a set-up that is in principle extendable to $d > 2$, and possibly able to use also fermions, instead than only bosons.

Chapter 4

Bosonic and fermionic link models in two dimensions: a proposal

In this Chapter we propose a scheme for the quantum simulation of quantum link models in two-dimensional lattices. Our approach considers spinor dipolar gases on a suitably shaped lattice, where the dynamics of particles in the different hyperfine levels of the gas takes place in one-dimensional chains coupled by the dipolar interactions. We show that at least four levels are needed. The present scheme does not require any particular fine-tuning of the parameters. We present a derivation of the parameters of the quantum link models by using a perturbative method. A comparison with other schemes for $(2+1)$-dimensional quantum link models present in literature is discussed. Finally, the extension to three-dimensional lattices is presented, and its subtleties are pointed out.

To be specific, we propose a quantum simulator for the $U(1)$ spin$-1/2$ pure Abelian QLM using spinor dipolar Bose-Einstein condensates (BECs) loaded in a spin-dependent optical lattice. With respect to Ref. [24], we use only bosonic atoms of spin-2, so that we have access to five internal states that, through angular momentum conservation in the various scattering channels, give rise to gauge invariance. As in Ref. [24], the robustness of gauge invariance is tied to the one of angular momentum conservation, and in the present proposal it is used to generate the plaquette term. The same principle can be achieved without conservation of angular momentum, provided the cold atomic parameters are properly tuned in the strong coupling regime. The resulting effective Hamiltonian describes the dynamics of the gauge field at third-order in perturbation theory for a square lattice, or at second-order for a triangular lattice.

The Chapter is organized as follows. In Sec. 4.1 we present our proposal using ultracold atomic platforms: we show how to construct our optical lattice and the ground state of the system (Sec. 4.1.1), and discuss how to obtain the effective Hamiltonian in perturbation theory (Sec. 4.1.2). In Sec. 4.1.3 we discuss the relation with the target gauge theory. In Sec. 4.2 we discuss possible

extensions and generalizations of our proposal. In Sec. 4.3 we summarize our results and present our conclusions.

4.1 Plaquette terms from angular momentum conservation

In this Section we describe how the plaquette interactions in the 2D Abelian spin-1/2 QLMs can be interpreted as a correlated hopping obtained through angular momentum conservation. The use of angular momentum conservation in scattering processes to ensure local gauge invariance was introduced, for the first time, in Ref. [24]. In that case, it guarantees that the gauge-matter interaction satisfies gauge invariance. By other side, plaquette terms are still obtained perturbatively. In contrast, our target model does not include matter and uses the conservation of angular momentum as a mean to obtain robust plaquette terms of the pure gauge theory. In this sense, the plaqutte term here is in treated on the same footing of the gauge-matter interaction in Ref. [24].

4.1.1 Structure of the optical lattice

In our proposal, we consider a spin-2 dipolar BEC loaded in a square optical lattice, whose structure is showed in the left panel of Fig. 4.1. The bosons are located on the vertices of the lattice, which has a spin-dependent structure: an atom can sit at a generic site $\mathbf{n}$ if it has the magnetic quantum number m_F associated with that site. In other words, the color with which the site $\mathbf{n}$ is painted, in Fig. 4.1, is associated with the magnetic quantum number of the atom that can sit here. This can be accomplished, in principle, by the realization of a state-dependent optical superlattice, with different periods and minima [152]. In Section 4.1.2 we provide an alternative construction where correlated hoppings are induced by a one-site one-body term in the Hamiltonian, i.e. $H_{\mathbf{i}} \sim h\, \epsilon_{\mathbf{i}m} b^{\dagger}_{\mathbf{i}m} b_{\mathbf{i}m}$, where h is large and $\epsilon_{\mathbf{i}m} \in \{0, 1\}$, penalizing or favoring, at the site $\mathbf{i}$, particles with different internal states. In this approach m_F can be any quantum number with which a superlattice of this form can be constructed. The details of the approach will be discussed in the next Subsection.

Moreover, we require the presence of asymmetric hopping amplitudes within the lattice: by denoting with t_x and t_y the horizontal and vertical hopping parameters, we assume that $t_x \gg t_y$, in a way that only horizontal hoppings processes are generated. With reference to the left panel of Fig. 4.1, this is represented by dotted ($\sim t_y$) and full ($\sim t_x$) lines. The simulated lattice, whose dynamics will be analyzed, is plotted in the right panel of Fig. 4.1. Here we associate each atom of the spinor dipolar BEC to a single link of the simulated lattice, and we assume that the hopping of the atoms can happen only along its diagonals, due to the requirement on t_x and t_y.

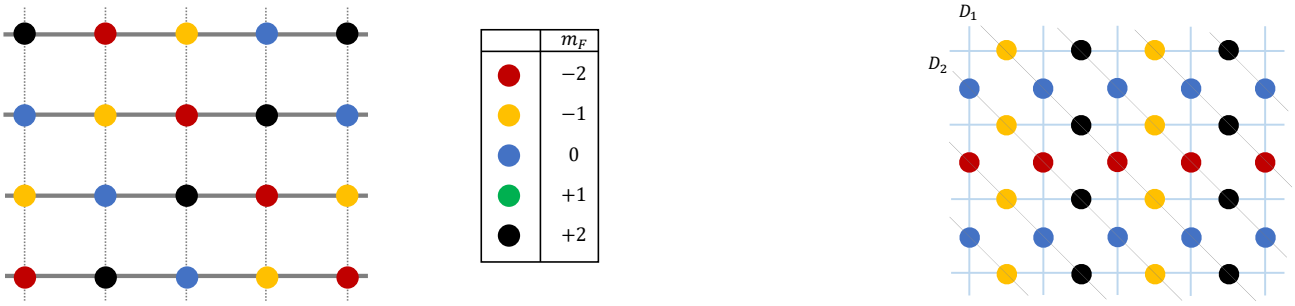

Figure 4.1: Left panel: spin-dependent optical lattice with atoms on the vertices in the five internal states $m_F = 0, \pm 1, \pm 2$, whose color code is reported in the table. The dotted vertical lines represent avoided hoppings. Right panel: simulated lattice (light blue lines) alongside the allowed hoppings on the original spin-dependent optical lattice (inclined grey lines). While it is easier to visualize the simulator as it is represented in the left panel, the mapping to the gauge theory is more transparent when the lattice is rotated by 45°, as in the right panel.

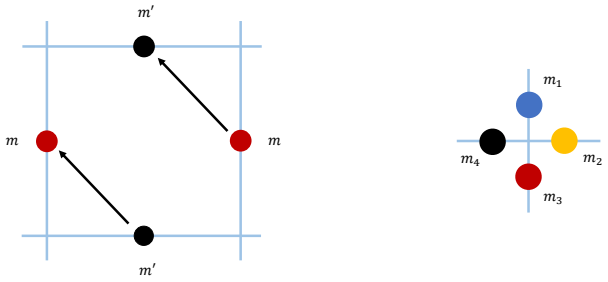

Figure 4.2: Left panel: generic plaquette structure in the simulated lattice with the same color appearing at opposite links. Right panel: generic vertex structure in the simulated lattice with all four different link colors meeting at a vertex.

With this choice the plaquette term is generated by correlated hoppings induced by angular momentum conservation. The geometric structure of the plaquette, as in left panel of Fig. 4.2, guarantees that the correspondent correlated hoppings generate the plaquette term. Additionally, by judicious choice of the four hyperfine levels, no correlated hoppings occur at vertices, as in left panel of Fig. 4.2. We anticipate that it is not enough to have four different colours meeting at a vertex, in order to forbid gauge symmetry breaking processes.

For these reasons, we consider two types of periodic sequences for the hyperfine levels along the diagonals in the right panel of Fig. 4.1:

$$\begin{aligned} &\mathrm{D}_1 : \; m_F = -1 \;\to\; 0 \;\to\; 2 \;\to\; -2 \;\to\; -1 \;\to\; \ldots, \\ &\mathrm{D}_2 : \; m_F = 0 \;\to\; -1 \;\to\; -2 \;\to\; 2 \;\to\; 0 \;\to\; \ldots, \end{aligned} \tag{4.1}$$

already depicted in Fig. 4.1. Only four out of five possible hyperfine levels are used in our proposal for the spin-dependent superlattice. However, the use of total spin 2 is necessary in order to avoid correlated hopping processes at the vertices (see the Appendix B.1 for more details).

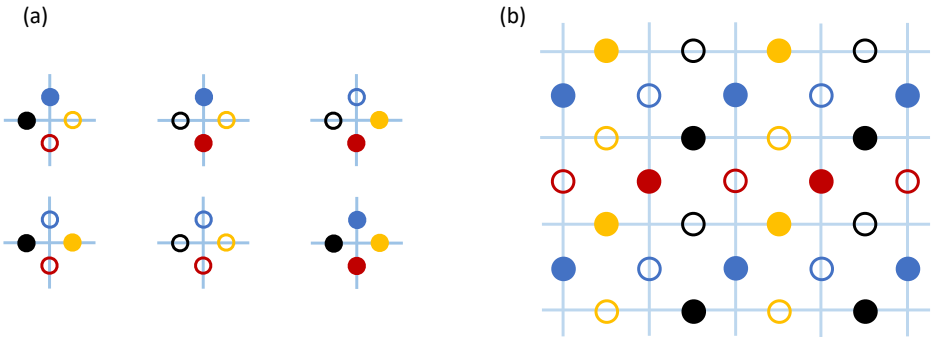

Figure 4.3: (a) The six vertices of the spin-dependent optical lattice compatible with Gauss' law. Filled circles represent sites occupied with a single particle, empty circles do not contain particles. (b) Fully flippable ground state of H_0, see Eq. 4.3, made of disconnected flippable plaquettes.

4.1.2 Effective gauge field dynamics

The above description guarantees that the plaquette terms are obtained directly, *without* the use of perturbation theory, as the most local processes allowed by conservation of angular momentum. By "most local", we emphasize that there are other processes which preserve angular momentum. For example, a particle hopping to its fourth neighbor (same color) along the diagonal in the right panel of Fig. 4.2. This process is "less local" in a rather concrete sense, and it is expected to be highly suppressed in the cold atomic dynamics. The purpose of this Subsection is twofold: first, we would like to show how the plaquette terms can emerge in perturbation theory, even without conservation of angular momentum, if the cold atomic parameters are properly tuned in the strong coupling regime. Second, we would like to quantify the aforementioned statement, which classifies the plaquette terms as the most local ones.

We consider a cold atomic Hamiltonian that has regular hopping terms along a one-dimensional line, a one-body potential that promotes the lattice structure described above, and angular momentum-preserving interactions among nearest neighbors. By performing a perturbative expansion for large amplitude values of the one-body potential, we can construct an effective Hamiltonian that exhibits gauge invariance at lowest orders, and contains all other angular momentum-conserving processes suppressed at higher orders. We also consider the hardcore bosons limit, so that we have, at most, one particle per site. In other words, there is a strong contact repulsion between bosons characterized by a parameter U_0 much larger than the relevant energy scales of the problem.

Explicitly, the full Hamiltonian reads $H = H_0 + H_1$ where

$$H_1 = H_{\text{hop}} + H_{\text{int}} \equiv -t_x \sum_{\langle \mathbf{i},\mathbf{j}\rangle_d, m} (b^\dagger_{\mathbf{i}m} b_{\mathbf{j}m} + \text{h.c.}) + \frac{1}{2} \sum_{\langle \mathbf{i},\mathbf{j}\rangle, m, m'} V^{\mathbf{ij}}_{mm'} b^\dagger_{\mathbf{i}m} b^\dagger_{\mathbf{j}m'} b_{\mathbf{i}m'} b_{\mathbf{j}m}, \tag{4.2}$$

with the operators satisfying the hardcore bosons commutation relations $[b_{\mathbf{i}m}, b^\dagger_{\mathbf{j}m'}] = \delta_{mm'}\delta_{\mathbf{ij}}(1 - 2b^\dagger_{\mathbf{i}m} b_{\mathbf{i}m})$. In addition to these terms we add a one-body term

$$H_0 = -h \sum_{\mathbf{i},m} \epsilon_{\mathbf{i}m} b^\dagger_{\mathbf{i}m} b_{\mathbf{i}m} \tag{4.3}$$

with $h \gg t_x, V^{\mathbf{ij}}_{mm'}$, and the function $\epsilon_{\mathbf{i}m}$ is such that it is equal to 1 if m is the hyperfine state associated with site $\mathbf{i}$ (according to Fig. 4.1) and 0 otherwise. This will enforce the desired lattice structure. Of course, this choice for h implies that we have two large energy scales in the system (h and U_0), and the further assumption that any effect of the on-site interaction is much beyond the scale we are interested in (see the Appendix B.2 for more details). We pause here to establish the connection with the previous Subsection. The sum of the two Hamiltonians (4.2) and (4.3) does not correspond exactly to the scenario described in 4.1.1. In fact, the hopping terms presented in (4.2) imply that particles with the same angular momentum can sit at nearest neighbor sites, in contrast to the situation described in Fig. 4.1, for example. In turn, the Hamiltonian (4.3) enforces this lattice structure through energy penalty. This allows the construction of the gauge theory as an effective theory at low energies, and the quantum numbers referred here could be different from angular momentum quantum numbers. However, the spin-dependent lattice structure represents a much more robust construction, as the plaquette terms rely on angular momentum conservation, and not on the large magnitude of h with respect to the other parameters of the model.

In the same spirit of Ref. [24], the idea is to prepare the system in a gauge invariant configuration that is a ground state of H_0. The dynamics generated by the full Hamiltonian $H = H_0 + H_1$ is gauge invariant at low energies, and our aim is to construct an effective Hamiltonian in perturbation theory, using h as large scale, giving rise to the plaquette interaction. We have then to characterize the ground states of H_0 that are compatible with the hardcore bosons constraint and with Gauss' law. Calling N the number of lattice sites, and N_p the number of particles in the lattice, we have two trivial cases, i.e. $N_p = 0$ (empty lattice) and $N_p = N$ (full lattice), for which the dynamics is completely frozen. The other possibilities are represented by gluing different vertices compatible with Gauss' law, reported in Fig. 4.3 (left panel), to form the full square lattice. The fully flippable ground state is composed by alternating filled anti-diagonals as showed in the right panel of Fig. 4.3.

We denote with $\mathcal{M}_0$ the ground state manifold of H_0. The system must be prepared in a state $|\alpha\rangle \in \mathcal{M}_0$, and we work in a subspace $\mathcal{M} \subset \mathcal{M}_0$ which is gauge invariant. As h is the largest scale in our system, we construct a low-energy Hamiltonian $H^{(\text{eff})}$ within $\mathcal{M}_0$, that includes the plaquette interactions as correlated hoppings emerging from H_1. Up to third-order in perturbation

theory, the effective Hamiltonian is

$$H^{(\text{eff})} = \frac{t_x^2}{h} \sum_{\langle \mathbf{i},\mathbf{j}\rangle_d, m, m'} n_{\mathbf{i}m} n_{\mathbf{j}m'} - \frac{1}{h} \sum_{\langle \mathbf{i},\mathbf{j}\rangle, m, m'} (V^{\mathbf{ij}}_{mm'})^2 n_{\mathbf{i}m} n_{\mathbf{j}m'} + \frac{1}{h^2} \sum_{\substack{\mathbf{i}',\mathbf{j},\mathbf{j}' \in \square \\ m,m'}} (V^{\mathbf{jj}'}_{mm'})^2 V^{\mathbf{j}'\mathbf{i}'}_{mm} n_{\mathbf{j}'m} n_{\mathbf{i}'m} n_{\mathbf{j}m'} + \frac{t_x^2}{h^2} \sum_{\substack{\mathbf{i},\mathbf{i}',\mathbf{j},\mathbf{j}' \in \square \\ m,m'}} V^{\mathbf{ii}'}_{mm'} b^\dagger_{\mathbf{j}'m} b^\dagger_{\mathbf{j}m'} b_{\mathbf{i}'m'} b_{\mathbf{i}m} + \text{h.c.}, \tag{4.4}$$

and we refer to Appendix B.2 for details on the computation. We observe that the last term in the previous equation corresponds exactly to the plaquette interaction, as the effect of two correlated hoppings and a spin-exchange interaction, deriving from the dipolar term in H_1. The pictorial virtual processes are showed in Fig. 4.4.

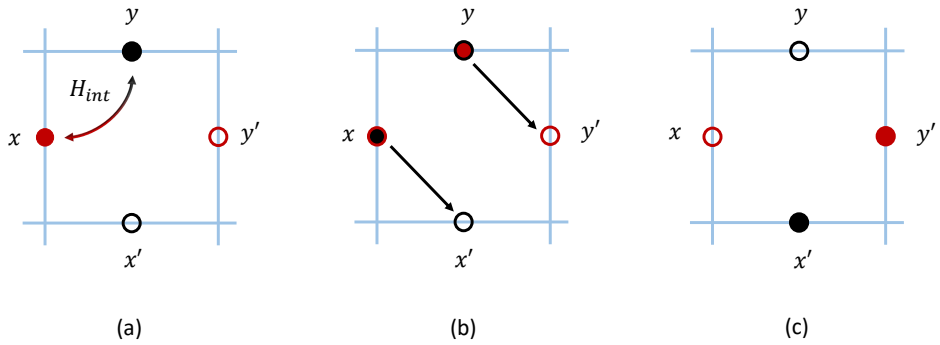

Figure 4.4: Virtual processes that build-up a plaquette flip, emerging at third-order in perturbation theory. (a) Spin-exchange interactions change the internal state of the atoms in the position $\mathbf{x}$, $\mathbf{y}$; (b) two hoppings from $\mathbf{x} \to \mathbf{x}'$ and $\mathbf{y} \to \mathbf{y}'$; (c) final state after the whole process, with the flipped plaquette.

The other terms appearing in the first line of Eq. (4.4) arise from the second-order of the perturbative expansion, and are related to back and forth hoppings ($\sim t_x^2/h$) and double spin-exchange ($\sim V^2/h$) between nearest neighbors. Similarly, the first term in the second line arises from the third-order of the expansion, and it is related to spin-exchange interactions ($\sim V^3/h^2$) within a given plaquette. These terms are not present in the initial model but are diagonal on the occupation number and, therefore, associated with products of the electric field at different links, in the gauge theory language. As a consequence, they are trivially gauge invariant.

4.1.3 Gauge theory interpretation

The effective model in Eq. (4.4) can be interpreted in the language of QLMs. We can identify

$$U_{\mathbf{i}m} = b^\dagger_{\mathbf{i}m}, \qquad U^\dagger_{\mathbf{i}m} = b_{\mathbf{i}m} \tag{4.5}$$

as the link operators of the associated LGT. In this way, the plaquette term has the desired form, and the mapping of the operators is such that the commutation relation of the QLMs are satisfied, using the hardcore bosonic commutation relations. Indeed, it is immediate to verify that

$$[U_{\mathbf{i}m}, U^{\dagger}_{\mathbf{j}m'}] = \delta_{\mathbf{ij}}\delta_{mm'}(2n_{\mathbf{i}m} - 1) = 2\delta_{\mathbf{ij}}\delta_{mm'}\left(n_{\mathbf{i}m} - \frac{1}{2}\right) \tag{4.6}$$

allowing for the identification of the electric field operator in terms of the particle number operator

$$E_{\mathbf{i}m} \equiv n_{\mathbf{i}m} - \frac{1}{2}. \tag{4.7}$$

As anticipated $[U_{\mathbf{i}m}, U^{\dagger}_{\mathbf{j}m'}] = 2\delta_{\mathbf{ij}}\delta_{mm'}E_{\mathbf{i}m}$. This is an explicit realization of the spin-1/2 QLMs, because, due to the hardcore boson constraint, the eigenvalues of $n_{\mathbf{i}m} \in \{0, 1\}$, and therefore the possible values of the electric fields are $E_{\mathbf{i}m} = \pm 1/2$. With this comparison, different particle sectors of the underlying bosonic theory are associated with different electric field sectors of the related QLM. While we have always assumed that the we were dealing with ultracold bosonic gases, the hardcore constraint makes the translation to fermionic link models trivial. As a consequence, and to the best of our knowledge, this constitutes the first proposal for the realization of the fermionic link models introduced in Ref.s [47, 48].

With the mapping in Eq. 4.5, the effective Hamiltonian derived in perturbation theory can be written in the gauge theoretical language as

$$\begin{aligned} H^{(\text{eff})} = \lambda_1 \sum_{\langle \mathbf{i},\mathbf{j}\rangle_d, m, m'} E_{\mathbf{i}m}E_{\mathbf{j}m'} - \sum_{\langle \mathbf{i},\mathbf{j}\rangle, m, m'} \lambda_2^{(mm')} E_{\mathbf{i}m}E_{\mathbf{j}m'} \\ + \sum_{\substack{\mathbf{i}',\mathbf{j},\mathbf{j}' \in \square \\ m,m'}} \lambda_3^{(mm')} E_{\mathbf{i}'m}E_{\mathbf{j}m'}E_{\mathbf{j}'m} - \sum_{\square} J^{(mm')}(U_{\square} + U^{\dagger}_{\square}) \end{aligned} \tag{4.8}$$

with $\lambda_1,\ \lambda_2,\ \lambda_3,\ J > 0$. We observe, as already commented, that the plaquette term is properly generated within this scheme alongside asymmetric terms containing the square of the electric field. The asymmetry in the sums and the different coefficients $\lambda_1,\ \lambda_2,\ \lambda_3$ are directly related to the construction of the spin-dependent optical lattice. The physics of the model in Eq. (4.8) can be analysed for some values of the parameters. We consider $\lambda_3 = 0$, to discuss what happens in the parameters space spanned by $\lambda_1,\ \lambda_2$. We also restrict our analysis to the half-filling case, since in this sector there is the fully flippable ground state of H_0. Clearly, for $\lambda_1 = \lambda_2 = 0$, our model is equivalent to the RK Hamiltonian with $\lambda = 0$. When the two parameters are switched on, we can discuss two limiting cases: for $\lambda_1 \gg \lambda_2$, the Hamiltonian favors the configurations in which the diagonals of the simulated lattice are independently filled as in the right panel of Fig. 4.3. In the opposite limit, i.e. for $\lambda_2 \gg \lambda_1$, the spin-exchange interaction between nearest neighbors dominates. When instead both the parameters are such that $\lambda_1,\ \lambda_2 \gg J$, this situation is exactly the one showed in Fig. 4.3. This is analogous to the $\lambda \to -\infty$ limit of the RK model, displaying

therefore a Néel state [16, 146]. We point out these features to highlight the fact that, despite the low-energy properties of Eq. (4.8) and the RK model are very similar, further considerations about the specific phases of our effective model at intermediate couplings may not be easy to guess. In general, we may expect that the two phase diagrams should be different, based on the different symmetries of Eq.s (4.8) and (1.29).

4.2 Extensions and generalizations

In this Section we discuss how to generalize our proposal to different cases. The most important is the extension to higher dimensions, and we discuss explicitly the $d = 3$ case. We then address how the proposal can be generalized to other geometries, with the aim to generate $U(1)$ plaquette terms in lower order perturbation theory and to extend our analysis to discrete gauge groups. Finally, we comment about the higher spin QLMs, closely related to the relaxation of the hardcore bosons constraint in the underlying microscopic model.

4.2.1 Higher dimensions: the $d = 3$ case

The extension to $d = 3$ is challenging for all the schemes that have been proposed so far in $d = 2$. In our proposal this is manifest by the increment of the number of atomic species. While the same perturbative method will exhibit gauge breaking terms, we argue that, by relying on angular momentum conservation, such terms are highly suppressed relatively to the gauge invariant dynamics.

To see this, we discuss how the extension to $d = 3$ would work by using the same lattice and the same number of internal states employed in $d = 2$, i.e. four out of five hyperfine levels of the spinor dipolar BEC. The principle that allowed the construction of the plaquette term in $d = 2$ was to associate the increase of the electric field in one of the links of the plaquette, with the decrease of one of the other links. We can then associate the change of two links with a single hopping term, and the full plaquette term with a correlated hopping. The resulting particles move in single (diagonal) lines. The exact same principles apply in $d = 3$. The extra dimension lifts the lines into planes, i.e., particles become confined in planes.

To identify these planes, it is useful to consider each link separately and construct the relative staples that constitute the set of all links which are coupled to the central one, as showed in Fig. 4.5. The centers of links of the lattice, where the particles reside, can be identified with the positions $(n_1, n_2, n_3) + \hat{\mu}/2$, with $\hat{\mu}$ one of the Cartesian unit vectors and n_ν integers. In Fig. 4.5 the cases $\mu = 1, 2, 3$ are represented in (a), (b) and (c) respectively. The links to which the particle can hop are colored the same as the particle. It becomes clear that particles at position

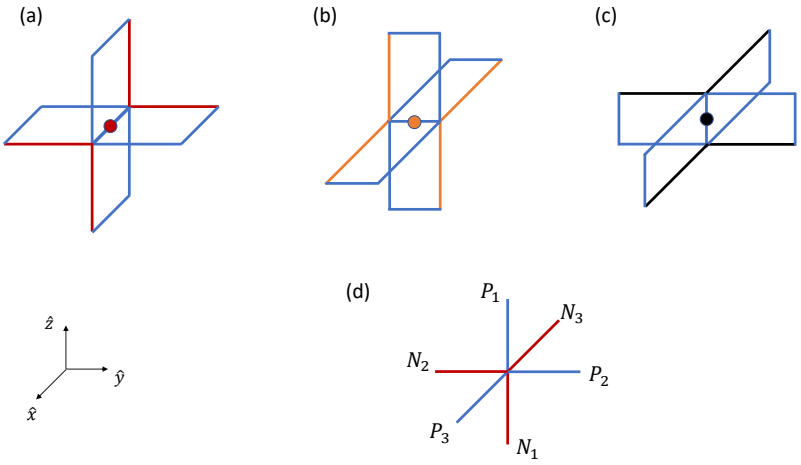

Figure 4.5: Structure of the staples for (a) x-links (red full dot), (b) y-links (orange full dot) and (c) z-links (black full dot) in $d = 3$. As in $d = 2$, we represent with blue links the target lattice. The full dots represent bosons. The colored links in (a)-(c) are the links that the particle can occupy after an hopping in the various possible directions. (d) Vertex structure in $d = 3$. The blue and red links identify the sublattices in which the particles moving in different planes can hop. The P_i, N_i are the possible internal states of the hardcore bosons at the given link.

$\mathbf{r} = (n_1, n_2, n_3) + \hat{\mu}/2$ can (only) hop to positions $\mathbf{r} \pm \hat{\mu}/2 \hat{\mp} \hat{\nu}/2$ with $\mu \neq \nu$. We can conclude that the planes along which the hardcore bosons move are described by the equation $\mathbf{r} \cdot \mathbf{n} = c$, where $\mathbf{n} = (1, 1, 1)$ and c is a constant that distinguishes the different parallel planes.

Having identified the planes, the subsequent task consists in identifying the values of angular momentum associated to each link in a way that allows for the generation of plaquette terms, but still forbids hoppings at the vertices, i.e. gauge symmetry breaking terms. The first part is constructed in complete parallel with the $d = 2$: by associating the same angular momentum to opposite links of the plaquette, we guarantee that the plaquette terms are such that conserve angular momentum. Guaranteeing that these are the only allowed processes is less straightforward. We refer to Fig. 4.5(d) to denote a generic vertex and call N_i and P_i the internal states of the two sublattices that are associated with two different planes. The full lattice is constructed by reflecting this vertex relatively to the different planes and gluing them, as represented in Fig. 4.6(a). The equations that must be imposed for N_i and P_i result from requiring two types of conditions. As a first point, differences of angular momentum across sublattices must be unequal so that such hoppings are removed from the dynamics. Secondly, within a sublattice, we must guarantee that each link does not have any neighbor with the same angular momentum in which it can hop to. These requirements lead to

$$|A_i - A_j| \neq |B_k - B_\ell|, \qquad \forall (i,j),(k,\ell) \in \{(1,2),(2,3),(3,1)\} \text{ and } A, B \in \{P, N\}, \tag{4.9}$$

$$N_i \neq N_j, \; P_i \neq P_j, \qquad N_i \neq P_j \qquad \forall i \neq j, \tag{4.10}$$

where the first equation comes from the first type of condition and the other two from the second. The inspection of these equations show that they cannot be satisfied with four levels, see Table 4.1

P_1	P_2	P_3	N_1	N_2	N_3
-3/2	1/2	7/2	-7/2	-5/2	7/2
-7/2	5/2	7/2	-7/2	-1/2	3/2
1/2	-3/2	7/2	-5/2	-7/2	7/2
5/2	-7/2	7/2	-1/2	-7/2	3/2

Table 4.1:: Some solutions to the Eq.s (4.9). As commented in the main text, it is impossible to satisfy them with the same number of internal levels employed in $d = 2$. To preserve the lattice structure and the scheme employed in the previous Section, we need five out of eight internal levels.

and the discussion in the caption. We conclude that to extend our scheme to $d = 3$ we have to increase the number of levels from four to *five* levels.

However, there is yet the problem that, even using five levels, we have the occurrence of gauge breaking terms of the form

$$H_{\rm GB} = -\frac{t_x t_y t_z}{h^2} \sum_{\mathbf{x},\mathbf{y}\in\Gamma} b^\dagger_{\mathbf{y}m} b_{\mathbf{x}m} \tag{4.11}$$

at the same order in perturbation theory as the plaquette term. If these terms are really competing with the plaquettes, the effective theory is not gauge invariant and this formulation needs further refinement. However, we remind that the presented perturbation theory scheme was introduced in order to offer a quantitative approach that shows how the plaquette term is the dominant dynamical process of the system, and that it can also emerge without conservation of angular momentum. If we follow the route of construction of plaquette terms solely by conservation of angular momentum, this process would correspond to tunneling to a third neighbor directly. In a real experimental setting, we expect that the atomic wave function can extend, even if slightly, to its nearest neighbors. Together with the dipolar interaction, which promotes exchange of angular momentum, the correlated hopping appears as the simplest dynamical process. In turn, the term above emerges through a triple hopping of a single particle, far beyond the point where the atomic wave function has an appreciable value, and is expected to be much more suppressed. We then expect that plaquette terms, which involve only nearest neighbors, are highly dominant over the above process.

In order to follow the perturbative approach, we need to use *ad hoc* hopping terms, which by the way must have a tunneling coefficient of opposite sign with respect to the sign of the $t_{x,y,z}$ hopping parameters entering the microscopic Hubbard Hamiltonian of Eq. (4.2). In principle, this can be accomplished by adding further lattices, one for each internal level, suitably located to allow just the needed hoppings. These have to be shaken lattices [**?**], in a way to enforce

the right sign for the hopping parameters. It is clear that this particular extension appears to be rather involved, and its realizability is far from being easy or conceivable. Finally, by modifying properly the superlattice structure, it could be possible to remove these third-order hoppings from the low-energy effective theory.

While it would be interesting to investigate if a suitable modification of the supperlatice would remove these terms in perturbation theory, we believe that the key advantage of the proposal is to tie the conservation of angular momentum to the correlated hopping that generates the plaquettes and, in that case, these processes should be irrelevant.

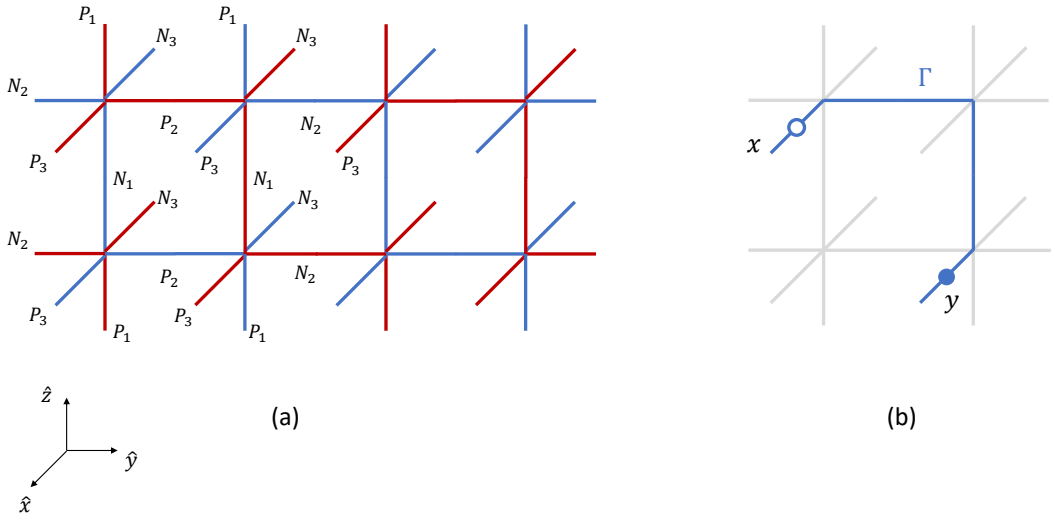

Figure 4.6: (a) Structure of the lattice in $d = 3$ with four out of five internal states. For the explicit values of the levels N_i, P_i we refer to Table 4.1. We highlight here with different colors the two sublattices in which the particles can hop, compatible with the planes identified in the main text. (b) Graphical structure of the gauge breaking terms that appear alongside the plaquettes, associated to a particle hopping from $\mathbf{x} \to \mathbf{y}$ along the blue path Γ.

4.2.2 Triangular lattice

The main purpose of this Section is to show that these principles are generalizable to other geometries and, inclusively, we can use fewer internal states to generate plaquette interactions in lower order in perturbation theory. In this specific case, we are able to use three consecutive internal states, i.e. a spin-1 dipolar BEC, to generate plaquettes at second-order in perturbation theory. Moreover, as we are going to discuss, the proposal looks arguably simpler in this geometry, if compared with the square lattice one. The phase diagram of the spin-1/2 QLMs on a triangular lattice, in the presence of the RK term, as been studied in [153].

The structure of the triangular lattice is presented in Fig. 4.7(b). The particles are constrained to hop along one-dimensional vertical lines, that we alternate with a set of two-level systems placed on the hypotenuses of the triangles. The sites of the spin-dependent optical lattice coincide with the sides of the target (triangular) lattice. According to the color code of Fig. 4.1, we use here the three internal states $m_F = 0, \pm 1$, that can be realized by using a spin-1 dipolar BEC. With this geometry, the plaquettes of the lattice can be identified graphically as in Fig. 4.7(a). They are made of three links and we adopt the convention $U_\triangle = U_z U_x U_y$, alongside the corresponding one for $U_\triangle^\dagger$. Here the Gauss' law takes a similar form, with the generator of gauge transformations being an oriented sum of the six links joining at each vertex of the triangular lattice. Explicitly $G(\mathbf{n}) = \sum_\mu [E_\mu(\mathbf{n}) - E_\mu(\mathbf{n} - \hat{\mu})]$, with μ representing the three directions x, y and z as in Fig. 4.7. By the judicious choice of the internal states for each site, again plaquette terms arise as the angular momentum conserving processes.

Again, this can be made precise by constructing an Hamiltonian along the same lines discussed before. If we denote by t_y the coefficient of the hopping term along the vertical lines, in the hardcore bosons limit the Hamiltonian reads

$$H_\triangle = H_{\rm hop} + H_{\rm int} \equiv -t_y \sum_{\langle \mathbf{i},\mathbf{j}\rangle_{\rm lines},m} (b^\dagger_{\mathbf{i}m} b_{\mathbf{j}m} + \text{h.c.}) + \frac{1}{2} \sum_{\langle \mathbf{i},\mathbf{j}\rangle,m,m'} V^{\mathbf{ij}}_{mm'} b^\dagger_{\mathbf{i}m} b^\dagger_{\mathbf{j}m'} b_{\mathbf{i}m'} b_{\mathbf{j}m}, \tag{4.12}$$

where the sum over nearest neighbors in the second term is extended to all the links of the triangular lattice, including the ones hosting the two-level systems. In turn, the hopping only occurs between neighbors along the line.

With this structure, we can proceed with perturbation theory exactly in the same logic of the square lattice, i.e. introducing H_0 as in Eq. (4.3) and take h as the largest scale in the system. While the first-order in the expansion vanishes, as in the square lattice, in this case the plaquette term emerges directly at second-order in perturbation theory. The effective Hamiltonian here contains two terms, i.e.

$$H^{(\rm eff)}_\triangle = -\frac{t_y^2}{h} \sum_{\langle \mathbf{i},\mathbf{j}\rangle_{\rm lines},m} n_{\mathbf{i}m}(1 - n_{\mathbf{j}m}) - \frac{t_y}{h} \sum_{\substack{\mathbf{i},\mathbf{j},\mathbf{k}\in\triangle \\ m,m'}} V^{\mathbf{jk}}_{mm'} b^\dagger_{\mathbf{k}m} b^\dagger_{\mathbf{j}m'} b_{\mathbf{k}m'} b_{\mathbf{i}m}, \tag{4.13}$$

where the first one is associated to back and forth hoppings along the lines, and the second one is the plaquette term. To make concrete the mapping with the gauge theory, we identify the link operators on the different sides of the triangle as

$$U_z = b^\dagger_{zm'} b_{zm}, \qquad U_y = b^\dagger_{ym}, \qquad U_x = b_{xm}, \tag{4.14}$$

making reference to the notation of Fig. 4.7(a). With this identification, the underlying LGT effective Hamiltonian has the form

$$H^{(\rm eff)}_\triangle = \lambda_\triangle \sum_{\langle i,j\rangle_{\rm lines},m} E_{\mathbf{i}m} E_{\mathbf{j}m} - \sum_\triangle J^{(mm')}_\triangle (U_\triangle + U^\dagger_\triangle). \tag{4.15}$$

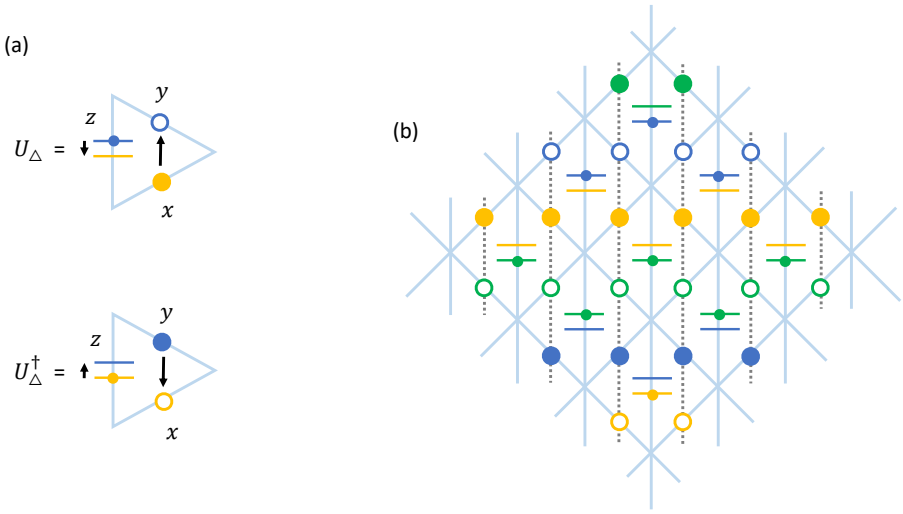

Figure 4.7: (a): Hopping processes generating the plaquette terms in the triangular lattice. (b): Structure of the triangular lattice using three internal states. The color code is the same of Fig. 4.1, while the horizontal lines are the two-level systems described in the main text. The grey dotted lines represent the $d = 1$ systems along which hopping processes can occur.

As in the square lattice case, we have the generation of the plaquette term plus an asymmetric term in the square of the electric field, due to the optical lattice structure. This is again different from the full RK model on the triangular lattice [153], and the various phases of the two models are in principle different.

4.2.3 Higher spin quantum link models

In Section 4.1.2 we showed how to simulate spin-1/2 QLMs using ultracold gases of hardcore bosons, i.e. working in the limit $U_0 \to \infty$. This allows for single particle occupations, and makes each link of the target lattice an effective spin-1/2 variable. Here we comment about the relaxation of the hardcore constraint on the ultracold bosons and about the quantum simulation of higher spin QLMs.

First of all, let us consider $U_0 \nrightarrow \infty$: then one could resort to a Schrieffer-Wolff transformation [154] to find the corresponding effective field theory and the terms generated by the finite U_0, i.e. the non-hardcore condition. Out of this procedure, one expects to obtain terms that can be incorporated at low energies in the parameters of the QLM: in other words, the QLM parameters are renormalized by U_0 (as an example see [155] for the computation in the case of the extended BH model at half-filling). Of course, this expectation is valid as soon that U_0 is varied in a way such that other phases appear.

The implementation of higher spin QLMs is related to the previous comment. Indeed, suppose that one is able to allow for multiple particles occupations at different sites of the optical lattice, e.g. that one can impose that in each site there may be at most a certain number of bosons of the same level. By imposing that the number of particles within the lattice is fixed, the above mentioned procedure could be used to obtain the simulation of higher spin QLMs. However, it is not a finite U_0 the key ingredient to have such models, but rather higher-body terms to fix the maximum occupation of the lattice sites.

4.3 Conclusions

In this Chapter we presented a proposal for the quantum simulation of Abelian spin-1/2 quantum link models (QLMs) using spinor dipolar Bose-Einstein condensates (BECs) loaded in spin-dependent optical lattice. We showed that plaquette interactions can be obtained by means of angular momentum conservation, and are directly related to correlated hoppings of bosons within a spin-dependent lattice.

In order to derive the effective theory corresponding to a gauge theory, we considered an extended Bose-Hubbard (BH) model with anisotropic hoppings and isotropic nearest neighbors interactions, with a further site-dependent energy penalty term to enforce the lattice structure. By means of a perturbative expansion we derived an effective Hamiltonian, whose gauge theoretical interpretation includes the plaquette interactions at third-order in perturbation theory. This process is associated to correlated hoppings of bosons within elementary squares, with a subsequent spin-dependent interaction to make their internal states compatible with the spin lattice structure. The use of angular momentum conservation in scattering processes to ensure gauge invariance was used in Ref. [24]: in that case, it guarantees that the gauge-matter interaction satisfies gauge invariance. By other side, plaquette terms are still obtained perturbatively. In contrast, our target model does not include matter and uses the conservation of angular momentum as a mean to obtain robust plaquette terms of the underlying pure gauge theory. The net result is that we have to use at least four internal states of a spinor dipolar gas, moving in one-dimensional chains coupled by the dipolar interactions. Without angular momentum conservation, on-site energies superimposed via additional superlattices are needed to produce the target lattice. We observe that to have a scheme valid far from the perturbative regime, i.e. where the on-site energies $H_i \propto h$ are not larger than other energy scales, or are even absent, requires that the particles can move and simultaneously be flipped, conserving angular momentum. That would give directly the plaquette terms, in exact parallel with gauge-matter coupling obtained in [24]. We think that it is worth to ascertain whether this can be concretely an advantage to simulate QLMs with respect to the perturbative scheme, where such requirements on the experimental control of the atoms are absent.

We further discussed possible extensions of our proposal to the triangular lattice, showing

that it is possible to lower the perturbative order at which the plaquette terms appear, with the proper choice of the spin-dependent lattice, and to higher spin QLMs, allowing for multiple site occupations with a fixed number of bosons. In this last case it is not trivial to generalize our proposal, since we get non-local effective interactions in the perturbative expansions, and the plaquette term is coupled to the electric field. Finally, our proposal can be generalized to the three-dimensional case by increasing the number of internal states employed in $d = 2$: with respect to the four levels used in $d = 2$, we need to use five internal states in $d = 3$. This is done by identifying the planes in which the particles move [48] and derive a set of equations for the internal states of the links in the third spatial directions. These equations can be satisfied at the cost of introducing extra atomic species. In the perturbative approach, gauge breaking terms emerge, which should be removed by adding *ad hoc* terms. These complications show, in our particular example, the difficulties of extending a scheme from $d = 2$ to $d = 3$.

To put our results in the wider context of quantum simulations of higher dimensional lattice gauge theories (LGTs), we observe that these last are currently challenging to realize in the realm of quantum simulators, even if there have been a lot of recent technical progresses in the field [127–130]. This is mainly due to local symmetry of the model, and its direct implementation in controllable physical systems. Our proposal employs many-body interaction symmetries to achieve this target. The main advantage of our scheme is to relate the local conservation of angular momentum to the gauge symmetric plaquette terms. Even in the perturbative approach, there is advantage coming from the order at which the plaquette terms come out with respect to Ref. [24], where it appears at fourth-order, here it shows up at third-order, involving only two correlated hoppings between bosons. A disadvantage is provided by the complications to generalize the scheme to $d = 3$, as discussed, anyway noticing that – to the best of our knowledge – the extension to $d = 3$ is an issue for all the schemes present in literature so far.

There are open questions that are worth to pursue. First of all, it would be interesting to understand the role of the additional terms coming from the perturbative expansion regarding the phase diagram of the model. In the gauge theoretical interpretation they are anisotropic in the electric field, and may give rise to a different phase diagram if compared with the Roksha-Kivelson (RK) Hamiltonian [39], based on symmetry arguments. From the condensed matter perspective, due to the extended nature of the Bose-Hubbard Hamiltonian, they could be related to supersolid phases [114–116]. Another important point regards the inclusion of matter. There is no straightforward way of doing this within this proposal but may be possible through the inclusion of ancillary particles. This difficulty is also present in the proposal of [21], where it is proposed a way to include static charges, but not dynamical ones. In the present proposal, static charges can be easily included by violating Gauss' law at the desired sites in the initial state. In the proposal of [24], instead, they include dynamical matter by increasing the number of fermionic species, in addition to the ancillary ones. Finally, it would be interesting to generalize the presented scheme to non-Abelian gauge theories. However, the advantage gained in encoding plaquettes in correlated

hopping is quickly lost by the increasing complicated substructure of the superlattice required by non-Abelian symmetries. A more reasonable goal may consist on considering discrete groups, in order to explore different physics and, possibly, simplify the superlattice structure.

Part III

Topological phases of lattice models

Chapter 5

Topology in condensed matter systems

In the last part of the Thesis we analyse the effects of static gauge fields on the dynamics of quantum particles [25, 94]. This is because, even if the back action of the matter fields is not considered, external gauge potentials provide a tool to play with the symmetries and the band structures of the model of interest, allowing for the investigation of novel topological phases in condensed matter systems. This last point raised a lot of interest in the scientific community in the recent years.

The role of topology in physics acquired a huge importance during the second half of the twentieth century. Indeed, prior to the 1980s, the Ginzburg-Landau theory [91] was the only framework able to characterize the stable phases of matter through a local order parameter, that is trivial in the disordered phase and non-trivial in the ordered one. Different ordered phases can be organized by how the order parameters transform under a symmetry operation. In this historical period this was the pillar for the study of phase transitions in condensed matter physics [125, 156].

The 1980 represents a turning point, due to the discovery of the integer quantum Hall effect (IQHE): this was the first example of a system showing no spontaneous symmetry breaking [157]. Von Klitzing and collaborators observed that at low temperature the energy spectra of a two-dimensional degenerate electron gas in a strong magnetic field display discrete energy bands, called Landau levels [157]. When the Fermi energy is in a gap between the energy levels, the system becomes insulating and the Hall conductance is quantized in units of e^2/h, being e the electric charge and h the Planck constant. This state breaks no symmetry, and the behaviour of the system depends on *topological invariants*, i.e. physical quantities independent of the geometry or microscopic properties of the system. Moreover, it was also argued that states confined to the edge of the system, called *edge states*, must carry the Hall current. There is a close relation between bulk topological invariants and the existence of these edge states, which is called *bulk-boundary correspondence*.

Four years later, in the 1984, thanks to the work of Berry about the geometric quantum phases [158], it emerged that the computation of the above mentioned topological invariants is related to the integral of the Berry field, over proper closed surfaces in momentum space. This was the first connection between the physical states that were not classified according to the Ginzburg-Landau paradigm and the realm of topology.

In this Chapter, we present the formalism of Berry's geometric quantum phases. In particular, we show that a quantum particle acquires a geometric phase under time evolution, called the *Berry phase*. This is a global, topological invariant related to a local, geometrical quantity called the *Berry curvature*. Finally, we present all these concept in three-dimensions, generalizing the topological phases to include *topological metals*. In particular, we will introduce the physical features of the Weyl semimetals, both in the continuum and on the lattice.

5.1 Berry phase and curvature

The theory of geometric phases can be seen as a manifestation of the adiabatic time evolution of Hamiltonians that are controlled by a time-dependent set of parameters [159]. We consider a set of parameters $\mathbf{a}(t)$, and an Hamiltonian $H[\mathbf{a}(t)]$ with a discrete and non-degenerate spectrum, without level crossing during the time evolution. According to the adiabatic theorem[1] [160, 161], the fact that the Hamiltonian is slowly changing should guarantee that the system remains in its evolving time-dependent ground state. This picture is however incomplete [158], and can be seen by considering the Schroedinger equation

$$i\partial_t \psi(t) = H[\mathbf{a}(t)]\psi(t) \tag{5.1}$$

with the introduction of the instantaneous set of eigenstates $\{\eta_k(t)\}$ such that

$$H[\mathbf{a}(t)]|\eta_k\rangle = \epsilon_k(t)|\eta_k\rangle, \qquad \psi(t) = \sum_k c_k(t)|\eta_k(t)\rangle. \tag{5.2}$$

By inserting this into the Schroedinger equation, we get a set of differential equations for the coefficients $c_k(t)$

$$\partial_t c_k(t) = -i\epsilon_k(t)c_k(t) - \sum_j c_j(t)\langle\eta_k(t)|\partial_t|\eta_j(t)\rangle. \tag{5.3}$$

Using the definition of instantaneous eigenstates introduced in Eq. (5.2) we have that

$$\langle\eta_k(t)|\partial_t|\eta_j(t)\rangle = \frac{\langle\eta_k(t)|\partial_t H(t)|\eta_j(t)\rangle}{\epsilon_j(t) - \epsilon_k(t)} \ll 1 \tag{5.4}$$

[1] A physical system remains in its instantaneous eigenstate if a given perturbation is acting on it slowly enough and if there is a gap between the eigenvalue and the rest of the Hamiltonian's spectrum.

within the assumptions of the adiabatic theorem. Thus we can solve for $c_k(t)$ by direct integration and find

$$c_k(t) = e^{i\alpha_{\rm dyn}(t)}e^{i\gamma(t)}, \qquad \psi(t) = \sum_k e^{i\alpha_{\rm dyn}(t)}e^{i\gamma(t)}|\eta_k(t)\rangle \tag{5.5}$$

where

$$\alpha_{\rm dyn}(t) \equiv -\int_0^t d\tau\ \epsilon_k(\tau), \qquad \gamma \equiv i\int_{\mathbf{a}(0)}^{\mathbf{a}(t)} \langle\eta_k|\nabla_{\mathbf{a}}|\eta_j\rangle \cdot d\mathbf{a}. \tag{5.6}$$

While $\alpha_{\rm dyn}$ is a dynamical phase, γ is the manifestation of the geometric aspects of the evolving system. When the Hamiltonian evolves adiabatically around a closed loop in the parameters space, the Berry phase is irreducible [158]. It can not be absorbed through a gauge transformation of the form $\psi(t) \to e^{i\mu}\tilde{\psi}(t)$ of the state, since there are closed loops such that

$$\oint_C \mathcal{A}\cdot d\mathbf{a} \bmod 2\pi \neq 0, \qquad \mathcal{A} \equiv i\langle\psi(\mathbf{a})|\nabla_{\mathbf{a}}|\psi(\mathbf{a})\rangle, \tag{5.7}$$

where C is a closed contour in the parameters space. This cyclic phase is observable, and it is called the *Berry phase*. For non-degenerate states, the freedom in the choice of the wave function is a local phase

$$\psi(\mathbf{a}) \ \to\ e^{i\theta(\mathbf{a})}\psi(\mathbf{a}), \qquad \mathcal{A} \ \to\ \mathcal{A} + \nabla_{\mathbf{a}}\theta. \tag{5.8}$$

This is reminiscent of the vector potential in electrodynamics, and for this analogy the field $\mathcal{A}$ is also referred to as the *Berry potential* (or field). Moreover, in $d = 3$ we can use the vector calculus to write that

$$\gamma = \oint_C \mathcal{A}\cdot d\mathbf{a} \bmod 2\pi = \int_{S(C)} \mathbf{\Omega}\cdot dS_{\mathbf{a}} \bmod 2\pi, \tag{5.9}$$

using the Stokes theorem, where $S(C)$ is a surface whose closed contour is C, and $dS_{\mathbf{a}}$ is the infinitesimal area element in the parameters space. Using again the analogy with electrodynamics, the field $\mathbf{\Omega}$ is like a magnetic field, and is called the *Berry curvature*. Its definition is

$$\mathbf{\Omega} \equiv \nabla_{\mathbf{a}} \times \mathcal{A} = \partial_\mu \mathcal{A}_\nu - \partial_\nu \mathcal{A}_\mu = -2\mathrm{Im}\langle\partial_\alpha\psi(\mathbf{a})|\partial_\beta\psi(\mathbf{a})\rangle. \tag{5.10}$$

This three-dimensional case highlighted a couple of similarities with the theory of electromagnetism, which is a $U(1)$ gauge theory. In this case, the gauge group is represented by the set of phases $e^{i\theta(\mathbf{a})}$: the relative vector potential and magnetic field are respectively the Berry field and curvature. The Berry phase, instead, can be seen as a flux through the closed surface $S(C)$, and being defined as the loop integral in Eq. (5.6), it is gauge-invariant and observable.

5.2 Chern number and topological invariants

The flux of the Berry curvature $\mathbf{\Omega}(\mathbf{a})$ through a closed surface S in the parameters space has a remarkable feature, i.e. it is a *quantized* quantity. This constitutes an example of a *topological*

invariant [159, 162]. If we specialize again to the $d = 3$ case and consider a spherical surface S^2, the quantization can be expressed as

$$C_1 = \frac{1}{2\pi} \int_{S^2} \mathbf{\Omega}(\mathbf{a}) \cdot dS_{\mathbf{a}} \in \mathbb{Z}. \tag{5.11}$$

The quantity C_1 is called *first Chern number*, and it is a robust topological invariant associated with physical observables, like the IQHE [157].

Concerning the characterization of topological invariants in condensed matter system, an important fact coming from the homotopy theory [163] is that if a given system has a finite number of bands N_{bands}, the sum of the Chern numbers associated to each band is zero

$$\sum_{k=1}^{N_{\text{bands}}} C_k = 0. \tag{5.12}$$

This statement implies that single-band systems can not have non-trivial topological invariants associated to their band structure. Therefore, to have non-trivial topological features in solid-state and condensed matter systems, we have to look at least to two-bands systems.

5.3 Three-dimensional topological metals

After the discoveries of the IQHE and its fractional counterpart [157, 164], several examples of topological phases were characterized in condensed matter systems. In particular, in 2010 the first three-dimensional topological systems involving all the previous features were the *topological insulators*, opening the door to novel phases of matter with bulk energy gaps and protected gapless edge states [165].

Later on, in 2011, another class of topological materials, called *Weyl semimetals* (WSMs) [166, 167], emerged as the first topological systems no longer constrained by a bulk energy gap protecting the topological nature of the energy bands. They are characterized by pairs of low-energy bulk excitations with linear dispersion, whose dynamics is described by the gapless Weyl equation. When the chemical potential coincides with the energy of the band-touching points, the system is a *topological semimetal*; if instead the chemical potential is not exactly equal to the band-touching energy the corresponding state of matter is called *topological metal* [168].

In a broad area of condensed matter physics, ranging from graphene [169] to high-T_c superconductors [123], two- and three-dimensional topological metals show electronic properties that can be described by Dirac and Weyl equations: the Dirac and Weyl particles describe the low-energy physics of real solid-state systems. While the physics originating the Weyl fermions in various systems may be different, the low-energy Hamiltonian descriptions and properties show the same Dirac points.

In the specific case of WSMs, that is the object of interest of this thesis, they have generated a lot of interest in the modern literature, as three-dimensional counterparts of graphene. There are also connections with the particle physics models of relativistic chiral fermions, solid-state topological and Chern insulators [26, 170]. Their peculiar electronic properties allow for the existence of protected surface states, novel responses to electromagnetic fields and charged Weyl fermions characterized by high mobilities.

In the next Sections we remind what are Weyl fermions in the continuum, in a way to introduce the Weyl Hamiltonian and the three main features that characterize a WSM. We pass then to the lattice framework, and present a class of lattice models hosting pairs of Weyl points in their spectra.

5.3.1 Weyl fermions

The massive Dirac equation for a particle of mass m, described by a spinor ψ, in $(d+1)$-dimensions reads

$$(i\gamma^\mu \partial_\mu - m)\psi = 0, \tag{5.13}$$

where the γ-matrices satisfy the algebra $\{\gamma^\mu, \gamma^\nu\} = 2\eta^{\mu\nu}$, with $\mu,\ \nu \in \{0, \dots, d\}$.

In odd spatial dimensions, i.e. when $d = (2k+1),\ k \in \mathbb{N}$, the Dirac equation can be written using the eigenstates of the fifth γ-matrix, which is defined as $\gamma^5 \equiv i^k \gamma^0 \gamma^1 \cdots \gamma^d$ [171]. If we move in momentum space in the spatial directions, where $\partial_i \to i p_i$, Eq. (5.13) can be written as

$$i\partial_t \psi = \gamma^0 m\psi + \sum_{j=1}^{d} \gamma^0 \gamma^j p_j \psi. \tag{5.14}$$

Due to the commutation properties of the γ-matrices, we have that $[\gamma^5, \gamma^0\gamma^j] = 0$. We notice that in even spatial dimensions, $d = 2k,\ k \in \mathbb{N}$, the matrix γ^5 reduces trivially to the identity matrix, and the previous rewriting is trivial.

We consider now two specific cases. For $d = 1$, we can represent the γ-matrices as $\gamma^0 = \sigma_z$, $\gamma^1 = i\sigma_y$ and $\gamma^5 = \gamma^0\gamma^1 = \sigma_x$, where σ are the Pauli matrices. In this case, the last equation reduces to

$$i\partial_t \psi = m\gamma^0 \psi + \gamma^0 \gamma^1 p_x \psi. \tag{5.15}$$

In the massless case, when $m = 0$, we can use the eigenstates of γ^5 to identify the underlying Hamiltonian. Indeed, by considering the states $\psi_\pm$ such that $\gamma^5 \psi_\pm = \pm\psi_\pm$, we have that

$$i\partial_t \psi_\pm = \pm p_x \psi_\pm, \tag{5.16}$$

that is the $(1+1)$-dimensional Weyl equation: it describes right-moving and left-moving chiral particles, whose dispersion relation is linear in the momentum, since $\epsilon(p_x) = \pm p_x$. We observe that when $m \neq 0$, the mass term causes the mix of the two chiralities.

Figure 5.1: Left panel: three-dimensional band dispersion relation $E(k)$ of two bands touching at two isolated Weyl points. The red (blue) outgoing (ingoing) arrows in the lowest cone represent the positive (negative) topological charge of the point. Right panel: Weyl nodes in the three-dimensional bulk Brillouin zone The ingoing (outgoing) arrows represent the negative (positive) topological charge. In the upper part of the cube, the topological surface state (yellow line) connects the projections of the Weyl points on the surface BZ (grey plane) .

We move now to $d = 3$. In this case, the γ-matrices are represented by the four-dimensional matrices $\gamma^0 = \mathbb{1} \otimes \sigma_x$, $\gamma^j = i\sigma_j \otimes \sigma_y$ and $\gamma^5 = -\mathbb{1} \otimes \sigma_z$. The Dirac equation reduces to

$$i\partial_t \psi_\pm = \mp \mathbf{p} \cdot \sigma \; \psi_\pm. \tag{5.17}$$

Out of this equation, which is the *Weyl equation* in $(3+1)-d$, we learn that the fermion propagates with spin that is parallel (or antiparallel) to its momentum. This defines the *chirality* $\chi = \pm 1$ of the Weyl fermion. From Eq. (5.17) it is immediate to read out the Hamiltonian, i.e.

$$\mathcal{H}(\mathbf{p}) = \chi \; \mathbf{p} \cdot \sigma, \tag{5.18}$$

which is called the *Weyl Hamiltonian*. Ultimately, this shows how Weyl fermions come out from the massless solutions of the relativistic Dirac equation.

5.3.2 Features of Weyl semimetals

In three-dimensional condensed matter systems, Weyl fermions may emerge as low-energy excitations of quantum materials. When two non-degenerate bands meet at isolated points in the Brillouin zone (BZ), close to the Weyl points they can be described using the Weyl Hamiltonian in Eq. (5.18).

The most prominent example is represented by WSMs. For these topological metals, the excitations in the bulk are gapless, but still the system has topological invariant and topologically protected gapless edge modes. In general the criteria to characterize WSM, at least in the standard case, are three [166, 168]:

1. linearly dispersing Weyl nodes in the bulk structure;
2. monopoles of Berry curvature originating at the location (in momentum space) of the Weyl points;
3. boundary modes connecting projections of Weyl nodes in the surface Brillouin zone (Fermi arcs).

In the remaining part of this Subsection, we elucidate the three items of the list, in a way to fully characterize the physics of WSMs.

Dispersion relation: Weyl nodes and density of states

We take as a reference the Weyl Hamiltonian in Eq. (5.18). Out of this, it is immediate to see that the dispersion relation is

$$\epsilon(\mathbf{p}) = \pm p \equiv \pm\sqrt{p_x^2 + p_y^2 + p_z^2}, \tag{5.19}$$

which is linear in the modulus of the momentum p. This gives rise to the conic structure showed in the left panel of Fig. 5.1, with the only difference that the cone of Eq. (5.19) is centered around $\mathbf{p} = \mathbf{0}$. Given this dispersion relation, we can compute the density of states

$$\rho(\epsilon) = \frac{1}{(2\pi)^3}\int_{\epsilon(\mathbf{k})=\epsilon} \frac{dS}{|\nabla_{\mathbf{p}}\epsilon(\mathbf{p})|} = \frac{\epsilon^2}{\pi^2}, \tag{5.20}$$

where dS is the infinitesimal surface element, and the surface integral is performed on a surface of constant energy $\epsilon(\mathbf{k}) = \epsilon$. The main property is that the density of states vanishes quadratically at the Weyl energy, a fact that is strongly related to the peculiar transport properties of WSMs, leading to a vanishing conductivity at low temperatures.

This simple computation for the Weyl Hamiltonian shows that the linearly dispersing Weyl points emerge quite naturally from the relative dispersion relation. This can be stated for a more general class of Hamiltonian [159]. Indeed, let us consider any system with a finite number of bands, and suppose that its Hamiltonian restricted to any couple of consecutive bands has the form

$$H = \mathbf{h}(\mathbf{p}) \cdot \sigma, \qquad \mathbf{h}(\mathbf{p}) \equiv (h_1(\mathbf{p}), h_2(\mathbf{p}), h_3(\mathbf{p})), \tag{5.21}$$

and we immediately read the dispersion relation

$$\epsilon_{\pm}(\mathbf{p}) = \pm\sqrt{h_1^2(\mathbf{p}) + h_2^2(\mathbf{p}) + h_3^2(\mathbf{p})}. \tag{5.22}$$

The expression for $\epsilon_\pm(\mathbf{p})$ implies that the two bands touch if $h_j(\mathbf{p})|_{\mathbf{p}=\mathbf{p}_0} = 0$, for a specific point $\mathbf{p}_0$ in momentum space. The role of the dimensionality here plays a crucial role. Indeed, in three dimensions the equation $h_{j_1}(\mathbf{p}) = 0$, for fixed j_1, defines a two-dimensional surface. The same happens if we consider $h_{j_2}(\mathbf{p}) = 0$, for $j_2 \neq j_1$. These two surfaces may intersect along lines, and if we introduce finally the third equation $h_{j_3}(\mathbf{p}) = 0$, with $j_3 \neq j_{1,2}$, the lines may intersect this last surface in isolated points in momentum space, without the need of fine-tuning [172]. In the two-dimensional case this would have been required necessarily to fine-tune one parameter.

Around the point $\mathbf{p} = \mathbf{p}_0$ we can linearize the Hamiltonian in Eq. (5.21) to obtain

$$H(\delta\mathbf{p}) = \epsilon_{\mathbf{p}_0} + \sum_{j=1}^{3} \mathbf{v}_j \cdot \delta\mathbf{p}\sigma_j, \qquad \delta\mathbf{p} \equiv \mathbf{p} - \mathbf{p_0}, \tag{5.23}$$

where $\epsilon_{\mathbf{p}_0}$ is the energy at the Weyl cone and $v_j \equiv \nabla_{\mathbf{p}} h_j(\mathbf{p})|_{\mathbf{p}=\mathbf{p}_0}$. This Hamiltonian describes Weyl nodes centered at $\mathbf{p} = \mathbf{p}_0$ in momentum space, with the possibility of having anisotropies in the spatial directions.

Monopoles of the Berry curvature

The eigenstates of the Weyl Hamiltonian in Eq. (5.18) are

$$\psi_\pm = \frac{\chi}{\sqrt{2p(p \pm \chi p_z)}} \begin{pmatrix} p_z \pm \chi p \\ p_x - i p_y \end{pmatrix}. \tag{5.24}$$

Out of them we can compute the components of the Berry fields and curvature, $\mathcal{A}_\pm(\mathbf{p})$ and $\mathbf{\Omega}_\pm(\mathbf{p})$, where we are considering $\mathbf{a} \equiv \mathbf{p}$ in the formalism of Sec. 5.1. Mathematically we have

$$\mathcal{A}_\pm(\mathbf{p}) = i\langle\psi_\pm(\mathbf{p})|\nabla_{\mathbf{p}}|\psi_\pm(\mathbf{p})\rangle, \qquad \mathbf{\Omega}_\pm(\mathbf{p}) = \nabla_{\mathbf{p}} \times \mathcal{A}_\pm(\mathbf{p}), \tag{5.25}$$

and using Eq. (5.24) we get that

$$\mathbf{\Omega}_\pm(\mathbf{p}) = \pm\frac{\chi}{2}\frac{\mathbf{p}}{p^3}. \tag{5.26}$$

This quantity is gauge-invariant, while the Berry field is gauge-dependent [159]. The mathematical structure of the Berry curvature in Eq. (5.26) has the form of a magnetic monopole field of charge $\pm\chi$ placed at the origin, since

$$\frac{1}{2\pi}\int_{S^2} \mathbf{\Omega}(\mathbf{p}) \cdot d\mathbf{S}_{\mathbf{p}} = \pm\chi. \tag{5.27}$$

We ultimately conclude that the Weyl points are monopoles in the BZ, with charges given by their chiralities, that can be considered as *topological charges* [168]. The sign of the charge indicates if the monopole represents a source or a sink (see both panels of Fig. 5.1).

Let us now consider a more general system with N Weyl points in its spectrum, located at $\mathbf{p} = \mathbf{p}_j$ and with chiralities χ_j, $j = 1, \ldots, N$. The total Berry curvature is

$$\mathbf{\Omega}(\mathbf{p}) = \sum_{j=1}^{N} \frac{\chi_j}{2} \frac{(\mathbf{p} - \mathbf{p}_j)}{p^3}. \tag{5.28}$$

We can integrate the divergence of this field over the whole BZ to get

$$\int_{\mathrm{BZ}(\mathbf{p})} d\mathbf{p}\ \nabla_{\mathbf{p}} \cdot \mathbf{\Omega}(\mathbf{p}) = 2\pi \sum_{j=1}^{N} \chi_j, \tag{5.29}$$

and further use the divergence theorem to rewrite the volume integral as

$$\int_{\mathrm{BZ}(\mathbf{p})} d\mathbf{p}\ \nabla_{\mathbf{p}} \cdot \mathbf{\Omega}(\mathbf{p}) = \int_{\partial \mathrm{BZ}(\mathbf{p})} dS_{\mathbf{p}} \cdot \mathbf{\Omega}(\mathbf{p}). \tag{5.30}$$

Since the BZ is topologically equivalent to a torus [104, 159], we have that $\partial\mathrm{BZ}(\mathbf{p})$ is trivial and the integral must vanish. We finally conclude that

$$\sum_{j=1}^{N} \chi_j = 0, \tag{5.31}$$

that is, the total chirality of Weyl nodes in the BZ is zero. This implies that, if Weyl nodes exist in a system, they must appear in pairs of opposite chiralities [173], constituting monopole-antimonopole pairs in the BZ, as in the right panel of Fig. 5.1.

Boundary modes: the Fermi arcs

A key property of WSMs is the presence of topological surface states reminiscent of topological insulators [165]. Since the Fermi surface is a set of discrete points in momentum space, these surface states, called *Fermi arcs*, stretch between the projections of the Weyl points on the surface BZ [166].

To concretely show what are the dispersion relation and wavefunction of the Fermi arcs, we consider a three-dimensional WSM with a boundary placed at $z = 0$ [174]. The starting point is again the Weyl Hamiltonian in Eq. (5.18), and we want to solve the system

$$\begin{cases} H(p_x, p_y, z)\psi = \epsilon_s \psi \\ N\psi|_{z=0} = 0, \end{cases} \tag{5.32}$$

where N is a generic Hermitian matrix parametrizing the boundary conditions of the system at $z = 0$. In Ref. [174] it is explicitly shown that the solution of the previous eigensystem, that gives

the dispersion relation ϵ_s and the wavefunction ψ_s of the surface states, is dictated by a single real boundary parameter θ. This is derived essentially by imposing the self-conjugacy of the Weyl Hamiltonian.

Since there is a boundary at $z = 0$, we can not consider p_z as a coordinate in momentum space, as there is no more the translation symmetry along the z-axis. We have then to consider $p_z \to -i\partial_z$ and solve the equation

$$H(p_x, p_y, -i\partial_z)\psi = \epsilon_s \psi \qquad \Rightarrow \qquad \begin{pmatrix} -i\partial_z - \epsilon_s & p_x - ip_y \\ p_x + ip_y & i\partial_z - \epsilon_s \end{pmatrix} \begin{pmatrix} \xi \\ \eta \end{pmatrix} = 0, \tag{5.33}$$

where in the last step we parametrized the field ψ using a 2-component spinor $\psi = (\xi, \eta)^T$ and exploited the structure of the Hamiltonian in terms of the Pauli matrices. The solution is

$$\begin{pmatrix} \xi \\ \eta \end{pmatrix} = e^{-\alpha(\epsilon_s)z} \begin{pmatrix} 1 \\ e^{2i\theta} \end{pmatrix}, \qquad \alpha(\epsilon_s) = p_x^2 + p_y^2 - \epsilon_s^2 > 0. \tag{5.34}$$

If we insert this into the eigensystem in Eq. (5.33), we find that the dispersion relation of the Fermi arc is

$$\epsilon_s(p_x, p_y, \theta) = -p_x \cos 2\theta - p_y \sin 2\theta, \qquad \alpha(p_x, p_y, \theta) = p_x \sin 2\theta - p_y \cos 2\theta. \tag{5.35}$$

It is explicit here the dependence on the boundary parameter. The Fermi arc is defined by $\epsilon_s = 0$, for vanishing chemical potential. Correspondingly, the wavefunction is

$$\psi_s(z) = \sqrt{\alpha(\epsilon_s)} e^{-\alpha(\epsilon_s)z} \begin{pmatrix} e^{-i\theta} \\ 1 \end{pmatrix}. \tag{5.36}$$

Due to the condition $\alpha(\epsilon_s) > 0$, the surface states exist only in a limited region of the momentum space.

To conclude, the dispersion relation of the Fermi arc is tangential to the Weyl cone and ends at the touching line on the Weyl cone. At zero energy, then, there is a Fermi arc in the surface BZ, ending at the Weyl points momenta.

Classification of Weyl points

In this Section we pointed out and clarified what are the features of an ideal WSM, and as a final part we give a symmetry argument to establish *a priori* what could be the number of Weyl points and their location in momentum space.

Due to the Kramers theorem, to have individually separed Weyl nodes we have to break either time-reversal (TR) or space-inversion (SI) symmetries [156, 159]. Let us then consider the Hamiltonian

$$H = \chi \sigma \cdot (\mathbf{p} - \mathbf{p_0}), \tag{5.37}$$

describing the Weyl node at $\mathbf{p} = \mathbf{p}_0$ with chirality χ, which transforms as

$$\text{TR}: \quad \mathbf{p} \to -\mathbf{p}, \quad \sigma \to -\sigma \quad \Rightarrow \quad H' = \chi\sigma \cdot (\mathbf{p} + \mathbf{p_0}), \tag{5.38}$$

$$\text{SI}: \quad \mathbf{p} \to -\mathbf{p}, \quad \sigma \to \sigma \quad \Rightarrow \quad H' = -\chi\sigma \cdot (\mathbf{p} + \mathbf{p_0}) \tag{5.39}$$

under the action of the above mentioned symmetries. This implies that for TR-invariant systems there must exist a Weyl point at $\mathbf{p} = -\mathbf{p}_0$ with the same chirality, while for SI-invariant systems the nodal point at $\mathbf{p} = -\mathbf{p}_0$ must have opposite chirality.

With this in mind, there are four possible cases:

1. presence of both symmetries: it is not possible to have individual Weyl points in momentum space, due to the Kramers theorem;
2. TR symmetry is broken in SI-invariant systems: there are at least two degenerate points at $\mathbf{p} = \pm\mathbf{p}_0$ with opposite topological charge;
3. SI symmetry is broken in TR-invariant systems: there are at least four Weyl points, because the doublet due to TR-invariance acquires a partner with opposite chirality;
4. absence of TR and SI symmetries: the position of the Weyl points may be everywhere in momentum space, and they may have different energies [173].

Out of this classification, we read that the simplest case of a model with a single pair of Weyl points with the same energy can be obtained by breaking explicitly TR symmetry and preserving, at the same time, SI symmetry.

5.3.3 A lattice model for Weyl semimetals: the Hofstadter model

To have a realization of the ideal WSM in a lattice model, we should consider a three-dimensional system that preserves SI symmetry and has the TR symmetry explicitly broken: this requires the presence of an external magnetic field, realizing the so-called *magnetic WSMs* [26, 159, 168, 170].

In generic dimensions, the physics of a single particle hopping on a hypercubic lattice in the presence of an external applied magnetic field is described by the *Hofstadter model*. In two dimensions, the Hofstadter model [89] is a paradigmatic example for the study of Chern insulators and the physics of the quantum Hall effect. Its spectrum as a function of the magnetic flux is the celebrated fractal Hofstadter butterfly, as showed in Fig. 5.2(a).

The three-dimensional version of the model on a cubic lattice with commensurate fluxes of the form $\Phi = 2\pi/n,\ n \in \mathbb{N}$, presents a complex and fractal spectrum as well [175, 176]. For $n = 2$,

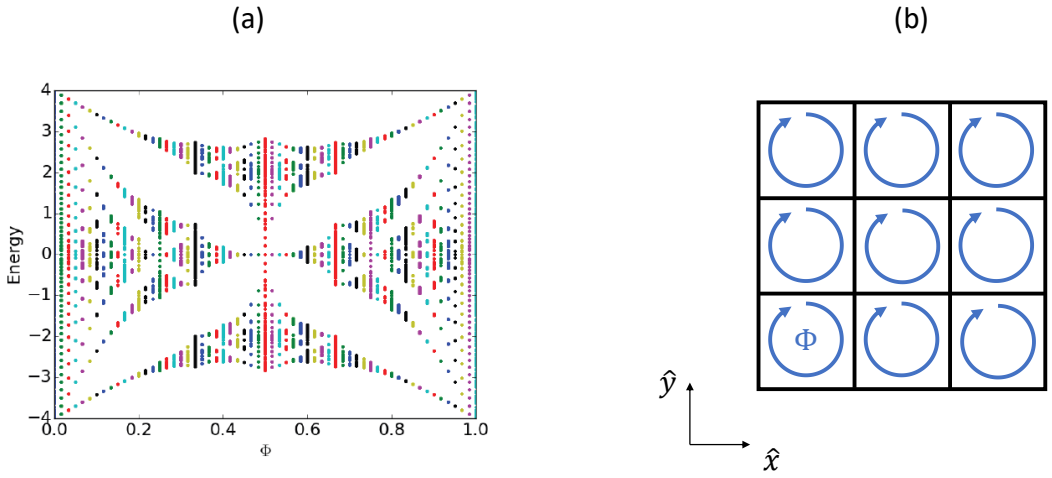

Figure 5.2: (a) Spectrum of the Hofstadter model in $d = 2$ for different magnetic fluxes Φ, reproducing the Hofstadter butterfly. The figure is taken from [38]. (b) Schematic illustration of the Hofstadter model on a square lattice, with magnetic flux Φ piercing the plaquettes of the lattice. The flux corresponds to the total phase accumulated by the wavefunction of a single particle which moves around the plaquette.

with $\Phi = \pi$, it realizes a WSM at half-filling [93, 177–179] which, in particular, does not break the physical TR and SI symmetries [180]. For $n \neq 2$, TR symmetry is broken and the system displays n connected energy bands. The spectrum is in general symmetric around zero energy due to the chiral sublattice symmetry. The Hamiltonian on a cubic lattice reads

$$H = -t \sum_{\mathbf{r},\hat{j}} c^{\dagger}_{\mathbf{r}+\hat{j}} e^{i\theta_j(\mathbf{r})} c_{\mathbf{r}} + \text{h.c.}, \qquad \theta_j(\mathbf{r}) = \int_{\mathbf{r}}^{\mathbf{r}+\hat{j}} \mathbf{A}(\mathbf{x}) \cdot d\mathbf{x}. \tag{5.40}$$

where t is the strenght of the hopping term, and the Peierls phases θ_j define the magnetic fluxes across all plaquettes.

Diagonalization of the model in momentum space

The Hofstadter model on a cubic lattice can be solved in momentum space, by taking advantage of the interplay between gauge and translational invariance in the presence of a commensurate background magnetic field. This allows for the introduction of the concept of a magnetic Brillouin zone (MBZ) [91], which can be defined for every choice of the gauge field $\mathbf{A}(\mathbf{x})$. We will focus on the case of a magnetic field $\Phi = 2\pi/n$ in all plaquettes ($n \in \mathbb{N}$), corresponding to a magnetic field $\mathbf{B} = \Phi\,(1,1,1)$. Other fluxes, such as $\Phi = 2\pi m/n$ ($m \in \mathbb{N}$), or orientations of the magnetic field, such as $\mathbf{B} \propto (0,1,1)$, yield analogous results.

Due to the presence of the Peierls phases in the Hamiltonian, the cubic lattice can be

decomposed in a certain number of independent sublattices, depending on the gauge choice. This arbitrariness can be used to determine the gauge generating the smallest number of the sublattices associated with Φ, i.e. the integer n. As analyzed in [94], on a $3d$ cubic lattice the minimal number of sublattices is given by n, and a convenient gauge to work with is the Hasegawa gauge [95], given by

$$\mathbf{A}(\mathbf{x}) = \Phi(0, x-y, y-x). \tag{5.41}$$

Within this gauge choice, the MBZ is

$$\text{MBZ}: \quad k_x \in \left[-\frac{\pi}{n}, \frac{\pi}{n}\right],\ k_y \in \left[-\frac{\pi}{n}, \frac{\pi}{n}\right],\ k_z \in \Big[-\pi, \pi\Big],. \tag{5.42}$$

The Hamiltonian can be written in terms of smaller independent blocks, the so-called magnetic bands. For each sublattice we have an associated band, and each one is n-fold degenerate. We observe that with $\mathbf{k} \in \text{MBZ}$ the allowed values for the momenta are N/n^2, and for each of them the matrix to be diagonalized has size $n \times n$. We then get N/n eigenvalues, each one with degeneracy n, matching the dimensionality of the problem in real space, see e.g. [94].

The expression of the Hofstadter Hamiltonian in momentum space is

$$\mathcal{H} = -t \sum_{\mathbf{k}\in\text{MBZ}} \sum_{\hat{j},s} c^\dagger_{s',\mathbf{k}} (T_{\hat{j}})_{s',s} e^{-i\mathbf{k}\cdot\hat{j}} c_{s,\mathbf{k}} + \text{h.c.}, \tag{5.43}$$

where s is an index labeling the sublattices, and the matrices $T_{\hat{j}}$ are

$$T_{\hat{x}} = \begin{pmatrix} 0 & 1 & 0 & 0 \\ 0 & 0 & \ddots & 0 \\ 0 & \cdots & 0 & 1 \\ 1 & 0 & \cdots & 0 \end{pmatrix}, \qquad T_{\hat{y}} = e^{-\frac{i\pi}{n}} \begin{pmatrix} 0 & \cdots & 0 & \varphi_0 \\ \varphi_1 & 0 & \cdots & 0 \\ 0 & \ddots & 0 & 0 \\ 0 & 0 & \varphi_{n-1} & 0 \end{pmatrix}, \qquad T_{\hat{z}} = \begin{pmatrix} \varphi_0 & 0 & \cdots & 0 \\ 0 & \varphi_{n-1} & 0 & 0 \\ 0 & 0 & \ddots & 0 \\ 0 & \cdots & 0 & \varphi_1 \end{pmatrix} \tag{5.44}$$

in the sublattice basis. In the previous expressions, we defined for the sake of simplicity $\varphi_l = e^{\frac{2\pi i l}{n}}$, with $l = 0, \ldots, n-1$. We observe that for $n \neq 2$ the matrices $T_{\hat{j}}$ are not invariant by the conjugate operation, reflecting the fact that time-reversal symmetry is broken by the presence of the external magnetic field. Moreover, the Hamiltonian in Eq. (5.40) has a chiral sublattice symmetry $c_{\mathbf{r}} \to (-1)^{x+y+z} c_{\mathbf{r}}$ that maps $\mathcal{H} \to -\mathcal{H}$. As a consequence, the model has a symmetric single-particle energy spectrum.

Chapter 6

Topological van Hove singularities at phase transitions in Weyl metals

In Chapter 5 we observed that Weyl semimetals (WSMs) [167, 181] are the simplest three-dimensional ($3d$) systems that combine a gapless spectrum with topological features. When their chemical potential matches the energy of the Weyl band-touching points, the Fermi surface shrinks to a discrete set of bulk points, and the low-energy transport properties are dominated by the topological surface features.

By shifting the chemical potential away from the Weyl nodes, the Fermi surface becomes in general a collection of two-dimensional Fermi sheets [182–184] surrounding, in momentum space, each band-touching point. They are characterized by a non-zero Chern number, realizing a topological metal [168]. By varying the chemical potential further away, the Fermi sheets typically merge, recovering trivial non-topological metallic states. This process not only constitutes a Lifshitz transition [185], due to the change of the topology of the Fermi surface, but it can also be seen as a *topological phase transition* (TPT) between two gapless states of matter, due to the change of the topological invariants associated with the Berry fluxes of the Fermi surface[1]. Therefore, not all the Lifshitz transitions are topological in this sense, and in the following we will refer to the non-topological Lifshitz transitions as *standard* Lifshitz transitions.

In this Chapter, we show that the TPTs between Weyl and trivial metallic phases are accompanied by van Hove (VH) singularities, as in the case of standard Lifshitz transitions, and they are signaled, in general, by peculiar magnetotransport features resulting from the vanishing chiral anomaly (see also [186]).

[1]To avoid any misunderstanding, we comment that very often the term TPT is used to denote a transition, as it occurs in 2D systems, where the gap closes and the topological invariants change. Here, we are considering 3D systems and the transition is between *gapless* phases, with a change of the topological invariants.

In $3d$ gapless systems, TPTs can be defined by changes of the topological invariants of the Fermi sheets, occurring at specific singular points. Additionally, Fermi surface singularities result in the presence of VH points, namely discontinuities in the energy derivative of the density of states (DOS). One can have a change in the topology of the Fermi surface, thus a Lifshitz transition [185], without a TPT. Therefore, not all the VH points are associated with TPTs. We will show that the TPTs between $3d$ topological and trivial metals, occurring when the chemical potential is varied, are characterized and accompanied by the appearance of VH singularities in the DOS.

As a case study, we will consider the $3d$ Hofstadter model, which offers a useful playground for modeling several topological metallic phases. Our choice is inspired by the recent progress in the engineering of quantum matter in artificial lattices with large effective magnetic fluxes, which encompasses many branches of many-body physics [187], including driven ultracold atoms trapped in an optical lattice [188–192], molecular nanostructures built with scanning tunneling microscopes [193, 194], moiré double-layer heterostructures [195, 196], and photonic crystals [197].

This Chapter is organized as follows: we firstly introduce the main general concept by analyzing a continuum model showing ideal Weyl points; we then discuss some characteristic properties of the TPTs based on their chiral anomaly signatures; in particular, we investigate the ballistic magnetotransport features of two toy models in proximity to the TPTs. After this first part we analyse the $3d$ Hofstadter model, and we present our result for generic magnetic fluxes. In the final part we summarize and present our conclusions.

6.1 General concept

To begin our discussion we use the minimal two-band toy model [183, 198–200] defined by:

$$H(\mathbf{k}) = \frac{v}{2k_0}\left(k_x^2 - k_0^2\right)\sigma_x + vk_y\sigma_y + vk_z\sigma_z - \mu\,. \tag{6.1}$$

For $\mu = 0$, the Hamiltonian (6.1) describes a WSM with two Weyl points of opposite topological charges located at $\mathbf{k}_W = (\pm k_0, 0, 0)$. Their linear dispersion is characterized by the same velocity v in all directions and the corresponding DOS quadratically vanishes at zero energy. For small variations of μ, the Fermi surface is composed by two (almost) spherical Fermi sheets of radius $|\mu/v|$ centered on each Weyl point, as in Fig. 6.1(c). These Fermi sheets are characterized by Chern numbers ± 1, matching the Weyl topological charges; thus the system is a topological metal [168, 182–184]. This topological phase survives until $|\mu| = vk_0/2$ (magenta lines in Fig. 6.2). Here, the two Fermi sheets become connected in the point $\mathbf{k_s} = (0, 0, 0)$, as in Fig. 6.1(b), with the result that the protected surface states completely overlap in momentum space with the zero-energy bulk states. For $|\mu| \geq vk_0/2$, there are paths within the Fermi surface connecting in momentum space the two Weyl points. $E_s \equiv vk_0/2$ is the minimum value of $|\mu|$ such that these paths open and, as a result, for $|\mu| = E_s$ the Fermi surface becomes a single connected surface with Chern number zero,

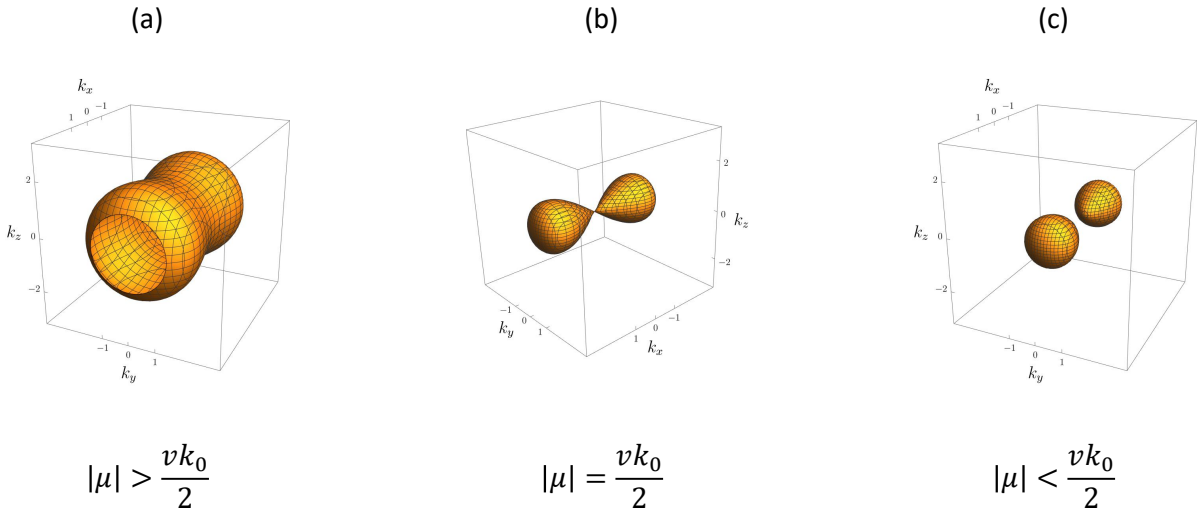

Figure 6.1: Fermi surfaces of the toy model in Eq. (6.1) for different values of the chemical potential. (a) $|\mu| > vk_0/2$: the Fermi surface has a single sheet enclosing the two Weyl points. (b) $|\mu| = vk_0/2$: the two blobs enclosing the Weyl points touch exactly at the van Hove singularity, showing the topological phase transition. (c) $|\mu| < vk_0/2$: two spherical sheets enclosing the Weyl points, each one with Chern number $C = \pm 1$, according to the chirality of the nodes.

as in Fig. 6.1(a), since it encloses two Weyl points with opposite charges. This is indeed a TPT between a topological metal at $|\mu| < E_s$ and a trivial metal for $|\mu| > E_s$.

In momentum space, $\mathbf{k_s}$ constitutes a saddle point for the energies of both bands, hence it gives rise to two VH singularities in the DOS $\rho(\epsilon)$ of the system at energies $\pm E_s$, which correspond to discontinuities in the derivative $d\rho/d\epsilon$, as shown in Fig. 6.2. These VH singularities can be observed through bulk transport measurements or the investigation of optical properties via ARPES techniques [26, 201, 202].

The concurrence of the TPT between topological and trivial metals and the appearance of a VH singularity in the DOS of the system is a general feature of Weyl metals. To be more specific, let us consider two energy bands connected by two Weyl points with opposite topological charges. These Weyl points may have different energies and different velocities (we exclude, however, the case of strongly tilted type-II Weyl points [203, 204]). For each path $\mathcal{K}$ between these two band-touching points in momentum space we can associate the differentiable function $\epsilon(\mathbf{k})$ with $\mathbf{k} \in \mathcal{K}$, describing the lowest band energy along $\mathcal{K}$. (analogous results are obtained for the highest bands). The Weyl points are local maxima of the energy. Therefore, for each $\mathcal{K}$, there exists at least one global minimum $\epsilon(\mathbf{k}_{\min})$. The TPT is located at $\mu = E_s$, where E_s is the maximum of the energy minima $\epsilon(\mathbf{k}_{\min})$ over the paths $\mathcal{K}$. This implies that $\nabla_k \epsilon(\mathbf{k_s}) = 0$. Then, E_s is a minimum of the energy along a path $\mathcal{K}$, but a maximum of the energy against variations of the path. Thus, in the most common scenario, it corresponds to a saddle point, and the vanishing of the velocity in this point

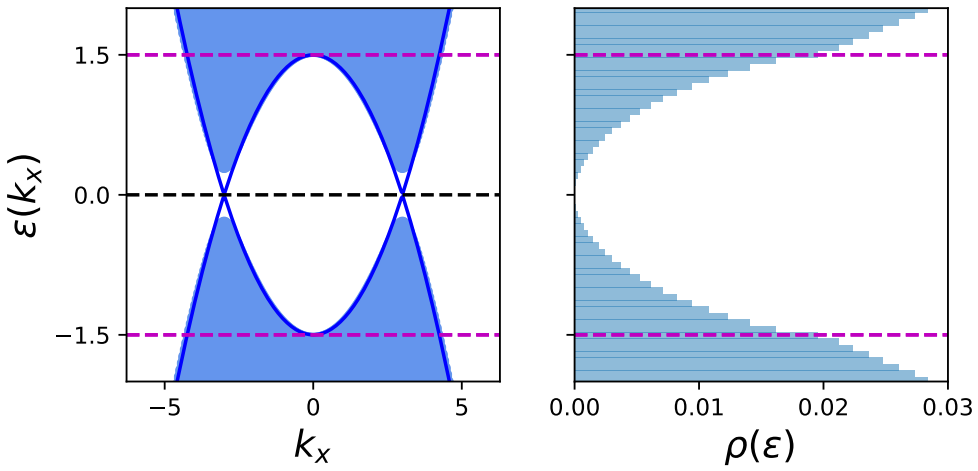

Figure 6.2: Dispersion relation of Eq. (6.1) for $k_z = 0$, alongside the associated DOS. We highlight the Weyl points energy $\epsilon = 0$ (black dashed line) and the VH singularities at $\epsilon = \pm E_s$ (magenta dashed lines). In this figure and in the following, energies are in units of t.

causes a VH singularity at $\epsilon = E_s$ (other situations with stronger VH singularities are possible as well).

The previous argument can also be rephrased by applying the Morse theory [205] to the differentiable function $\epsilon(\mathbf{k})$. In this framework, the critical points of $\epsilon(\mathbf{k})$, such that $\nabla_k \epsilon(\mathbf{k}) = 0$, correspond to a change in the topology of the level sets of the function, i.e. the Fermi surfaces. In addition, the presence of the Weyl points ensure the change in the Chern number giving rise to a TPT. In realistic tight-binding models, however, several additional VH singularities may appear that are not related to TPTs and that correspond to standard Lifshitz transitions. Therefore, in the following, we will distinguish *topological* VH singularities from trivial VH singularities.

The topological VH singularities we discussed so far are based on a variation of the Chern number of the Fermi sheets by ± 1. More complicated scenarios may be verified in systems presenting multi-Weyl points [206–210], or other kinds of band touching points with multiple topological charges [211–213].

Let us consider, for instance, the case of double Weyl points with topological charge ± 2. In these models, characterized by the presence of additional symmetries, additional topological VH singularities can appear that are associated with the merging of two Fermi sheets with Chern numbers ± 2. The set of TPTs in these gapless systems, however, is richer: when considering models with multiple bands, further band-touching points may cause TPTs in which a Fermi sheet with Chern number ± 2 split into two sheets with Chern number ± 1. These kinds of TPTs are not associated with VH singularities because they occur in correspondence with Weyl points connecting different bands, rather than saddle points appearing in a single band.

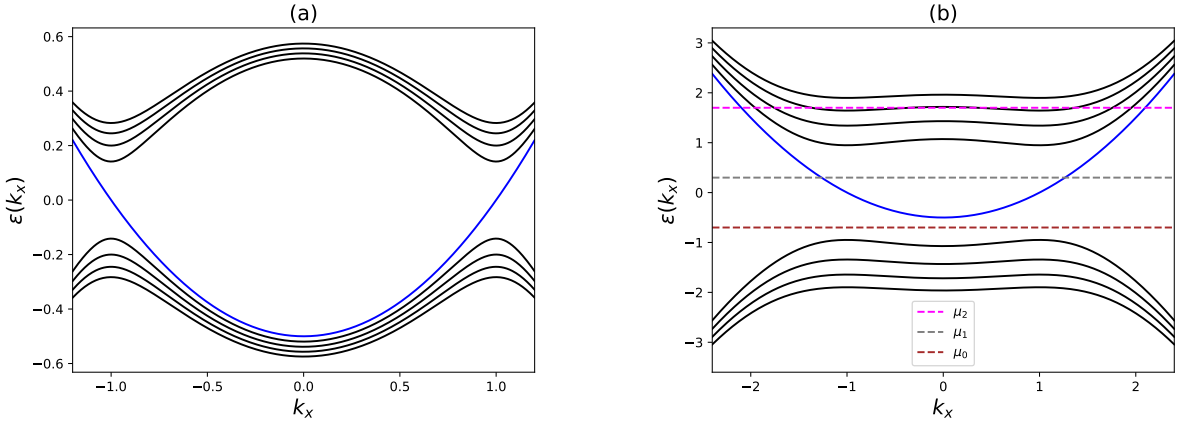

Figure 6.3: Landau levels $\epsilon_n(\mathbf{k})$ at fixed $k_y = k_z = 0$, up to $n = 5$, in the case of negative magnetic field in the two regimes $|B| < B_c$ (a), and $|B| > B_c$ (b). The chiral Landau level ($n = 0$) is plotted in blue. For large magnetic fields we distinguish the three regimes discussed in the main text: $\mu_0 \in (-\sqrt{|B|}, E_s)$ (brown dashed line), $\mu_1 \in [E_s, \sqrt{|B|})$ (gray dashed line), and $\mu_2 \geq \sqrt{|B|}$ (magenta dashed line).

6.2 Signatures of the chiral anomaly in the topological phases

Across a TPT, the topological invariants associated with the Fermi sheets change: in a topological metallic phase, the system presents disjoint Fermi sheets with different Chern numbers, which give rise to signatures associated with the onset of chiral anomaly [168]. Chiral anomaly is indeed one of the main distinguishing features of the topological phases and in the following we investigate the related response of a Weyl system upon the introduction of parallel magnetic and electric fields, when the chemical potential varies across a TPT.

6.2.1 Ideal Weyl points

We refer in particular to the toy model in Eq. (6.1), and we consider the application of a magnetic field along the direction of the Weyl points, i.e. $\mathbf{B} = B\hat{x}$. The dispersion of the corresponding Landau levels $\varepsilon_n^{\pm}(k_x)$ is easily calculated as a function of B [186]:

$$\varepsilon_n^{\pm}(\mathbf{k}) = \pm\sqrt{|B|n + \frac{v^2(k_x^2 - k_0^2)^2}{4k_0^2}}, \tag{6.2}$$

$$\varepsilon_0(\mathbf{k}) = -v\ \mathrm{sgn}(B)\frac{k_x^2 - k_0^2}{2k_0}. \tag{6.3}$$

The Landau level at $n = 0$ displays an opposite chiral behavior in proximity to the two Weyl points at $k_x = \pm k_0$. This chirality is exchanged when changing the sign of the magnetic field B, as a

result of the different wave function of the $n = 0$ Landau level. Hereafter we fix $B < 0$, but the following considerations hold for $B > 0$ and opposite energies. At fixed magnetic field, we can distinguish different regimes of the system depending on μ.

For weak magnetic fields $|B| < B_c = E_s^2$, the system is gapless for any μ, and indeed in Fig. 6.3 (a) there is at least one partially filled Landau level for any chemical potential. In this case, for $\mu < -E_s$ only non-chiral Landau levels contribute to the zero-temperature conductance of the system, while for $\mu > -E_s$ also the chiral $n = 0$ Landau level conducts. Based on the construction by Nielsen and Ninomiya [173], we conclude that the conservation of chirality of the bulk states is broken for $\mu > -E_s$.

At stronger fields, $|B| > B_c$ (the so-called quantum limit), the situation is qualitatively different and we can identify four regimes: for $\mu \geq \sqrt{|B|}$ [see μ_2 in Fig. 6.3 (b)] all the Landau levels $\varepsilon_n^+(\mathbf{k})$ contribute to the zero-temperature conductance; for $\mu \in [-E_s, \sqrt{|B|})$ [see μ_1 in Fig. 6.3 (b)] only the chiral Landau level contributes to the bulk conductance; for $\mu < -E_s$ [see μ_0 in Fig. 6.3 (b)] an insulating phase appears; for other values of μ only the non-chiral Landau levels $\varepsilon_n^-(\mathbf{k})$ conduct.

In summary, for the trivial phase at $|\mu| > E_s$ there exists a critical value of the magnetic field amplitude B_c above which an insulating phase appears. Within the topological phase at $|\mu| < E_s$, instead, the chiral Landau levels always contributes to the magnetoelectric transport, and, in particular, the system displays chiral anomaly. Another consequence of chiral anomaly is that in the topological phase for $|\mu| < E_s$, the system necessarily displays chiral Fermi arcs localized on any surface parallel to $\hat{x}$. In the trivial phase $|\mu| > E_s$, the Fermi arcs may instead vanish depending on the surface properties [200]. This implies that the topological phase necessarily displays anomalous Hall conductivity, which, instead, may vanish in the trivial phase.

6.2.2 Multiple Weyl points

The above argument relies on the assumption of an ideal Weyl semimetal with a single pair of Weyl points. In the following, we extend it to a more general class of Weyl systems, characterized by multiple pairs of Weyl points. We focus in particular on systems displaying a collection of well-separated Weyl dipoles, each constituted by two Weyl points with opposite charges displaced by a small momentum distance. Our analysis of the Landau levels in Eqs. (6.2),(6.3) can indeed be generalized to Hamiltonians of the form

$$H(\mathbf{k}) = \sum_{j=x,y,z} g_j(k_j)\sigma_j - \mu, \tag{6.4}$$

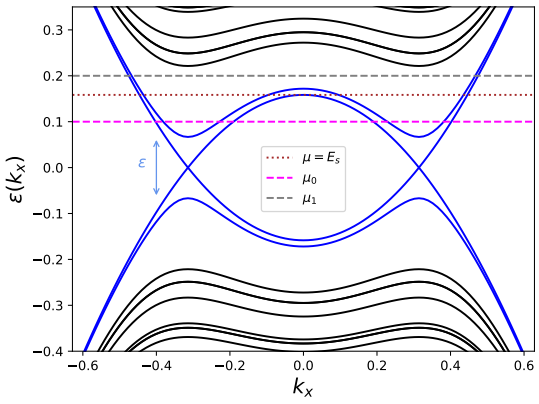

Figure 6.4: Landau levels $\varepsilon_n(\mathbf{k})$ of the model in Eq. (6.6) at fixed $k_z = \pi/2$, in the case of positive magnetic field $B \gtrsim B_c$. The chiral Landau levels ($n = 0$) are plotted in blue. We show two of the four regimes discussed in the main text: $\mu_0 \in [\epsilon, E_s]$ (magenta dashed line), $\mu_1 \in [E_s, \varepsilon_{1,\min}]$ (grey dashed line). The saddle point energy E_s (dotted brown line) is reported too.

and, to present a concrete example, we consider the following model of spin 1/2 fermions on a cubic lattice:

$$H_{\rm lat} = -\frac{v}{2\sin k_0}\sum_{\mathbf{r}}\left(c^\dagger_{\mathbf{r}+\hat{x}}\sigma_x c_{\mathbf{r}} + \text{H.c.}\right) + v\cot k_0 \sum_{\mathbf{r}} c^\dagger_{\mathbf{r}}\sigma_x c_{\mathbf{r}} \\ - \mu\sum_{\mathbf{r}} c^\dagger_{\mathbf{r}} c_{\mathbf{r}} + \frac{v}{2}\sum_{j=y,z}\sum_{\mathbf{r}}\left(ie^{i\theta_j(\mathbf{r})}c^\dagger_{\mathbf{r}+\hat{j}}\sigma_j c_{\mathbf{r}} + \text{H.c.}\right). \tag{6.5}$$

Here and in the following we set the lattice spacing to unit value. When the phases θ_j vanish, no magnetic field is present and the model displays four Weyl dipoles at $\mu = 0$, each oriented along k_x and with charges separated by $2k_0$, which we assume to be much smaller than π. In this case, $H_{\rm lat}$ describes a system that replicates four times the toy model in Eq. (6.5), with the four Weyl dipoles displaced by π in the k_y and k_z directions of the BZ, and characterized by alternating orientations. The topological VH singularities lie at energy $E_s = v\tan(k_0/2)$.

The Peierls phases θ_j introduce a magnetic field in the system, and, analogously to the previuous example, we consider a magnetic field $\mathbf{B} = B\hat{x}$ parallel to the Weyl dipoles. We adopt a Landau gauge and we set $\theta_y(\mathbf{r}) = 0$ and $\theta_z(\mathbf{r}) = By$. In this case, k_x, k_z are conserved momenta, and the problem is effectively reduced to a collection of $1d$ systems:

$$H(k_x, k_z) = \frac{v}{2}\sum_y\left(ic^\dagger_{y+1}\sigma_y c_y + \text{H.c.}\right) - v\sum_y c^\dagger_y\left[\frac{(\cos k_x - \cos k_0)}{\sin k_0}\sigma_x + \sin(k_z + By)\,\sigma_z + \mu\right]c_y. \tag{6.6}$$

This choice of the magnetic field gives rise to a set of Landau levels for each Weyl dipole, analogous to the ones discussed for the ideal Weyl model. In particular, we expect two chiral Landau levels

approaching zero energy and $k_x = \pm k_0$ for each chirality. Based on commensurability effects between B and the Weyl point momentum distance, however, these chiral Landau levels may display avoided crossings, determined by the non-linear momentum dependence along k_y and k_z of the original lattice model (see [214–216]). Depending on the value of B, these avoided crossings may affect all the chiral Landau levels, or only a subset (as in the case of Fig. 6.4), and they introduce a further energy scale in the problem, which we label with ϵ. This splitting of the chiral Landau levels can be considerable (see Fig. 6.4) and was discussed in [214, 216] for the ideal Weyl system in Eq. (6.5) with a magnetic field orthogonal to the Weyl point separation. However, an estimate of this energy scale in our model is a non-trivial problem, related to the solution of the generalized Harper model obtained by setting $k_x = \pm k_0$ in Eq. (6.6). Intuitively, we expect that ϵ grows with B, and with the ratio $2k_0/\pi$ between the separation in momentum space of the Weyl points in the same dipole and the momentum distance of different dipoles, but given its non-monotonic behavior in B, the ballistic transport properties of the system (6.6) are difficult to predict around zero energy.

Another effect of the non-linear perturbations of the dispersion of the cones, is that the critical field B_c for the onset of the quantum limit decreases below E_s^2. For a weak splitting of the chiral Landau levels, at fixed $B \gtrsim B_c$, we identify four main regimes (see Fig. 6.4):

1. for $\mu \lesssim \epsilon$, the conductance depends on the detail of the splitting of the chiral Landau levels, and, for specific values of B and system sizes, insulating phases may appear (consistently with the analysis in [214–216]);

2. for $\epsilon \lesssim |\mu| \lesssim E_s$, instead, the chiral Landau levels stemming from all the monopoles contribute to the bulk conductance G (see μ_0 in Fig. 6.4); thus, in the limit of ballistic transport[2].

$$G = \frac{4e^2}{h}\left(\frac{L^2}{2\pi l_B^2}\right), \tag{6.7}$$

   where L^2 is the area of the section of the system orthogonal to $\mathbf{B}$, and l_B is the magnetic length of the system;

3. for $|\mu| \in (E_s, \varepsilon_{1,\min}]$, where $\varepsilon_{1,\min}$ is the minimum of the energy of the non-chiral Landau levels, only the chiral Landau levels with a given chirality contribute to the transport (see μ_1 in Fig. 6.4), therefore

$$G = \frac{2e^2}{h}\left(\frac{L^2}{2\pi l_B^2}\right). \tag{6.8}$$

[2]We remind that the *ballsitic regime*, in the context of transport phenomena for Weyl metals, is defined by the condition $L > L_m \sim D/B$, where D is the diffusion coefficient $D \sim v_F \ell$, related to the mean-free path, and B is the applied external magnetic field. This has to be distinguished from the *diffusive regime*, where instead $L < L_m$.

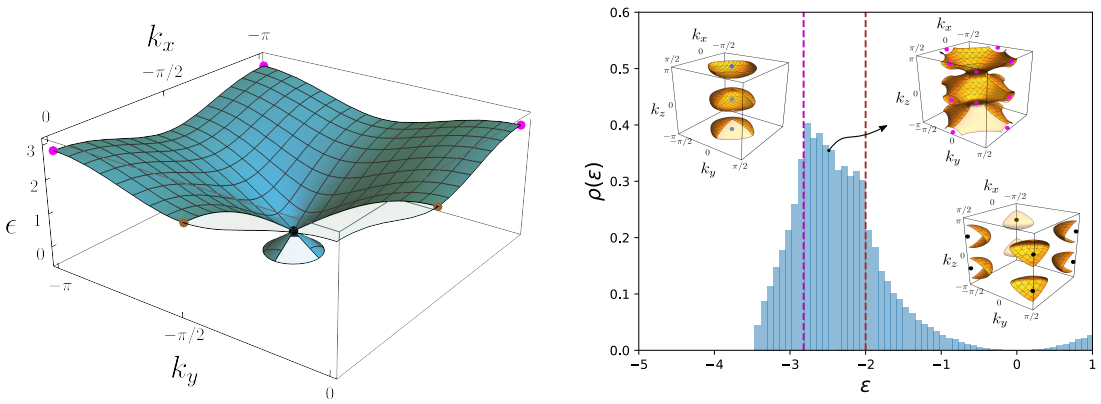

Figure 6.5: Left panel: second band in Eq. (6.10) for $k_z = \pi/2$ centered around the point $\mathbf{k}_{\mathbf{W}}^{-,-}$, together with the topological (brown dots) and trivial (magenta dots) VH singularities. Right panel: Hofstadter model DOS for $n = 2$ and $\epsilon \leq 1$. We highlight the topological (brown dashed lines) and trivial (magenta dashed lines) VH singularities. Insets: Fermi surfaces in the MBZ for the different regions of μ explored in the text, highlighting the main points in momentum space.

4. for $|\mu| > \varepsilon_{1,\min}$ also the Landau levels with $n \neq 0$ contribute to the conductance, increasing it at least by

$$\Delta G = \frac{4e^2}{h}\left(\frac{L^2}{2\pi l_B^2}\right). \tag{6.9}$$

In conclusion, at $|\mu| = E_s$ we expect a considerable variation in the number of channels contributing to the magnetotransport properties of the system in the large magnetic field regime; this gives rise to a peculiar discontinuity in the conductivity which drops from $G = 4\,(e^2/h)\,(L^2/2\pi l_B^2)$ on the topological side to $G = 2\,(e^2/h)\,(L^2/2\pi l_B^2)$ on the trivial side. Importantly, the aforementioned transport features do not appear, in general, if the system undergoes a standard Lifshitz transition.

6.3 The three-dimensional Hofstadter model

To investigate how trivial and topological metallic phases alternate in lattice models and the corresponding patterns of VH singularities, we consider, as a case study, the $3d$ Hofstadter model. We consider the Hamiltonian in Eq. (5.40) on a cubic lattice with commensurate magnetic fluxes $\Phi = 2\pi/n$ in all plaquettes ($n \in \mathbb{N}$), corresponding to a magnetic field $\mathbf{B} = \Phi\,(1,1,1)$ in units of the magnetic flux quantum.

6.3.1 Varying the magnetic flux

To study the model in Eq. (5.40) it is convenient to choose the Hasegawa gauge [95] $\mathbf{A}(\mathbf{r}) = \Phi(0, x-y, y-x)$ for the definition of the θ phases [94]. In the following, the behavior of the DOS, and the properties and location of the VH singularities, are studied for different values of $n \geq 2$.

The Weyl semimetal appearing at $n = 2$ is characterized by the band dispersion:

$$\epsilon(\mathbf{k}) = \pm 2t\sqrt{\cos^2 k_x + \cos^2 k_y + \cos^2 k_z}. \tag{6.10}$$

as explained in Section 5.3.3. It presents four inequivalent Weyl nodes in the magnetic Brillouin zone (MBZ), at $\mathbf{k_W}^{\pm,\pm} = (\pm\pi/2, \pm\pi/2, \pi/2)$. When $|\mu| < E_s \equiv 2t$, the Fermi surface is composed of four sheets with Chern number ± 1. As expected, at $\mu = \pm 2t$ the system undergoes a TPT, and the Fermi sheets merge in a single surface with vanishing Chern number. This phase transition is accompanied by a topological VH singularity, generated by the saddle points in $\mathbf{k_s} = (\pm\pi/2, \pm\pi/2, 0)$ (and the corresponding permutations within the MBZ; see the brown dots in Fig. 6.5). In the lowest band, the energy Hessian $\partial_{k_i}\partial_{k_j}\epsilon$ at the saddle points is diagonal with eigenvalues $2t\,\{1, -1, -1\}$, corresponding indeed to a minimum of the energy along the line joining two opposite Weyl points and to a local maximum in the orthogonal directions (the opposite happens in the highest band).

By inspecting the DOS and the spectrum, we clearly see other singularities at $\epsilon = \pm 2\sqrt{2}t$ corresponding to additional saddle points at $(0, 0, \pi/2)$ and the analogous points; see Fig. 6.5. These additional VH singularities can be understood by considering the behavior of the system for $-2\sqrt{3}t < \mu < -2\sqrt{2}t$, close to the minimum of the lowest band. In this regime, the Fermi surface is constituted by inequivalent disconnected sheets in the MBZ surrounding each band minimum (upper left inset in fig. 6.5). Each sheet has a vanishing Chern number. When $\mu = -2\sqrt{2}t$, these Fermi sheets merge in a single surface with zero Chern number (upper right inset in fig. 6.5), and the corresponding saddle points of the spectrum have a diagonal Hessian with eigenvalues $2t\,\{1, 1, -1\}$. The topology of the Fermi surface changes at this energy, thus the system undergoes a Lifshitz phase transition between two topologically trivial metallic phases [185]. Therefore, we label the VH singularities at $\mu = \pm 2\sqrt{2}t$ as topologically trivial.

Similar features characterize the Hofstadter model with $n = 3$. In this case, the three bands of the model are separated by inequivalent pairs of Weyl points: within the MBZ there are two Weyl cones between the first two bands located at energy $\epsilon = -\sqrt{3}t$ [95], and the symmetric cones between the second and third band at $\epsilon = \sqrt{3}t$. The system is thus in a Weyl semimetal phase when the chemical potential matches these energy levels, and the DOS vanishes quadratically at $\epsilon = \pm\sqrt{3}t$. By varying μ around the Weyl points, the system is in a metallic Weyl phase with disconnected Fermi sheets; the lowest and highest bands behave qualitatively as the bands in the $n = 2$ model. The central band, instead, presents two TPTs from the topological phases at $|\mu| > t$ to a trivial phase for $|\mu| < t$. Besides these topological VH singularities, we can detect other VH singularities corresponding to local extrema of the three energy bands. At the level of the Fermi

n	Energy (Weyl points → **boldface**; Topological VH singularities → red)
2	-2 **0** 2
3	-2.42 $-\sqrt{\mathbf{3}}$ -1.03 1.03 $\sqrt{\mathbf{3}}$ 2.42
4	-2.70 **-2.17** -1.63 -0.34 **0** 0.34 1.63 **2.17** 2.70
5	-2.71 **-2.34** -1.96 1.96 **2.34** 2.71
6	-2.67 **-2.43** -2.18 2.18 **2.43** 2.67
7	-2.60 **-2.50** -2.40 2.40 **2.50** 2.60

Table 6.1:: Energies of the Weyl points and their associated topological VH singularities for $2 \leq n < 8$.

surface, these singularities signal the appearance of particle or hole pockets, thus of trivial Fermi sheets, and do not change the topological properties of the system.

Let now consider $n \geq 3$. For n smaller than a "critical" value n_c, found to be $n_c = 8$, the DOS of the system shows isolated zeros at $\epsilon = \mp\epsilon_{w,n}$, corresponding to Weyl points that separate the lowest (and the highest) energy bands from the others. This result for n_c is consistent with the observation by Hasegawa [95] that, for $\Phi \lesssim 4\pi/31$, all the bands in the model overlap in energy. For $n < 8$, the filling at the Weyl point with negative energy is thus $\nu = \frac{1}{n}$, generalizing the well-known result for $n = 2$.

Around the energies $\epsilon_{w,n}$, the band structure is qualitatively similar to the $n = 2$ case: there are two energy thresholds $E^{\mp}_{s,n}$, corresponding to saddle points, which determine topological VH singularities, thus the system is in a topological metal phase for $E^{-}_{s,n} < |\mu| < E^{+}_{s,n}$. Additional trivial VH singularities appear at different energies, signaling trivial Lifshitz transitions.

The case $n = 4$ stands on its own, since a zero of the DOS is found also at $\epsilon = 0$, corresponding to two Weyl cones. These points overlap in energy with additional local extrema of the central bands, which are quadratically tangent to $\epsilon = 0$. As a consequence, in this case the DOS vanishes as $\rho(\epsilon) \sim \sqrt{|\epsilon|}$, and not quadratically, at $\epsilon = 0$, and the topological saddle points are doubled accordingly (see Appendix C.3). In particular, for $\mu \simeq 0$, the Fermi surface is made by four disconnected sheets: two of them enclose the bands' stationary points, with Chern numbers equal to zero, while the remaining enclose the Weyl points, with Chern number ± 1.

Concerning smaller fluxes, i.e. $n \geq n_c$, $\rho(\epsilon)$ does not display any zero. As a consequence, there are ranges of μ for which the system is in a multiband metallic state, whose Fermi surface contains sheets generated from consecutive bands.

Nonetheless, the system presents Weyl points at the energy $\epsilon = E_w$ between the first and the second band (and possibly between higher bands), whose presence is "hidden" by the band overlap. In this case, an additional VH singularity appears, which is associated with the minimum

of the second band, with energy $E_m < E_w$ (see Appendix C.2). This singularity signals a Lifshitz non-TPT between two topological metals, i.e. a single band metal for $\mu < E_m$ and a multiband metal for $\mu > E_m$, which corresponds to the opening of an electron pocket. The topological VH singularity is located at the lower energy $E_s^- < E_m$. Similar hidden Weyl points appear also between the intermediate bands for $n = 5, 6, 7$.

Our results on the Weyl points and their corresponding topological VH singularities for the Hofstadter model with $n < 8$ are summarized in the Table 6.1.

To conclude this Section, we comment about the characterization of the TPTs in the $3d$ Hofstadter model using the chiral anomaly ballistic transport signatures discussed above. The study of the magnetotransport in this model is a non-trivial task due to the commensurability effects induced by the presence of the magnetic field [217]. On general ground, the Landau levels analysis presented in Sec. 6.2 can be applied to the 3D Hofstadter model when considering small variations of the magnetic fluxes around a commensurate value in finite-size systems. In particular, a small flux perturbation of strength $|\delta\phi| = 2\pi/q$ around the value $\phi = 2\pi/n$ (with $q \gg n$) introduces a volume scale dependent on q below which the Nielsen-Ninomiya argument for the appearence of the chiral anomaly is expected to hold, in analogy to similar results for the DOS obtained in [180, 217]. A full analysis of the dependence on the magnetic perturbation of the Weyl points in the $3d$ Hofstadter model and their magnetotransport properties is a subject certainly deserving of further study.

6.4 Conclusions

We showed that the topological phase transitions (TPTs) in Weyl metals are signaled by the appearance of Van Hove (VH) singularities. As a function of the chemical potential, these transitions occur between a trivial phase, with a connected Fermi surface, and a topological phase, displaying disconnected Fermi sheets with non-zero Chern numbers. The related topological VH singularities manifest themselves as cusps in the DOS and are caused by the saddle points of the momentum space paths joining Weyl points with opposite chiralities. Their transport signatures may be enhanced for models displaying higher-order saddle points, whereas, in general, we expect them to vanish for strongly tilted (type-II) Weyl semimetals [203, 204].

To characterize these TPTs between different metallic states, we investigated some of the effects of the chiral anomaly and the Landau levels structure of these systems. Indeed, the chiral anomaly gives rise to peculiar behaviors in the magnetotransport of Weyl semimetals [218–221] and it allows us to distinguish topological and trivial phases. In particular, we studied the ballistic bulk magnetoconductance of relevant Weyl metal toy models. We verified that for sufficiently high magnetic fields with suitable orientation, the conductance of these systems displays a characteristic

reduction by varying the chemical potential across a topological VH singularity from the topological to the trivial phase. In the case of ideal Weyl systems in this extreme quantum limit, insulating phases may appear in the trivial phase under strong magnetic fields [186, 214–216]; for models with multiple pairs of Weyl points instead, the most common scenario corresponds to halving of the conductance. This discontinuity of the magnetoconductance is typical of the topological VH transitions, and it does not appear for standard Lifshitz transitions.

As an illustrative example of the onset of topological VH singularities, interesting *per se*, we investigated the Hofstadter model on a $3d$ cubic lattice as a function of the magnetic flux Φ of the form $\Phi = 2\pi/n$, which hosts several trivial and topological gapless phases when n is varied, and is relevant for the study of novel superconducting materials [222, 223]. For $n < 8$, its lowest bands do not overlap, and we identified the TPTs by inspecting directly the singular points of the DOS. For $n \geq 8$ the bands overlap, and Lifshitz transitions between single and multiband metallic phases can be identified. Our analysis opens the possibility of defininig a $3d$ analog of the Hofstadter butterfly by distinguishing it as a function of the flux and the chemical potential trivial and topological gapless phases.

Analogous features can be investigated for generic fluxes of the form $\Phi = 2\pi m/n$ and generic filling. For each $m > 1$, we expect the existence of a critical value of n, which separates phases without and with overlapping bands. In any case presenting Weyl cones between neighboring bands, TPTs are identified by the topological VH singularities. The behavior of the model for general m/n is non-trivial due to the fractal nature of the spectrum; a natural question, however, would be to verify the existence of a general limit Φ_c of the critical flux for large m (and study its dependence on the filling).

Depending on the physical system of interest, the topological VH singularities discussed in this Chapter can be detected through different methods, e.g. ARPES techniques, scanning tunneling spectroscopy and microscopy, and optical and transport measurements [26]. The Hofstadter model can be realized in ultracold atom quantum simulations with artificial gauge fluxes [187–189, 191]. In this context, several techniques have been successfully applied to detect the presence of band-touching points, including Landau-Zener scattering processes [224], interferometric experiments [225] and Bragg spectroscopy [226]. Furthermore, very recent works allow for the experimental realization of Weyl semimetals by engineering $2d$ and $3d$ spin-orbit couplings [227], presenting different methods to locate the position of the Weyl nodes in momentum space and to measure the Berry curvature [228].

Finally, we comment that it would be interesting to study the fate of the topological VH singularities and the associated topological phase transitions discussed here in the case of higher-order Weyl metals, such as the ones studied in [229, 230], and when the dimension d is increased. Moreover, a deserving line of activity could be the study of the role of the topological VH singularities in the determination of the superconducting/superfluid-metal critical temperature

transition when an attractive interaction is introduced [223], especially when it may be tailored in order to preserve the topological properties.

Part IV

Appendix

Appendix A

A gauge invariant reformulation and applications to mean-field computations

Here we provide additional information about the gauge invariant mean-field application of the formalism presented in Chapter 2. More work on these lines is currently pursued.

A.1 $(1+1)-d$ Abelian gauge theory in different constructions

We reformulate the pure gauge action in Eq. (1.23) in $(1+1)-d$, using both the symmetric and the asymmetric constructions. Explicitly we have that

$$S_G = \frac{1}{e^2}\sum_{\mathbf{n}}\left[1-\frac{U_{01}(\mathbf{n})+U_{01}^{\dagger}(\mathbf{n})}{2}\right]. \tag{A.1}$$

Using firstly the symmetric construction, we simply have $A_0 = \Delta_0\phi + \bar{F}_{01}/2$ and $A_1 = \Delta_1\phi + \bar{F}_{10}/2$ at each site $\mathbf{n}$ of the lattice. For the moment, we do not specific the boundary conditions and keep the discussion at a general level. We denote with $\bar{U}_{\mu\nu}$ the plaquette written in terms of the variables $\bar{F}_{\mu\nu}$, whose expression is

$$\bar{U}_{01}(\mathbf{n}) = \exp\left[i\frac{e}{2}\mathcal{F}(\mathbf{n})\right], \qquad \mathcal{F}(\mathbf{n}) = \bar{F}_{01}(\mathbf{n}) + \bar{F}_{10}(\mathbf{n}+\hat{0}) - \bar{F}_{10}(\mathbf{n}) - \bar{F}_{10}(\mathbf{n}+\hat{1}). \tag{A.2}$$

The action is then

$$S_{\text{sym}} \equiv \frac{1}{e^2}\sum_{\mathbf{n}}\left[1-\frac{1}{2}(\bar{U}_{01}(\mathbf{n})+\bar{U}_{01}^{\dagger}(\mathbf{n}))\right], \tag{A.3}$$

but the strips $\bar{F}_{10}$, $\bar{F}_{01}$ are not independent, as they satisfy Eq. (2.26). At the level of partition function, we include the Mandelstam constraints as

$$Z_{\text{sym}} = \int \mathcal{D}\bar{F}_{10}\mathcal{D}\bar{F}_{01}\; e^{-\beta S_{\text{sym}}}\;\delta(\mathcal{G}(\mathbf{n})), \tag{A.4}$$

$$\mathcal{G}(\mathbf{n}) \equiv \sum_{\mathbf{n}} [\bar{F}_{01}(\mathbf{n}) + \bar{F}_{10}(\mathbf{n}) - \bar{F}_{10}(\mathbf{n}+\hat{0}) - \bar{F}_{01}(\mathbf{n}+\hat{1})]. \tag{A.5}$$

A.1.1 Exact resolution of the Mandelstam constraint

Particularly simple here is to resolve the constraint, and sum over one of the two fields. For example, we can express $\mathcal{F}(\mathbf{n})$ only in terms of $\bar{F}_{01}$ and get

$$\mathcal{F}(\mathbf{n}) = 2[\bar{F}_{01}(\mathbf{n}) - \bar{F}_{01}(\mathbf{n}+\hat{1})] \;\Rightarrow\; \bar{U}_{01} = \exp\big\{\{ie[\bar{F}_{01}(\mathbf{n}) - \bar{F}_{01}(\mathbf{n}+\hat{1})]\}\big\}. \tag{A.6}$$

This is nothing but the plaquette U_{01} reformulated within the asymmetric construction $\{\phi, \bar{F}_{01}\}$. This is not surprising, since the partition function of the theory Z, whatever is the reformulation, must be the same. Therefore we must have $Z_{\rm sym} = Z_{\rm asym}$. which is

$$Z_{\rm asym} = \int \mathcal{D}\bar{F}_{01} \underbrace{\left(\int \mathcal{D}\bar{F}_{10}\, e^{-\beta S_{\rm sym}}\, \delta(\mathcal{G}(\mathbf{n})) \right)}_{\equiv e^{-\beta S_{\rm asym}}} = \int \mathcal{D}\bar{F}_{01}\, e^{-\beta S_{\rm asym}}. \tag{A.7}$$

This defines the reformulated action in the asymmetric construction as a function of the symmetric one:

$$S_{\rm asym} = -\frac{1}{\beta} \log \left(\int \mathcal{D}\bar{F}_{10}\, e^{-\beta S_{\rm sym}}\, \delta(\mathcal{G}(\mathbf{n})) \right). \tag{A.8}$$

As a quick comment, this can be generalized also to higher dimensions: the difficulty, as already discussed in Section 2.4, regards the integration of the Mandelstam constraints, which may be in general a non-trivial task. This highlights the fact that the asymmetric construction is the only one with the minimum number of independent variables[1].

A.1.2 Constraint imposed at the mean-field level

Let us forget about the exact integration of the constraint, and discuss what happens if we try to deal with it at the mean-field level. The proper way to do this would be to write the $\delta(\mathcal{G})$ in its exponential form

$$Z_{\rm sym} = \int \mathcal{D}\bar{F}_{\mu\nu} e^{-\beta S_{\rm sym}[\bar{F}]}\, \delta(\mathcal{G}(\mathbf{n})) = \int_{-\infty}^{+\infty} d\eta \int \mathcal{D}\bar{F}_{\mu\nu}\, e^{-\beta S_{\rm sym}[\bar{F}] + i\eta\mathcal{G}(\mathbf{n})}, \tag{A.9}$$

where $\eta \in \mathbb{R}$. Since we want to take $W = \langle \bar{U}_\mu \rangle$ as (gauge invariant) order parameter, it would be better to further change variables to the links and rewrite the functional as

$$Z_{\rm sym} = \int_{-\infty}^{+\infty} d\eta \int \mathcal{D}\bar{U}_\mu\, |J(\bar{U}_\mu)|\, e^{-\beta S_{\rm sym}[\bar{U}] + i\eta\mathcal{G}(\mathbf{n})}, \tag{A.10}$$

[1]This however does not mean that it is automatically the best choice to begin with, if the purpose is to build proper approximation schemes for the starting theory.

both for open and periodic boundary conditions, up to the determinant of the Jacobian of the change of variables $|J(\bar{U}_\mu)|$. Therefore, we can take

$$W \equiv \langle \bar{U}_\mu \rangle = \left\langle \exp\left\{ ie \sum_{\mu\neq\nu} \alpha^\nu \bar{F}_{\mu\nu} \right\} \right\rangle \tag{A.11}$$

as order parameter in the effective action $S_{\text{eff}} \equiv S_{\text{sym}} - i\eta/\beta \cdot \mathcal{G}(\mathbf{n}) - \log|J(\bar{U}_\mu)|$, and perform the functional derivatives with respect to $\bar{U}_\mu$ directly, in order to derive the self-consistent equations.

Besides these observations, holding in general dimensions, for $d = 1$ we have that

$$\begin{cases} \bar{U}_0 = e^{ie\bar{F}_{01}/2} \\ \bar{U}_1 = e^{ie\bar{F}_{10}/2} \end{cases} \quad \rightarrow \quad \begin{cases} \bar{F}_{01} = \frac{2}{ie}\log \bar{U}_0 \\ \bar{F}_{10} = \frac{2}{ie}\log \bar{U}_1 \end{cases} \quad , \qquad |J(\bar{U}_\mu)| = \frac{4}{e^2}\frac{1}{\bar{U}_0\bar{U}_1}, \tag{A.12}$$

and the effective action is

$$S_{\text{eff}}[\bar{U}] = S_{\text{sym}}[\bar{U}_0, \bar{U}_1] - \sum_{\mathbf{n}} \log \bar{U}_0(\mathbf{n})\bar{U}_1(\mathbf{n}) - \frac{2\eta}{e\beta}\sum_{\mathbf{n}} \log\left[\frac{\bar{U}_0(\mathbf{n})\bar{U}_1(\mathbf{n}+\hat{0})}{\bar{U}_1(\mathbf{n})\bar{U}_0(\mathbf{n}+\hat{1})}\right]. \tag{A.13}$$

By writing $\bar{U} = W + \delta\bar{U}$, and assuming $W \in \mathbb{R}$ for the mean-field ansatz, we have that

$$S_{\text{sym}}[\delta\bar{U}] - \log|J(\delta\bar{U})| = \frac{1}{e^2}\left[1 - \left(W^3 + \frac{2e^2}{W}\right)(\delta\bar{U} + \delta\bar{U}^\dagger)\right] + \frac{2W^4}{e^2} - 2\log W, \tag{A.14}$$

while the ratio appearing in the Mandelstam constraints reduces to

$$\frac{\bar{U}_0(\mathbf{n})\bar{U}_1(\mathbf{n}+\hat{0})}{\bar{U}_1(\mathbf{n})\bar{U}_0(\mathbf{n}+\hat{1})} = \frac{W^2 + 2W\delta\bar{U} + O(\delta\bar{U})^2}{[W+\delta\bar{U}]^2} = 1 + O(\delta\bar{U})^2. \tag{A.15}$$

The meaning of this is that, if we neglect higher orders in the fluctuations, the Mandelstam constraints vanish at the mean-field order, since we have $\log[1+O(\delta\bar{U})^2] \to 0$ in the effective action. Therefore, using this order parameter W, at the mean-field level the symmetric construction does not see the Mandelstam constraints. They are taken into account only by going at subsequent order in the mean-field expansion.

The effective action then reduces to $S_{\text{eff}}[\delta\bar{U}] \rightarrow S_{\text{sym}}[\delta\bar{U}] - \log|J(\delta\bar{U})|$, with W that satisfies the self-consistent equation

$$\frac{\delta S_{\text{eff}}}{\delta\bar{U}} = 0 \qquad \Rightarrow \qquad 2\beta\tilde{W} = \frac{I_1(2\beta\tilde{W})}{I_0(2\beta\tilde{W})}, \qquad \tilde{W} \equiv \left(W^3 + \frac{2e^2}{W}\right), \tag{A.16}$$

where

$$I_0(x) \equiv \frac{1}{\pi}\int_0^\pi e^{x\cos\theta}\, d\theta, \qquad I_1(x) \equiv \frac{1}{\pi}\int_0^\pi e^{x\cos\theta}\cos\theta\, d\theta \tag{A.17}$$

are standard modified Bessel functions.

The structure of Eq. (A.16) is consistent with the Eq. (1.47) presented in Chapter 1: more precisely, the functional form is the same, while its argument changes. If we consider the specific case of $d = 1$ in Eq. (1.47), the field h coincides with W in the notation of the present Section. Within our formalism, instead, we have $h = \tilde{W}$, accounting for the Jacobian of the change of coordinates, while the Mandelstam constraints are not taken into account at the mean-field level.

Appendix B

Bosonic and fermionic link models in two dimensions: a proposal

We provide here additional details about the proposal of the quantum simulator presented in Chapter 4.

B.1 Determination of the number of species

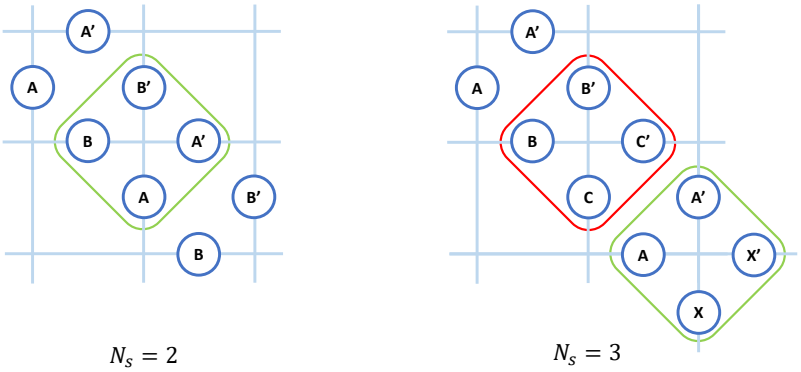

Figure B.1: Lattice structure with $N_s = 2$ (left panel) and $N_s = 3$ (right panel) internal states. The quantum numbers are denoted respectively with A, B and C. The primed letters denote a different permutations of the internal states along the two lattice diagonals. The green (red) square encloses the vertices that are problematic (correct) in the spirit of our proposal.

We motivate here the choice of four internal states for our proposal on the square lattice. To do this, we show what are the inconsistencies when less internal states are considered in the construction of the spin-dependent optical lattice.

APPENDIX B. BOSONIC AND FERMIONIC LINK MODELS IN TWO DIMENSIONS: A PROPOSAL

Let us firstly discuss the case of $N_s = 2$ internal states (left panel of Fig. B.1). We consider two diagonals of the lattice, with generic internal levels A, B and A', B' that can assume only two integer values. If we want to generate the plaquette term through angular momentum conservation, we have to impose the condition

$$\Delta_1 = B' - A', \qquad \Delta_2 = B - A \qquad \Rightarrow \qquad \Delta_1 + \Delta_2 = 0. \tag{B.1}$$

By imposing this condition, no matter what follows in the diagonal, we get unwanted problems at the subsequent vertex (see the green square in the left panel of Fig. B.1). Indeed, for any value of A, B and A', B', there could be hopping processes at the vertices, that within our proposal we want to avoid.

If we try to repeat the same reasoning with $N_s = 3$ internal levels (right panel of Fig. B.1), we can solve this inconsistency in the first vertex (red square in Fig. B.1) by choosing C and C' such that $\Delta_1 + \Delta_2 = 0$, and at the same time $\Delta_3 + \Delta_2 \neq 0$, with $\Delta_3 = C' - C$. We have then two different types of plaquettes in this scheme. However, inconsistencies arise again when we go to the subsequent vertex (green square in the right panel of Fig. B.1), and try to combine A, A' with X, X' that could be either B (B') or C (C') internal states. Also in this case, for any X, X' there are unwanted hopping processes at this vertex.

The solution to this is to use four internal states, but this is still not enough. To avoid hopping at the vertices throughout all the lattice, there must be two internal states m, m' such that their difference is $|m - m'| > 1$, as in our proposal of Fig. 4.1, and this is the reason why we introduce four out of five internal states.

B.2 Perturbation theory contributions

We present here the computations in perturbation theory that give rise to the effective model in Eq. (4.4). The starting point is the full Hamiltonian $H = H_1 + H_0$, with $h \gg t_x$, $V^{ij}_{mm'}$. Making reference to the definition of $\mathcal{M}_0$ given in the main text, we define respectively the projector on $\mathcal{M}_0$ and the restricted inverse of $(H_0 - E_0)$ as

$$\mathcal{P}_0 = \sum_{\alpha \in \mathcal{M}_0} |\alpha\rangle\langle\alpha|, \qquad \mathcal{K} = \sum_{\alpha \notin \mathcal{M}_0} \frac{|\alpha\rangle\langle\alpha|}{E_0(\alpha) - E_0(0)}, \tag{B.2}$$

where E_0 is the eigenvalue of H_0, and proceed with the computations order by order [150]. At first order the contribution is $H_1^{(\text{eff})} = \mathcal{P}_0 H_1 \mathcal{P}_0$, and it is always zero. This is because, both for the hopping and interaction term, with a single application of H_1 we move out of the ground state manifold. Therefore, once $\mathcal{P}_0$ acts again, the projection gives zero. At second order we have

$H_2^{(\text{eff})} = -\mathcal{P}_0 H_1 \mathcal{K} H_1 \mathcal{P}_0$, and the two non-trivial contributions are

$$\mathcal{P}_0 H_{\text{hop}} \mathcal{K} H_{\text{hop}} \mathcal{P}_0 = -\frac{t_x^2}{h} \sum_{\langle x,x' \rangle_d, m, m'} n_{xm}(1 - n_{x'm'}), \tag{B.3}$$

$$\mathcal{P}_0 H_{\text{int}} \mathcal{K} H_{\text{int}} \mathcal{P}_0 = -\frac{1}{h} \sum_{\langle x,y \rangle, m, m'} (V_{mm'}^{xy})^2 n_{xm} n_{ym'}. \tag{B.4}$$

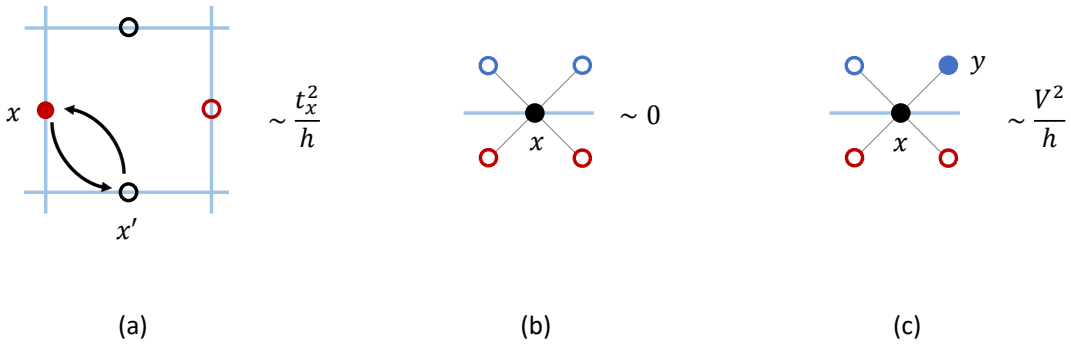

Figure B.2: Virtual processes at second order in perturbation theory. In all the panels, light blue lines are representing the target lattice, while grey lines the optical one, according to the convention of the main text. (a) Back and forth hopping process $x \to x' \to x$, generating the term in Eq. (B.4). This process can happen if x is occupied and x' is empty, independently of the other two sites of the plaquette. (b)-(c): Processes associated to the $H_{\text{int}} - H_{\text{int}}$ contribution of Eq. (B.4). The only trivial situation is when all of the nearest neighbors of x are empty.

The graphical representation of the virtual processes associated to these two terms is showed in Fig. B.2. Concerning the hopping contribution, it is associated to back and forth hopping processes happening along the diagonals; for the interaction part, we have that two generic nearest neighbors in the optical lattice interact mutually. These are the only processes that do not vanish when projected back to the ground state manifold $\mathcal{M}_0$.

At third order we get two non-trivial contribution, including the plaquette term already commented in the main text. The mathematical structure of the effective Hamiltonian is

$$H_3^{(\text{eff})} = \mathcal{P}_0 H_1 \mathcal{K} H_1 \mathcal{K} H_1 \mathcal{P}_0 - \frac{1}{2}\{\mathcal{P}_0 H_1 \mathcal{K}^2 H_1 \mathcal{P}_0, \mathcal{P}_0 H_1 \mathcal{P}_0\} \equiv \tilde{H}_3 + \tilde{H}_2, \tag{B.5}$$

where $\tilde{H}_2$ is a combination of lower order terms, and $\tilde{H}_3$ is the real third order contribution. Due to the fact that

$$\tilde{H}_2 = -\frac{1}{2}\{\mathcal{P}_0 H_1 \mathcal{K}^2 H_1, H_1^{(\text{eff})}\} \tag{B.6}$$

and since $H_1^{(\text{eff})} = 0$, this term vanishes. We are left only with $\tilde{H}_3$, and among the various contributions the only non-trivial ones are $\mathcal{P}_0 H_{\text{int}} \mathcal{K} H_{\text{hop}} \mathcal{K} H_{\text{hop}} \mathcal{P}_0$, generating the plaquette term,

and $\mathcal{P}_0 H_{\rm int}\mathcal{K}H_{\rm int}\mathcal{K}H_{\rm int}\mathcal{P}_0$, due to the spin-exchange interactions within a given plaquette. We make reference to Fig. B.3 for the representation of the virtual process in this last case, which is constrained to have the sites x', y, y' in the plaquettes occupied by particles compatible with the spin-dependent lattice structure.

The total third order contribution is therefore

$$\tilde{H}_3 = \frac{t_x^2}{h^2} \sum_{\substack{x,x',y,y' \in \square \\ m,m'}} V_{mm'}^{xx'} b_{y'm}^\dagger b_{ym'}^\dagger b_{x'm'} b_{xm} + \text{h.c.} + \frac{1}{h^2} \sum_{\substack{x',y,y' \in \square \\ m,m'}} (V_{mm'}^{yy'})^2 V_{mm}^{y'x'} n_{y'm} n_{x'm} n_{ym'}. \tag{B.7}$$

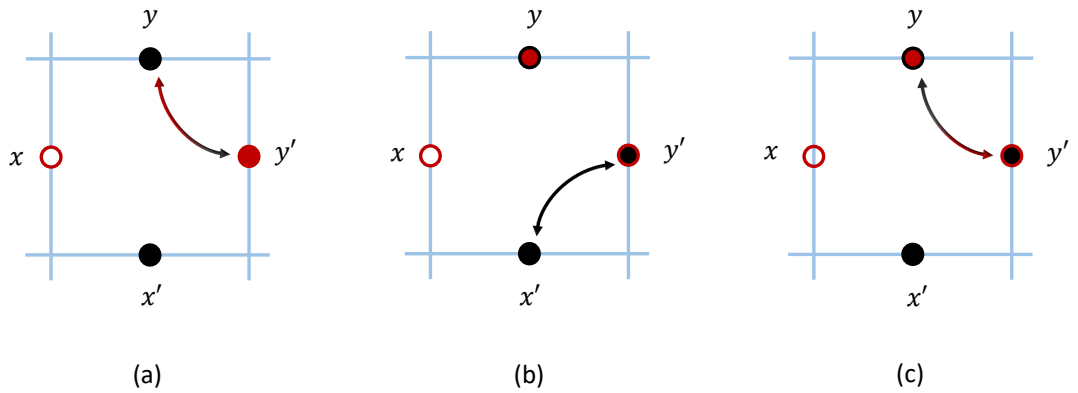

Figure B.3: Virtual processes due to three spin-exchange interactions at third order in perturbation theory. We have the spin-exchange between $y - y'$ (a), followed by the ones involving $y' - x'$ (b) and again $y' - y$ (c). The final state here coincides with the initial one. This process can happen if all the three involved sites contain the bosons in the proper initial states, according to the lattice structure. In all the panels, light blue lines are representing the target lattice, while grey lines the optical one, according to the convention of the main text.

Appendix C

Phase transitions in Weyl metals

We report here additional details and analysis for the Hofstader model in $d = 3$, supporting the description reported in Chapter 6.

C.1 Properties of the density of states of the $3D$ Hofstadter model

There are some general features that can be identified from the DOS profiles, which are displayed in Fig. C.1 for $n \leq 8$. We consider, in particular, the behavior of the topological metal phase at filling $\nu \approx 1/n$.

The quantities we adopt to characterize the energy features as a function of n are as follows: the bottom of the lowest band of the system, i.e. the lowest eigenvalue ϵ_{min} of the Hamiltonian; the energy location ϵ_0 of the first zero of the DOS; and the number N_w of inequivalent Weyl points in the MBZ at ϵ_0. We also numerically checked that the filling ν_w of the system in the Weyl phase at $\mu = \epsilon_0$ is $1/n$, as expected from the diagonalization of the $n \times n$ Hamiltonian (5.43). These quantities are summarized in Table C.1 (given the chiral sublattice symmetry, symmetric results hold for $\epsilon > 0$).

The position of ϵ_0 is determined through the identification of the DOS zeros. Its value decreases as a function of n, and thus for decreasing magnetic fluxes, as can be clearly seen in the left panel of Fig. C.2, where we display the function $\epsilon_0 \sim n^{-b}$, with $b \approx -2.8$, as a guide for the eye on top of the estimated values of ϵ_0.

Qualitatively, the same behavior of ϵ_0 is observed for $\epsilon_{\min}$, as shown in the central panel of Fig. C.2. Here we consider magnetic fields up to $n \leq 50$, using the Lanczos algorithm [231] to get

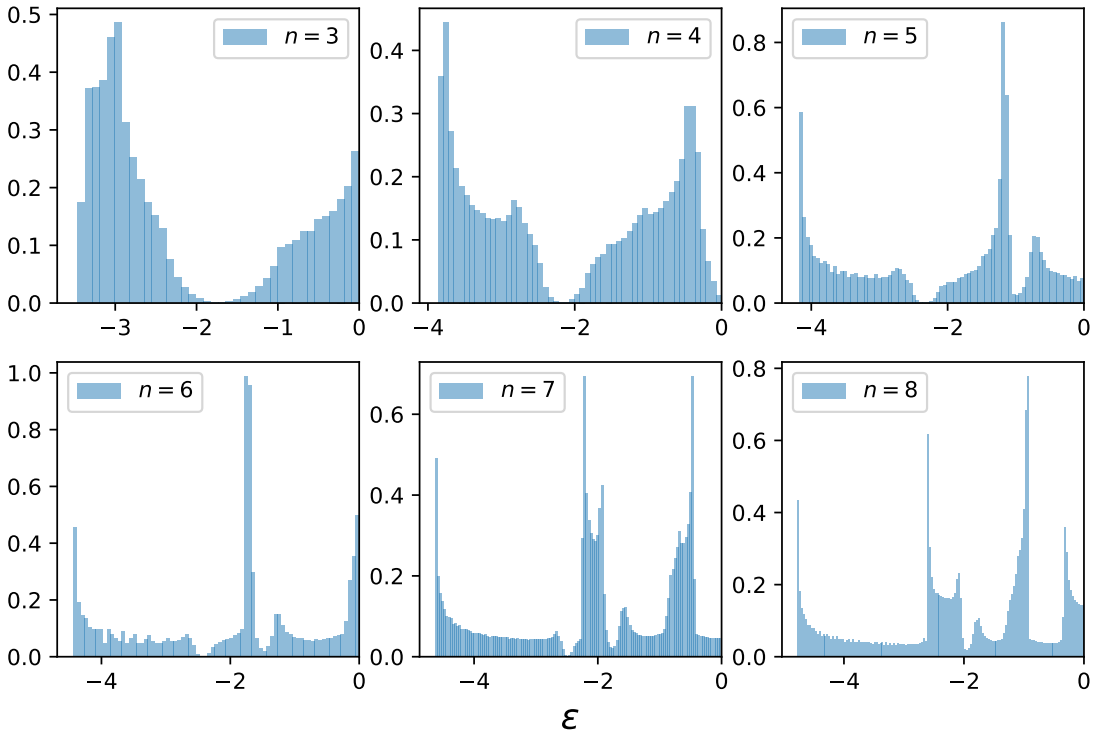

Figure C.1: Normalized DOS profiles from $n = 3$ to $n = 8$, obtained with the exact diagonalization of the Hofstadter Hamiltonian on a finite cubic system of linear size $L = 120$ (except for $n = 7$, where we considered $L = 119$). Because the energy spectrum is symmetric with respect to the origin, we plot the profiles for $\epsilon < 0$.

the lowest eigenvalue of Eq. (5.43). To characterize this decreasing behavior, we fit the data with the function

$$\epsilon_{min} = \alpha + \frac{\beta}{n^{\gamma}}. \tag{C.1}$$

The optimal parameters are found to be $\alpha = -6.09(1)$, $\beta = 6.8(1)$ and $\gamma = 0.79(1)$.

Regarding the number N_w of inequivalent Weyl points in the MBZ, since the system has inversion symmetry but no time-reversal symmetry, its minimum value is 2, allowing for the existence of a pair of Weyl nodes with opposite momenta at the same energy [159, 168]. For $n < 8$ we exactly observe two nodes at $\epsilon = \epsilon_0$, as reported in Table C.1: therefore, within the MBZ, the Hofstadter model hosts the minimum number of nodes compatible with the symmetries of the system, being an example of the so-called ideal Weyl semimetals [232, 233]. Denoting with $\mathbf{k}_0^{(\pm)}$ the positions of the Weyl nodes in momentum space, the effective Hamiltonian around them can

n	ϵ_{min}	ϵ_0	N_w	ν_w
3	-3.46	-1.75	2	1/3
4	-3.86	-2.18	2	1/4
5	-4.18	-2.32	2	1/5
6	-4.43	-2.43	2	1/6
7	-4.63	-2.49	2	1/7
8	-4.78	/	/	/

Table C.1:: Parameters as a function of the integer n. We report the bottom of the energy bands ϵ_{min}, the energy location ϵ_0, the related number N_w of Weyl points and the filling ν_w of the Weyl semimetal phase (energies in units of t). For $n = 8$ the DOS does not display zeros, therefore it is not possible to properly identify ϵ_0, N_w and ν_w from it. The values are calculated for a discretized MBZ with a mesh of L^3 points with $L = 120$ (except for $n = 7$, where we considered $L = 119$). By doing finite-size scaling with a dependence of the form $\alpha + \beta/L^\gamma$, one finds values compatible with those of the table in the first two columns with error ≈ 0.01.

be written as

$$\mathcal{H}(\delta\mathbf{k}) = f(\delta\mathbf{k})\,\mathbb{1} + \sum_{i,j=x,y,z} (\delta k)_i v_{ij} \sigma_j, \tag{C.2}$$

with $\delta\mathbf{k} = \mathbf{k} - \mathbf{k}_0^{(\pm)}$. The function $f(\delta\mathbf{k})$ represents the overall tilt of the Weyl cone, while the tensor v_{ij} contains the velocity vectors. Their specific form can be computed by expanding the Hamiltonian (5.43) around the Weyl points, and then computing the low-energy Hamiltonian (C.2) using degenerate perturbation theory. Since there do not exist directions along which the tilt dominates over the pure Weyl part, the Weyl points are of type I. The contributions of these points to the DOS are still quadratic, but the presence of the tilt and anisotropies makes the computations of the DOS coefficients not analytically doable [234].

We finally investigate the difference between the minima of the first and the second bands $\Delta\epsilon = \epsilon^1_{min} - \epsilon_{min}$, in order to verify that for $\Phi \ll 1$ and filling $\nu \ll 1$ the lattice structure becomes negligible, and the system can be described by its continuum counterpart [95]. We therefore expect $\Delta\epsilon \sim n^{-1}$, in agreement with a Landau levels description of the model. We plot the energy difference $\Delta\epsilon$ as a function of the magnetic field in Fig. C.2, observing the expected behavior.

C.2 Topological van Hove singularities and Weyl points

We investigate in this Appendix how the energy difference between ϵ_0 and the topological VH singularity vanishes as a function of n. Denoting with $\epsilon^{(R)}_m > \epsilon_0$ the energy of the first topological

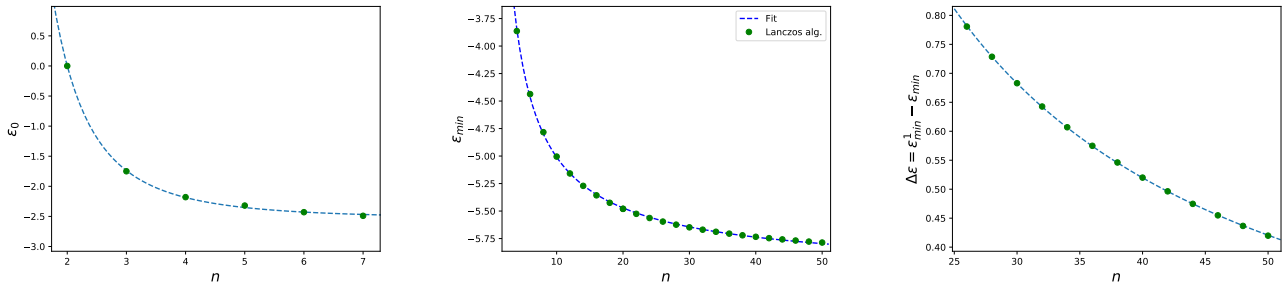

Figure C.2: Left panel: Weyl node energy ϵ_0, for $n \leq 6$, (a dotted function $\epsilon_0 = n^{-2.8} + \kappa$ is depicted as a guide for the eye). Central panel: ϵ_{min}, for $n \leq 50$ together with the fit function in Eq. (C.1). Right panel: $\Delta\epsilon$, for $25 \leq n \leq 50$, superimposed with the function $\Delta\epsilon \propto n^{-1}$. All the estimated values are obtained through a finite-size scaling analysis, up to $L = 120$.

VH singularity found by increasing the energy from the Weyl points, we define the parameter

$$\delta \equiv \epsilon_m^{(R)} - \epsilon_0, \tag{C.3}$$

whose plot as a function of n is shown in Fig. C.3. Apart from the special value of $n = 2$, we observe a net linear trend, therefore we interpolate the data with a linear function of the form $\delta = \tau n + q$. The obtained parameters are $\tau = -0.16(1)$, $q = 1.20(5)$, and the value of n such that the energy difference closes, i.e. $\delta = 0$, corresponds to 7.6(2).

The associated critical value of the flux $\phi_c = 2\pi/n_c$ is consistent with the estimate found by Hasegawa [95]. In his work, he observed how the energy bands of the Hofstadter model overlap for several pairs (m, n), associated with the flux $\Phi = 2\pi m/n$, finding that this happens for fluxes $\phi > \phi_c$, with ϕ_c associated with $(m_c, n_c) = (4, 31) \sim (1, 8)$.

Our analysis on the critical points of the energy bands supports this argument, allowing us to conclude that the contribution of the Weyl point in the DOS for $n \geq 8$ is always screened by the presence of other states from the upper band overlapping at the same energy (see, for example, the right panel of Fig. C.3). In this case, the Weyl semimetal phase disappears, and the system enters a more general topological metallic phase. Quantitatively, this is parametrized by the behavior of $\delta(n)$, which linearly closes at $n_c \in (7, 8)$. As a consequence, the DOS for $n > n_c$ no longer displays any zero at ϵ_0, despite the presence of Weyl points.

C.3 The case $n = 4$ at zero energy

For $n = 4$, the Hofstadter model shows a peculiar behavior at $\epsilon = 0$. Indeed, at this energy there are two crossing points for the central bands, exactly in correspondence of the two momenta

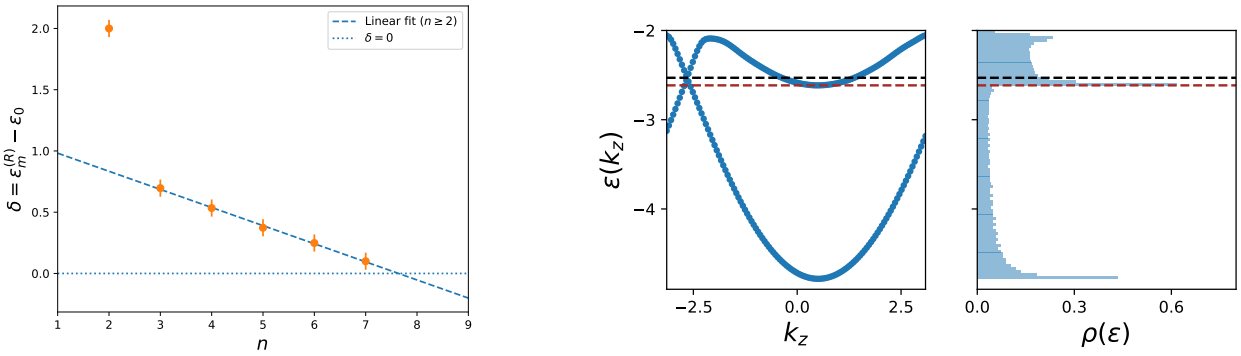

Figure C.3: Left plot: energy difference δ as a function of n, for $n \leq 8$. We also plot $\delta = \tau n + q$ (see the text), with the estimated parameters values (blue dashed line) and the line $\delta = 0$ (black dotted line), for which the energy difference closes. The errorbars in the plot are estimated through a binning analysis on the DOS profiles. Right plot: two lowest energy bands at fixed $k_x = k_x^{(w)}$, $k_y = k_y^{(w)}$ (left panel), alongside the DOS of the model (right panel) for $n = 8$. We highlight the VH singularity associated with the minimum of the second band at energy E_m (brown dashed line) and the energy position of the Weyl nodes $E_w > E_m$ (black dashed line).

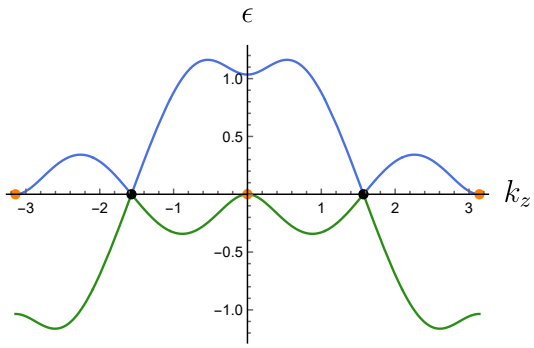

Figure C.4: Plot of the central bands of the Hofstadter model with $n = 4$ at fixed $k_x = k_y = 0$. We highlight the stationary points $\mathbf{k} = (0, 0, \pm\pi)$, $(0, 0, 0)$ at $\epsilon = 0$ (orange dots) together with the Weyl points (black dots).

$\mathbf{k}_0^{(\pm)} = (0, 0, \pm\pi/2)$. At the same energy there are also two stationary points of the crossing bands, namely a maximum of the second band at $\mathbf{k}_M = (0, 0, 0)$ and a minimum of the third band at $\mathbf{k}_m = (0, 0, \pi)$, as shown in Fig. C.4. We expand the dispersion relations around these points, determining the eigenvalues of the Hessian and the behavior of the DOS at $\epsilon = 0$. The functional forms of the DOS around them are [235, 236]

$$\rho_m(\epsilon \simeq 0) = \begin{cases} A\sqrt{\epsilon}, & \epsilon > 0, \\ O(\epsilon), & \epsilon < 0, \end{cases} \qquad \rho_M(\epsilon \simeq 0) = \begin{cases} A\sqrt{-\epsilon}, & \epsilon < 0, \\ O(\epsilon), & \epsilon > 0, \end{cases} \tag{C.4}$$

where the coefficient A, which depends on the curvature of the energy band around the stationary point, turns out to be the same for both the functions, since the Hessians of the dispersion relations in $\mathbf{k}_m$ and $\mathbf{k}_M$ are equal and opposite, giving rise to the same modulus of the curvature.

The total contribution to the DOS at $\epsilon = 0$ is the sum of the single DOS at the stationary points and at the Weyl points

$$\rho(\epsilon = 0) = \rho_m + \rho_M + \rho_W = A\sqrt{|\epsilon|} + B\epsilon^2, \tag{C.5}$$

where B is a numerical factor encoding the effects of the tilt and the anisotropy of the Weyl cones [234]. From Eq. (C.5) we conclude that the behavior of the DOS around $\epsilon = 0$ is not quadratic, due to the presence of stationary points at the same energy of the Weyl ones.

Acknowledgments

These years in Sissa have been incredibly intense, both from the personal and professional points of view. I would like to thank here the various people that allowed me to finish this experience and enriched me as a physicist and science man.

First, I want to thank my supervisor Andrea, with whom I spent days of discussions about physics (and beyond!) during the last three years. Even if for some points we are divergent, so to say, it would be unfair to focus only on these ones. I prefer here to highlight how much enthusiasm you put in your work, with different ideas and huge curiosity in various research areas. This is one of the things I liked the most, and that also allowed me to discover new topics, even if not directly connected to my past formation or research field.

I thank then Michele, which is probably the professor with whom I interacted more in these years out of SISSA community. We spent hours discussing on Skype and working together, and every time I was impressed by your knowledge and experience about physics. It was (and, hopefully, will be) a pleasure to work with you, and to meet you personally the last year at GGI, to share dinners and coffee breaks and go, also with you, beyond the physical context.

A special thank goes to Joao. We started as scientific collaborators, but I think we became friends now after three years. We share different interests, as football, reading and music, and for this reason our discussions were never boring. The biggest pleasure for me was to meet you personally in Zurich, and the month I spent here allowed me to discover the man beyond the scientist. You were kind and hospital with me, and I will never forget this. Finally, I finish by thanking you for all the times you were patient with me, to listen to my vents and complaints during these years.

Unfortunately, due to the pandemic situation, the opportunities to go around the world were not so much. Despite this, I was lucky to meet collaborators that enriched me in different context, starting from our discussion about physics and going, again, beyond that. I refer in particular to Ettore, Luca, Mimmo, Alessio, Marcello and Stefano. In various forms you always encouraged me to proceed, not to push me down, even when I doubted of myself, and I was not sure about my future after the PhD. Your suggestions, comments and feedbacks meant a lot for me, being like fireflies in a shaded period.

I thank Marina and his research team in Zurich, for the hospitality and the opportunity to spend a month working with you. I enjoyed the various seminars and group meeting that we attended, and you gave me the opportunity to brush up things that I didn't see since my master degree in Pisa. Last but not least, coffee breaks and dinners with the other guys were a good occasion to know you also outside the work environment. I will remember this as one of the best experiences that I did during these years of PhD.

Finally, a big thank to the whole SISSA community, and to the Statistical Physics group, for the big opportunity you gave me in the last four years, starting from the first year to these last days of my journey here in Trieste. Journal clubs, discussions in the corridors, Zoom and Skype calls, lunches and coffee breaks were an important part of this experience, leaving me with the message that research life is not only inside the offices, but it can grow also in "unofficial" contexts like these.

References

[1] P. Fontana, J.C. Pinto Barros and A. Trombettoni, *Reformulation of gauge theories in terms of gauge invariant fields*, *Annals of Physics* **436** (2022) 168683.

[2] P. Fontana, J.C. Pinto Barros and A. Trombettoni, *Quantum simulator of link models using spinor dipolar ultracold atoms*, *arXiv preprint arXiv:2210.14836* (2022) .

[3] P. Fontana, M. Burrello and A. Trombettoni, *Topological van hove singularities at phase transitions in weyl metals*, *Phys. Rev. B* **104** (2021) 195127.

[4] P. Fontana, *Scaling behavior of ising systems at first-order transitions*, *Journal of Statistical Mechanics: Theory and Experiment* **2019** (2019) 063206.

[5] M. Peskin and D. Schroeder, *An introduction to Quantum Field Theory*, Addison-Wesley Pub. Co., Reading, Mass (1995).

[6] M.D. Schwartz, *Quantum Field Theory and the Standard Model*, Cambridge University Press (2013).

[7] M. Maggiore, *A Modern Introduction to Quantum Field Theory*, OUP Oxford (2005).

[8] X.-G. Wen, *Quantum Field Theory of Many-body Systems*, OUP Oxford (2004).

[9] M. Levin and X.-G. Wen, *Colloquium: Photons and electrons as emergent phenomena*, *Rev. Mod. Phys.* **77** (2005) 871.

[10] K.G. Wilson, *Confinement of quarks*, *Phys. Rev. D* **10** (1974) 2445.

[11] J. Kogut and L. Susskind, *Hamiltonian formulation of wilson's lattice gauge theories*, *Phys. Rev. D* **11** (1975) 395.

[12] H.J. Rothe, *Lattice Gauge Theories: an Introduction*, World Scientific Publishing Company (2005).

[13] M. Creutz, *Quarks, gluons and lattices*, Cambridge Monographs on Mathematical Physics, Cambridge University Press (1985).

[14] M. Troyer and U.-J. Wiese, *Computational complexity and fundamental limitations to fermionic quantum monte carlo simulations*, *Physical review letters* **94** (2005) 170.

[15] K. Fukushima and T. Hatsuda, *The phase diagram of dense qcd*, *Reports on Progress in Physics* **74** (2010) 014001.

[16] U.-J. Wiese, *Ultracold quantum gases and lattice systems: quantum simulation of lattice gauge theories*, *Annalen der Physik* **525** (2013) 777.

[17] E. Zohar, J.I. Cirac and B. Reznik, *Quantum simulations of lattice gauge theories using ultracold atoms in optical lattices*, *Report on Progress in Physics* **79** (2016) .

[18] M.C. Bañuls, R. Blatt, J. Catani, A. Celi, J.I. Cirac, M. Dalmonte et al., *Simulating lattice gauge theories within quantum technologies*, *The European Physical Journal D* **74** (2020) 1.

[19] R. Blatt and C. Roos, *Quantum simulations with trapped ions*, *Nature Physics* **8** (2012) 277.

[20] A. Houck, H. Türeci and J. Koch, *On-chip quantum simulation with superconducting circuits*, *Nature Physics* **8** (2012) 292.

[21] A. Celi, B. Vermersch, O. Viyuela, H. Pichler, M.D. Lukin and P. Zoller, *Emerging two-dimensional gauge theories in rydberg configurable arrays*, *Phys. Rev. X* **10** (2020) 021057.

[22] I. Bloch, J. Dalibard and S. Nascimbène, *Quantum simulations with ultracold quantum gases*, *Nature Physics* **8** (2012) 267.

[23] S. Elitzur, *Impossibility of spontaneously breaking local symmetries*, *Phys. Rev. D* **12** (1975) 3978.

[24] E. Zohar, J.I. Cirac and B. Reznik, *Quantum simulations of gauge theories with ultracold atoms: Local gauge invariance from angular-momentum conservation*, *Phys. Rev. A* **88** (2013) 023617.

[25] B. M., L. L., P. S. and T. A., *Abelian gauge potentials on cubic lattices*, In *Advances of Quantum Mechanics* (2017) 47.

[26] B.Q. Lv, T. Qian and H. Ding, *Experimental perspective on three-dimensional topological semimetals*, *Rev. Mod. Phys.* **93** (2021) 025002.

[27] A. Wipf, *Statistical Approach to Quantum Field Theory: An Introduction*, Lecture Notes in Physics, Springer, 2013 ed. (2012).

[28] C. Gattringer and C. Lang, *Quantum chromodynamics on the lattice: an introductory presentation*, vol. 788, Springer Science & Business Media (2009).

[29] M. Creutz, *Monte carlo study of quantized su(2) gauge theory*, *Phys. Rev. D* **21** (1980) 2308.

[30] M. Creutz and K.J.M. Moriarty, *Numerical studies of wilson loops in su(3) gauge theory in four dimensions*, *Phys. Rev. D* **26** (1982) 2166.

[31] J.D. Stack, *Heavy-quark potential in su(3) lattice gauge theory*, *Phys. Rev. D* **29** (1984) 1213.

[32] K.D. Born, E. Laermann, N. Pirch, T.F. Walsh and P.M. Zerwas, *Hadron properties in lattice qcd with dynamical fermions*, *Phys. Rev. D* **40** (1989) 1653.

[33] K. Bowler, D. Chalmers, A. Kenway, R. Kenway, P. G.S. and D. Wallace, *A critique of quenched hadron mass calculations*, *Physics Letters B* **162** (1985) 354.

[34] C. Michael and M. Teper, *The glueball spectrum in su(3)*, *Nuclear Physics B* **314** (1989) 347.

[35] T. Yoshié, Y. Iwasaki and S. Sakai, *Hadron spectrum on a 243 × 60 lattice*, *Nuclear Physics B - Proceedings Supplements* **17** (1990) 413.

[36] E. Laermann, R. Altmeyer, K. Born, W. Ibes, R. Sommer, T. Walsh et al., *Qcd with dynamical fermions*, *Nuclear Physics B - Proceedings Supplements* **17** (1990) 436.

[37] M. D'Elia, *High-temperature qcd: theory overview*, *Nuclear Physics A* **982** (2019) 99.

[38] M. Dalmonte and S. Montangero, *Lattice gauge theory simulations in the quantum information era*, *Contemporary Physics* **57** (2016) 388.

[39] D.S. Rokhsar and S.A. Kivelson, *Superconductivity and the quantum hard-core dimer gas*, *Phys. Rev. Lett.* **61** (1988) 2376.

[40] D. Horn, *Finite matrix models with continuous local gauge invariance*, *Physics Letters B* **100** (1981) 149.

[41] P. Orland and D. Rohrlich, *Lattice gauge magnets: Local isospin from spin*, *Nuclear Physics B* **338** (1990) 647.

[42] S. Chandrasekharan and U.J. Wiese, *Quantum link models: A discrete approach to gauge theories*, *Nuclear Physics B* **492** (1997) 455.

[43] P. Widmer, D. Banerjee, F.-J. Jiang and U.-J. Wiese, *Crystalline confinement*, *PoS* **LATTICE 2013** (2014) 333.

[44] D. Banerjee, S. Caspar, F.-J. Jiang, J.-H. Peng and U.-J. Wiese, *Nematic confined phases in the $u(1)$ quantum link model on a triangular lattice: An opportunity for near-term quantum computations of string dynamics on a chip*, *arXiv preprint arXiv:2107.01283* (2021) .

[45] D. Banerjee and A. Sen, *Quantum scars from zero modes in an abelian lattice gauge theory on ladders*, *Phys. Rev. Lett.* **126** (2021) 220601.

[46] R. Moessner, S.L. Sondhi and E. Fradkin, *Short-ranged resonating valence bond physics, quantum dimer models, and ising gauge theories*, *Phys. Rev. B* **65** (2001) 024504.

[47] D. Banerjee, E. Huffman and L. Rammelmüller, *Exploring bosonic and fermionic link models on* $(3+1)-$ *d tubes*, *arXiv preprint arXiv:2201.07171* (2022) .

[48] D. Banerjee, E. Huffman and L. Rammelmüller, *Introducing fermionic link models*, *arXiv preprint arXiv:2111.00300* (2021) .

[49] J.-M. Drouffe and J.-B. Zuber, *Strong coupling and mean field methods in lattice gauge theories*, *Physics Reports* **102** (1983) 1 .

[50] P.A.M. Dirac, *Gauge-invariant formulation of quantum electrodynamics*, *Canadian Journal of Physics* **33** (1955) 650.

[51] S. Mandelstam, *Quantum electrodynamics without potentials*, *Annals of Physics* **19** (1962) 1.

[52] J. Kijowski and G. Rudolph, *New lattice approximation of gauge theories*, *Phys. Rev. D* **31** (1985) 856.

[53] J. Kijowski and G. Rudolph, *The functional integral on the gauge orbit space for a non-abelian higgs model*, *Nuclear Physics B* **325** (1989) 211 .

[54] J. Kijowski and G. Rudolph, *Spinor electrodynamics in terms of gauge-invariant quantities*, *Lett. Math. Phys.* **29** (1993) 103.

[55] J. Kijowski, G. Rudolph and M. Rudolph, *Functional integral of qed in terms of gauge-invariant quantities*, *Lett. Math. Phys.* **33** (1995) 139.

[56] J. Kijowski, G. Rudolph and M. Rudolph, *Gauge invariant formulation and bosonization of the Schwinger model*, *Phys. Lett. B* **419** (1998) 285.

[57] J. Kijowski, G. Rudolph and M. Rudolph, *Towards an effective field theory of qed*, `hep-th/9909113`.

[58] S. Coleman, R. Jackiw and L. Susskind, *Charge shielding and quark confinement in the massive schwinger model*, *Annals of Physics* **93** (1975) 267 .

[59] S. Coleman, *More about the massive schwinger model*, *Annals of Physics* **101** (1976) 239 .

[60] R. Brower, S. Chandrasekharan and U.-J. Wiese, *Qcd as a quantum link model*, *Phys. Rev. D* **60** (1999) 094502.

[61] O. Bär, R. Brower, B. Schlittgen and U.-J. Wiese, *Quantum link models with many rishon flavors and with many colors*, *Nuclear Physics B - Proceedings Supplements* **106-107** (2002) 1019.

[62] E. Rico, M. Dalmonte, P. Zoller, D. Banerjee, M. Bögli, P. Stebler et al., *So(3) "nuclear physics" with ultracold gases*, *Annals of Physics* **393** (2018) 466.

[63] I. Raychowdhury and J.R. Stryker, *Loop, string, and hadron dynamics in su(2) hamiltonian lattice gauge theories*, *Phys. Rev. D* **101** (2020) 114502.

[64] D.B. Kaplan and J.R. Stryker, *Gauss's law, duality, and the hamiltonian formulation of u(1) lattice gauge theory*, 1806.08797.

[65] J.F. Haase, L. Dellantonio, A. Celi, D. Paulson, A. Kan, K. Jansen et al., *A resource efficient approach for quantum and classical simulations of gauge theories in particle physics*, 2006.14160.

[66] J. Bender and E. Zohar, *A gauge redundancy-free formulation of compact qed with dynamical matter for quantum and classical computations*, 2008.01349.

[67] M.B. Halpern, *Field-strength and dual variable formulations of gauge theory*, *Phys. Rev. D* **19** (1979) 517.

[68] L. Durand and E. Mendel, *Field-strength formulation of gauge theories: Transformation of the functional integral*, *Phys. Rev. D* **26** (1982) 1368.

[69] E. Mendel and L. Durand, *Field-strength formulation of gauge theories. the hamiltonian approach in the abelian theory*, *Phys. Rev. D* **30** (1984) 1754.

[70] R. Giles, *Reconstruction of gauge potentials from wilson loops*, *Phys. Rev. D* **24** (1981) 2160.

[71] R. Loll, *Lattice gauge theory in terms of independent wilson loops*, *Nuclear Physics B - Proceedings Supplements* **30** (1993) 224.

[72] R. Loll, *Loop approaches to gauge field theories*, *Theoretical and Mathematical Physics* **93** (1992) 1415.

[73] J.P. Greensite and B. Lautrup, *Phase transitions and mean-field methods in lattice gauge theory*, *Physics Letters B* **104** (1981) 41.

[74] Brézin, E., *Quantum field theory and statistical mechanics*, *J. Phys. Colloques* **43** (1982) C3.

[75] G.G. Batrouni, *Gauge-invariant mean-plaquette method for lattice gauge theories*, *Nuclear Physics B* **208** (1982) 12.

[76] O. Akerlund and P. de Forcrand, *Mean distribution approach to spin and gauge theories*, *Nuclear Physics B* **905** (2016) 1.

[77] J. Greensite and R. Höllwieser, *Relative weights approach to su(3) gauge theories with dynamical fermions at finite density*, *Phys. Rev. D* **94** (2016) 014504.

[78] P. Gaete, *On gauge-invariant variables in qed*, *Z Phys C - Particles and Fields* **76** (1997) 355.

[79] G. 't Hooft, *A property of electric and magnetic flux in non-abelian gauge theories*, *Nuclear Physics B* **153** (1979) 141 .

[80] G. Mack and V. Petkova, *Sufficient condition for confinement of static quarks by a vortex condensation mechanism*, *Annals of Physics* **125** (1980) 117.

[81] G. 't Hooft, *Some twisted self-dual solutions for the yang-mills equations on a hypertorus*, *Communications in Mathematical Physics* **81** (1981) 267.

[82] U.J. Wiese, *Lattice quantization of topological excitations, finite volume effects, and the use of C-periodic boundary conditions*, Habilitationsschrift, RWTH Aachen (1993).

[83] Y. Makeenko, *Methods of Contemporary Gauge Theory*, Cambridge Monographs on Mathematical Physics, Cambridge University Press, Cambridge (2002).

[84] M. Creutz, *Gauge fixing, the transfer matrix, and confinement on a lattice*, *Phys. Rev. D* **15** (1977) 1128.

[85] C. Hamer, Z. Weihong and J. Oitmaa, *Series expansions for the massive schwinger model in hamiltonian lattice theory*, *Phys. Rev. D* **56** (1997) 55.

[86] J.C. Pinto Barros, M. Dalmonte and A. Trombettoni, *Long-range interactions from u(1) gauge fields via dimensional mismatch*, *Journal of Statistical Mechanics: Theory and Experiment* **2018** (2018) 103103.

[87] J.C. Pinto Barros, M. Dalmonte and A. Trombettoni, *String tension and robustness of confinement properties in the schwinger-thirring model*, *Phys. Rev. D* **100** (2019) 036009.

[88] L.D. Landau and E.M. Lifshitz, *Quantum Mechanics; Non-relativistic Theory*, Butterworth-Heinemann (1981).

[89] D.R. Hofstadter, *Energy levels and wave functions of bloch electrons in rational and irrational magnetic fields*, *Phys. Rev. B* **14** (1976) 2239.

[90] M. Al-Hashimi and U.-J. Wiese, *Discrete accidental symmetry for a particle in a constant magnetic field on a torus*, *Annals of physics* **324** (2009) 343.

[91] E.M. Lifschitz and L.P. Pitaevskii, *Statistical Physics, Part 2*, Pergamon Press (1980).

[92] P.G. Harper, *Single band motion of conduction electrons in a uniform magnetic field*, *Proc. Phys. Soc. A* **68** (1955) 874.

[93] J.B. Marston and I. Affleck, *Large-n limit of the hubbard-heisenberg model*, *Phys. Rev. B* **39** (1989) 11538.

[94] M. Burrello, I. Fulga, L. Lepori and A. Trombettoni, *Exact diagonalization of cubic lattice models in commensurate abelian magnetic fluxes and translational invariant non-abelian potentials*, *J. Phys. A: Math. Theor. 50, 455301* (2017) .

[95] Y. Hasegawa, *Generalized flux states on 3-dimensional lattice*, *Journal of the Physical Society of Japan* **59** (1990) 4384.

[96] Y. Frishman and J. Sonnenschein, *Non-perturbative field theory: from two-dimensional conformal field theory to QCD in four dimensions*, Cambridge University Press, Cambridge (2010).

[97] L. Barbiero, C. Schweizer, M. Aidelsburger, E. Demler, N. Goldman and F. Grusdt, *Coupling ultracold matter to dynamical gauge fields in optical lattices: From flux attachment to $\mathbb{Z}_2$ lattice gauge theories*, *Science Advances* **5** (2019) eaav7444.

[98] T. Chanda, J. Zakrzewski, M. Lewenstein and L. Tagliacozzo, *Confinement and lack of thermalization after quenches in the bosonic schwinger model*, *Phys. Rev. Lett.* **124** (2020) 180602.

[99] L. Cardarelli, S. Greschner and L. Santos, *Deconfining disordered phase in two-dimensional quantum link models*, *Phys. Rev. Lett.* **124** (2020) 123601.

[100] U. Borla, R. Verresen, F. Grusdt and S. Moroz, *Confined phases of one-dimensional spinless fermions coupled to Z_2 gauge theory*, *Phys. Rev. Lett.* **124** (2020) 120503.

[101] W.D. Phillips, *Nobel lecture: Laser cooling and trapping of neutral atoms*, *Rev. Mod. Phys.* **70** (1998) 721.

[102] S.H. Autler and C.H. Townes, *Stark effect in rapidly varying fields*, *Phys. Rev.* **100** (1955) 703.

[103] M. Lewenstein, A. Sanpera and V. Ahufinger, *Ultracold Atoms in Optical Lattices: Simulating quantum many-body systems*, Oxford University Press (2012).

[104] N.D.M. Neil W. Ashcroft, *Solid state physics*, Solid State Physics, Holt, Rinehart and Winston, 1 ed. (1976).

[105] D. Jaksch, C. Bruder, J.I. Cirac, C.W. Gardiner and P. Zoller, *Cold bosonic atoms in optical lattices*, *Phys. Rev. Lett.* **81** (1998) 3108.

[106] H. Feshbach, *Unified theory of nuclear reactions*, *Annals of Physics* **5** (1958) 357.

[107] H. Feshbach, *A unified theory of nuclear reactions. ii*, *Annals of Physics* **19** (1962) 287.

[108] U. Fano, *Effects of configuration interaction on intensities and phase shifts*, *Phys. Rev.* **124** (1961) 1866.

[109] C. Chin, R. Grimm, P. Julienne and E. Tiesinga, *Feshbach resonances in ultracold gases*, *Rev. Mod. Phys.* **82** (2010) 1225.

[110] H.S. C. J. Pethick, *Bose-Einstein condensation in dilute gases*, Cambridge University Press, 2nd ed ed. (2008).

[111] Y. Kawaguchi and M. Ueda, *Spinor bose–einstein condensates*, *Physics Reports* **520** (2012) 253.

[112] D.M. Stamper-Kurn and M. Ueda, *Spinor bose gases: Symmetries, magnetism, and quantum dynamics*, *Rev. Mod. Phys.* **85** (2013) 1191.

[113] K. Eckert, L. Zawitkowski, M.J. Leskinen, A. Sanpera and M. Lewenstein, *Ultracold atomic bose and fermi spinor gases in optical lattices*, *New Journal of Physics* **9** (2007) 133.

[114] A. Van Otterlo, K.-H. Wagenblast, R. Baltin, C. Bruder, R. Fazio and G. Schön, *Quantum phase transitions of interacting bosons and the supersolid phase*, *Phys. Rev. B* **52** (1995) 16176.

[115] B. Capogrosso-Sansone, C. Trefzger, M. Lewenstein, P. Zoller and G. Pupillo, *Quantum phases of cold polar molecules in 2d optical lattices*, *Phys. Rev. Lett.* **104** (2010) 125301.

[116] C. Zhang, A. Safavi-Naini, A.M. Rey and B. Capogrosso-Sansone, *Equilibrium phases of tilted dipolar lattice bosons*, *New Journal of Physics* **17** (2015) 123014.

[117] S. Giovanazzi, A. Görlitz and T. Pfau, *Tuning the dipolar interaction in quantum gases*, *Phys. Rev. Lett.* **89** (2002) 130401.

[118] M. Baranov, L. Dobrek, K. Goral, L. Santos and M. Lewenstein, *Ultracold dipolar gases - a challenge for experiments and theory*, *Physica Scripta* **T102** (2002) 74.

[119] T. Lahaye, C. Menotti, L. Santos, M. Lewenstein and T. Pfau, *The physics of dipolar bosonic quantum gases*, *Reports on Progress in Physics* **72** (2009) 126401.

[120] I. Bloch, J. Dalibard and W. Zwerger, *Many-body physics with ultracold gases*, *Rev. Mod. Phys.* **80** (2008) 885.

[121] W. Hofstetter and T. Qin, *Quantum simulation of strongly correlated condensed matter systems*, *Journal of Physics B: Atomic, Molecular and Optical Physics* **51** (2018) 082001.

[122] R.P. Feynman, *Simulating physics with computers*, *International Journal of Theoretical Physics* **21** (1982) 467.

[123] P.A. Lee, N. Nagaosa and X.-G. Wen, *Doping a mott insulator: Physics of high-temperature superconductivity*, *Rev. Mod. Phys.* **78** (2006) 17.

[124] K.L. Hur and T. Maurice Rice, *Superconductivity close to the mott state: From condensed-matter systems to superfluidity in optical lattices*, *Annals of Physics* **324** (2009) 1452.

[125] J. Cardy, *Scaling and Renormalization in Statistical Physics*, Cambridge lecture notes in physics 5, Cambridge University Press (1996).

[126] S. Sachdev, *Quantum Phase Transitions*, Cambridge University Press, 2 ed. (2011).

[127] M. Bañuls, R. Blatt, Catani and J. et al., *Simulating lattice gauge theories within quantum technologies*, *The European Physical Journal D* **74** (2020) 165.

[128] M.C. Bañuls and K. Cichy, *Review on novel methods for lattice gauge theories*, *Rep. Prog. Phys.* **83** (2020) .

[129] M. Aidelsburger, L. Barbiero and A.e.a. Bermudez, *Cold atoms meet lattice gauge theory*, *Philosophical Transactions of the Royal Society A: Mathematical, Physical and Engineering Sciences* **380** (2022) 20210064.

[130] C.W. Bauer, Z. Davoudi, A.B. Balantekin and et al., *Quantum simulation for high energy physics*, *arXiv preprint arXiv:2204.03381* (2022) .

[131] E. Zohar and B. Reznik, *Confinement and lattice quantum-electrodynamic electric flux tubes simulated with ultracold atoms*, *Phys. Rev. Lett.* **107** (2011) 275301.

[132] E. Zohar, J.I. Cirac and B. Reznik, *Simulating compact quantum electrodynamics with ultracold atoms: Probing confinement and nonperturbative effects*, *Phys. Rev. Lett.* **109** (2012) 125302.

[133] E. Zohar, J.I. Cirac and B. Reznik, *Simulating $(2+1)$-dimensional lattice qed with dynamical matter using ultracold atoms*, *Phys. Rev. Lett.* **110** (2013) 055302.

[134] H. Weimer, M. Müller, I. Lesanovsky, P. Zoller and H.P. Büchler, *A rydberg quantum simulator*, *Nature Physics* **6** 382.

[135] L. Tagliacozzo, A. Celi, A. Zamora and M. Lewenstein, *Optical abelian lattice gauge theories*, *Annals of Physics* **330** (2013) 160.

[136] L. Tagliacozzo, A. Celi, P. Orland, M.W. Mitchell and M. Lewenstein, *Simulation of non-abelian gauge theories with optical lattices*, *Nature Communications* **4** (2013) .

[137] A. Mezzacapo, E. Rico, C. Sabín, I.L. Egusquiza, L. Lamata and E. Solano, *Non-abelian su(2) lattice gauge theories in superconducting circuits*, *Phys. Rev. Lett.* **115** (2015) 240502.

[138] T. Banks, L. Susskind and J. Kogut, *Strong-coupling calculations of lattice gauge theories: (1 + 1)-dimensional exercises*, *Phys. Rev. D* **13** (1976) 1043.

[139] P. Sala, T. Shi, S. Kühn, M.C. Bañuls, E. Demler and J.I. Cirac, *Variational study of u(1) and su(2) lattice gauge theories with gaussian states in* $1+1$ *dimensions*, *Phys. Rev. D* **98** (2018) 034505.

[140] E. Zohar and J.I. Cirac, *Removing staggered fermionic matter in* $u(n)$ *and* $su(n)$ *lattice gauge theories*, *Phys. Rev. D* **99** (2019) 114511.

[141] D. Banerjee, M. Dalmonte, M. Müller, E. Rico, P. Stebler, U.-J. Wiese et al., *Atomic quantum simulation of dynamical gauge fields coupled to fermionic matter: From string breaking to evolution after a quench*, *Phys. Rev. Lett.* **109** (2012) 175302.

[142] K. Kasamatsu, I. Ichinose and T. Matsui, *Atomic quantum simulation of the lattice gauge-higgs model: Higgs couplings and emergence of exact local gauge symmetry*, *Phys. Rev. Lett.* **111** (2013) 115303.

[143] E.F.P.M.G. Notarnicola, S. Ercolessi, G. Pascazio and F. Pepe, *Discrete abelian gauge theories for quantum simulations of qed*, *Journal of Physics A: Mathematical and Theoretical Physics* **48** (2015) .

[144] Y. Kuno, K. Kasamatsu, Y. Takahashi, I. Ichinose and T. Matsui, *Real-time dynamics and proposal for feasible experiments of lattice gauge–higgs model simulated by cold atoms*, *New Journal of Physics* **17** (2015) .

[145] K. Stannigel, P. Hauke, D. Marcos, M. Hafezi, S. Diehl, M. Dalmonte et al., *Constrained dynamics via the zeno effect in quantum simulation: Implementing non-abelian lattice gauge theories with cold atoms*, *Phys. Rev. Lett.* **112** (2014) 120406.

[146] D. Banerjee, F.-J. Jiang, P. Widmer and U.-J. Wiese, *The (2 1)-d iu/i(1) quantum link model masquerading as deconfined criticality*, *Journal of Statistical Mechanics: Theory and Experiment* **2013** (2013) P12010.

[147] D. Banerjee, E. Huffman and L. Rammelmüller, *Introducing fermionic link models*, arXiv:2111.00300 [hep-lat] (2021) [2111.00300].

[148] P. KJordan, *Der zusammenhang der symmetrischen und linearen gruppen und das mehrkörperproblem*, *Zeitschrift für Physik* **94** (1935) .

[149] S. Ben-Menahem, *Confinement in compact qed for low couplings*, *Phys. Rev. D* **20** (1979) 1923.

[150] C.E. Soliverez, *An effective hamiltonian and time-independent perturbation theory*, *Journal of Physics C: Solid State Physics* **2** (1969) 2161.

[151] T. Graß, M. Lewenstein and A. Bermudez, *Dual trapped-ion quantum simulators: an alternative route towards exotic quantum magnets*, *New Journal of Physics* **18** (2016) 033011.

[152] B. Yang, H.-N. Dai, H. Sun, A. Reingruber, Z.-S. Yuan and J.-W. Pan, *Spin-dependent optical superlattice*, *Phys. Rev. A* **96** (2017) 011602.

[153] R. Moessner and S.L. Sondhi, *Resonating valence bond phase in the triangular lattice quantum dimer model*, *Phys. Rev. Lett.* **86** (2001) 1881.

[154] J.R. Schrieffer and P.A. Wolff, *Relation between the anderson and kondo hamiltonians*, *Phys. Rev.* **149** (1966) 491.

[155] D. Giuliano, D. Rossini, P. Sodano and A. Trombettoni, *Xxz spin-$\frac{1}{2}$ representation of a finite-u bose-hubbard chain at half-integer filling*, *Phys. Rev. B* **87** (2013) 035104.

[156] A. Altland and B. Simons, *Condensed Matter Field Theory*, CUP, 2ed ed. (2010).

[157] K. von Klitzing, G. Dorda and M. Pepper, *New method for high-accuracy determination of the fine-structure constant based on quantized hall resistance*, *Phys. Rev. Lett.* **45** (1980) 494.

[158] M.V. Berry, *Quantal phase factors accompanying adiabatic changes*, *Proc. R. Soc. Lond.* **392** (1984) 45.

[159] M. El-Batanouny, *Advanced Quantum Condensed Matter Physics: One-Body, Many-Body, and Topological Perspectives*, Cambridge University Press (2020).

[160] J.J. Sakurai, *Modern quantum mechanics*, Addison-Wesley Pub. Co, rev. ed ed. (1994).

[161] M. Born and V. Fock, *Beweis des adiabatensatzes*, *Zeitschrift für Physik* **51** (1928) 165.

[162] D.J. Thouless, M. Kohmoto, M.P. Nightingale and M. den Nijs, *Quantized hall conductance in a two-dimensional periodic potential*, *Phys. Rev. Lett.* **49** (1982) 405.

[163] J.E. Avron, R. Seiler and B. Simon, *Charge deficiency, charge transport and comparison of dimensions*, *Communications in Mathematical Physics* **159** (1994) 399 .

[164] D.C. Tsui, H.L. Stormer and A.C. Gossard, *Two-dimensional magnetotransport in the extreme quantum limit*, *Phys. Rev. Lett.* **48** (1982) 1559.

[165] J.E. Moore and L. Balents, *Topological invariants of time-reversal-invariant band structures*, *Phys. Rev. B* **75** (2007) 121306.

[166] X. Wan, A.M. Turner, A. Vishwanath and S.Y. Savrasov, *Topological semimetal and fermi-arc surface states in the electronic structure of pyrochlore iridates*, *Phys. Rev. B* **83** (2011) 205101.

[167] A.A. Burkov and L. Balents, *Weyl semimetal in a topological insulator multilayer*, *Phys. Rev. Lett.* **107** (2011) 127205.

[168] A. Burkov, *Weyl metals*, *Annual Review of Condensed Matter Physics* **9** (2018) 359.

[169] A.H. Castro Neto, F. Guinea, N.M.R. Peres, K.S. Novoselov and A.K. Geim, *The electronic properties of graphene*, *Rev. Mod. Phys.* **81** (2009) 109.

[170] N.P. Armitage, E.J. Mele and A. Vishwanath, *Weyl and dirac semimetals in three-dimensional solids*, *Rev. Mod. Phys.* **90** (2018) 015001.

[171] H. Weyl, *Gravitation and the electron*, *Proceedings of the National Academy of Sciences of the United States of America* **15** (1929) 323 .

[172] O. Vafek and A. Vishwanath, *Dirac fermions in solids: From high-tc cuprates and graphene to topological insulators and weyl semimetals*, *Annual Review of Condensed Matter Physics* **5** (2014) 83.

[173] H.B. Nielsen and M. Ninomiya, *The adler-bell-jackiw anomaly and weyl fermions in a crystal*, *Physics Letters B* **130** (1983) 389.

[174] K. Hashimoto, T. Kimura and X. Wu, *Boundary conditions of weyl semimetals*, *Progress of Theoretical and Experimental Physics* **2017** (2017) .

[175] M. Koshino, H. Aoki, K. Kuroki, S. Kagoshima and T. Osada, *Hofstadter butterfly and integer quantum hall effect in three dimensions*, *Phys. Rev. Lett.* **86** (2001) 1062.

[176] M. Koshino, H. Aoki, T. Osada, K. Kuroki and S. Kagoshima, *Phase diagram for the hofstadter butterfly and integer quantum hall effect in three dimensions*, *Phys. Rev. B* **65** (2002) 045310.

[177] R.B. Laughlin and Z. Zou, *Properties of the chiral-spin-liquid state*, *Phys. Rev. B* **41** (1990) 664.

[178] L. Lepori, G. Mussardo and A. Trombettoni, $(3+1)$ *massive dirac fermions with ultracold atoms in frustrated cubic optical lattices*, *Europhysics Letters* **92** (2010) 50003.

[179] T. Dubček, C.J. Kennedy, L. Lu, W. Ketterle, M. Soljačić and H. Buljan, *Weyl points in three-dimensional optical lattices: Synthetic magnetic monopoles in momentum space*, *Phys. Rev. Lett.* **114** (2015) 225301.

[180] L. Lepori, I.C. Fulga, A. Trombettoni and M. Burrello, *pt-invariant weyl semimetals in gauge-symmetric systems*, *Phys. Rev. B* **94** (2016) 085107.

[181] X. Wan, A.M. Turner, A. Vishwanath and S.Y. Savrasov, *Topological semimetal and fermi-arc surface states in the electronic structure of pyrochlore iridates*, *Phys. Rev. B* **83** (2011) 205101.

[182] F. Haldane, *Attachment of surface" fermi arcs" to the bulk fermi surface:" fermi-level plumbing" in topological metals*, *arXiv preprint arXiv:1401.0529* (2014) .

[183] R. Okugawa and S. Murakami, *Dispersion of fermi arcs in weyl semimetals and their evolutions to dirac cones*, *Phys. Rev. B* **89** (2014) 235315.

[184] D. Gosálbez-Martínez, I. Souza and D. Vanderbilt, *Chiral degeneracies and fermi-surface chern numbers in bcc fe*, *Phys. Rev. B* **92** (2015) 085138.

[185] G.E. Volovik, *Topological lifshitz transitions*, *Low Temperature Physics* **43** (2017) 47.

[186] T. Louvet, M. Houzet and D. Carpentier, *Signature of the chiral anomaly in ballistic weyl junctions*, *Journal of Physics: Materials* **1** (2018) 015008.

[187] M. Aidelsburger, S. Nascimbene and N. Goldman, *Artificial gauge fields in materials and engineered systems*, *Comptes Rendus Physique* **19** (2018) 394.

[188] M. Aidelsburger, M. Atala, M. Lohse, J.T. Barreiro, B. Paredes and I. Bloch, *Realization of the hofstadter hamiltonian with ultracold atoms in optical lattices*, *Phys. Rev. Lett.* **111** (2013) 185301.

[189] H. Miyake, G.A. Siviloglou, C.J. Kennedy, W.C. Burton and W. Ketterle, *Realizing the harper hamiltonian with laser-assisted tunneling in optical lattices*, *Phys. Rev. Lett.* **111** (2013) 185302.

[190] N. Goldman, G. Juzeliūnas, P. Öhberg and I.B. Spielman, *Light-induced gauge fields for ultracold atoms*, *Reports on Progress in Physics* **77** (2014) 126401.

[191] M. Aidelsburger, M. Lohse, C. Schweizer, M. Atala, J.T. Barreiro, S. Nascimbène et al., *Measuring the chern number of hofstadter bands with ultracold bosonic atoms*, *Nature Physics* **11** (2015) 162.

[192] C. Weitenberg and J. Simonet, *Tailoring quantum gases by floquet engineering*, *arXiv preprint arXiv:2102.07009* (2021) .

[193] S.N. Kempkes, M.R. Slot, S.E. Freeney, S.J. Zevenhuizen, D. Vanmaekelbergh, I. Swart et al., *Design and characterization of electrons in a fractal geometry*, *Nature physics* **15** (2019) 127.

[194] M. Fremling, M. van Hooft, C.M. Smith and L. Fritz, *Existence of robust edge currents in sierpiński fractals*, *Phys. Rev. Research* **2** (2020) 013044.

[195] C.R. Dean, L. Wang, P. Maher, C. Forsythe, F. Ghahari, Y. Gao et al., *Hofstadter's butterfly and the fractal quantum hall effect in moiré superlattices*, *Nature* **497** (2013) 598.

[196] B. Hunt, J.D. Sanchez-Yamagishi, A.F. Young, M. Yankowitz, B.J. LeRoy, K. Watanabe et al., *Massive dirac fermions and hofstadter butterfly in a van der waals heterostructure*, *Science* **340** (2013) 1427.

[197] T. Ozawa, H.M. Price, A. Amo, N. Goldman, M. Hafezi, L. Lu et al., *Topological photonics*, *Rev. Mod. Phys.* **91** (2019) 015006.

[198] K.-Y. Yang, Y.-M. Lu and Y. Ran, *Quantum hall effects in a weyl semimetal: Possible application in pyrochlore iridates*, *Phys. Rev. B* **84** (2011) 075129.

[199] J. Chesta Lopez, L.E.F. Foa Torres and A.S. Nunez, *Multiterminal conductance at the surface of a weyl semimetal*, *Phys. Rev. B* **97** (2018) 125419.

[200] M. Burrello, E. Guadagnini, L. Lepori and M. Mintchev, *Field theory approach to the quantum transport in weyl semimetals*, *Phys. Rev. B* **100** (2019) 155131.

[201] A. Pal, M. Chinotti, L. Degiorgi, W. Ren and C. Petrovic, *Optical properties of ybmnbi2: A type ii weyl semimetal candidate*, *Physica B: Condensed Matter* **536** (2018) 64.

[202] D.V. Efremov, A. Shtyk, A.W. Rost, C. Chamon, A.P. Mackenzie and J.J. Betouras, *Multicritical fermi surface topological transitions*, *Phys. Rev. Lett.* **123** (2019) 207202.

[203] A.A. Soluyanov, D. Gresch, Z. Wang, Q. Wu, M. Troyer, X. Dai et al., *Type-ii weyl semimetals*, *Nature* **527** (2015) 495.

[204] Y. Xu, F. Zhang and C. Zhang, *Structured weyl points in spin-orbit coupled fermionic superfluids*, *Phys. Rev. Lett.* **115** (2015) 265304.

[205] C. Nash and S. Sen, *Topology and Geometry for Physicists*, Academic Press (1983).

[206] C. Fang, M.J. Gilbert, X. Dai and B.A. Bernevig, *Multi-weyl topological semimetals stabilized by point group symmetry*, *Phys. Rev. Lett.* **108** (2012) 266802.

[207] L. Lepori, I.C. Fulga, A. Trombettoni and M. Burrello, *Double weyl points and fermi arcs of topological semimetals in non-abelian gauge potentials*, *Phys. Rev. A* **94** (2016) 053633.

[208] S.-M. Huang, S.-Y. Xu, I. Belopolski, C.-C. Lee, G. Chang, T.-R. Chang et al., *New type of weyl semimetal with quadratic double weyl fermions*, *Proceedings of the National Academy of Sciences* **113** (2016) 1180.

[209] Q. Chen and G.A. Fiete, *Thermoelectric transport in double-weyl semimetals*, *Phys. Rev. B* **93** (2016) 155125.

[210] B. Sbierski, M. Trescher, E.J. Bergholtz and P.W. Brouwer, *Disordered double weyl node: Comparison of transport and density of states calculations*, *Phys. Rev. B* **95** (2017) 115104.

[211] B. Bradlyn, J. Cano, Z. Wang, M.G. Vergniory, C. Felser, R.J. Cava et al., *Beyond dirac and weyl fermions: Unconventional quasiparticles in conventional crystals*, *Science* **353** (2016) aaf5037.

[212] I.C. Fulga, L. Fallani and M. Burrello, *Geometrically protected triple-point crossings in an optical lattice*, *Phys. Rev. B* **97** (2018) 121402(R).

[213] I.C. Fulga and A. Stern, *Triple point fermions in a minimal symmorphic model*, *Phys. Rev. B* **95** (2017) 241116(R).

[214] C.-K. Chan and P.A. Lee, *Emergence of gapped bulk and metallic side walls in the zeroth landau level in dirac and weyl semimetals*, *Phys. Rev. B* **96** (2017) 195143.

[215] P. Kim, J.H. Ryoo and C.-H. Park, *Breakdown of the chiral anomaly in weyl semimetals in a strong magnetic field*, *Phys. Rev. Lett.* **119** (2017) 266401.

[216] D.R. Saykin, K.S. Tikhonov and Y.I. Rodionov, *Landau levels with magnetic tunneling in a weyl semimetal and magnetoconductance of a ballistic p−n junction*, *Phys. Rev. B* **97** (2018) 041202(R).

[217] S. Roy, M. Kolodrubetz, J.E. Moore and A.G. Grushin, *Chern numbers and chiral anomalies in weyl butterflies*, *Phys. Rev. B* **94** (2016) 161107(R).

[218] J. Xiong, S.K. Kushwaha, T. Liang, J.W. Krizan, M. Hirschberger, W. Wang et al., *Evidence for the chiral anomaly in the dirac semimetal na3bi*, *Science* **350** (2015) 413.

[219] X. Huang, L. Zhao, Y. Long, P. Wang, D. Chen, Z. Yang et al., *Observation of the chiral-anomaly-induced negative magnetoresistance in 3d weyl semimetal taas*, *Phys. Rev. X* **5** (2015) 031023.

[220] H. Li, H. He, H.-Z. Lu, H. Zhang, H. Liu, R. Ma et al., *Negative magnetoresistance in dirac semimetal cd3as2*, *Nature Communications* **7** (2016) .

[221] A.C. Niemann, J. Gooth, S.-C. Wu, S. Bäßler, P. Sergelius, R. Hühne et al., *Chiral magnetoresistance in the weyl semimetal nbp*, *Scientific Reports* **7** (2017) .

[222] S. Ran, I.-L. Liu, Y.S. Eo, D.J. Campbell, P.M. Neves, W.T. Fuhrman et al., *Extreme magnetic field-boosted superconductivity*, *Nature Physics* **15** (2019) 1250.

[223] M.J. Park, Y.B. Kim and S. Lee, *Geometric superconductivity in 3d hofstadter butterfly*, *arXiv preprint arXiv:2007.16205* (2020) .

[224] L.-K. Lim, J.-N. Fuchs and G. Montambaux, *Bloch-zener oscillations across a merging transition of dirac points*, *Phys. Rev. Lett.* **108** (2012) 175303.

[225] L. Duca, T. Li, M. Reitter, I. Bloch, M. Schleier-Smith and U. Schneider, *An aharonov-bohm interferometer for determining bloch band topology*, *Science* **347** (2015) 288.

[226] P.T. Ernst, S. G¨otze, J.S. Krauser, K. Pyka, D.-S. L¨uhmann, D. Pfannkuche et al., *Probing superfluids in optical lattices by momentum-resolved bragg spectroscopy*, *Nature Phys.* **6** (2010) 56–61.

[227] Z.-Y. Wang, X.-C. Cheng, B.-Z. Wang, J.-Y. Zhang, Y.-H. Lu, C.-R. Yi et al., *Realization of ideal weyl semimetal band in ultracold quantum gas with 3d spin-orbit coupling*, *Science* **372** (2021) 271.

[228] N.R. Cooper, J. Dalibard and I.B. Spielman, *Topological bands for ultracold atoms*, *Rev. Mod. Phys.* **91** (2019) 015005.

[229] H.-X. Wang, Z.-K. Lin, B. Jiang, G.-Y. Guo and J.-H. Jiang, *Higher-order weyl semimetals*, *Phys. Rev. Lett.* **125** (2020) 146401.

[230] S.A.A. Ghorashi, T. Li and T.L. Hughes, *Higher-order weyl semimetals*, *Phys. Rev. Lett.* **125** (2020) 266804.

[231] C. Lanczos, *An iteration method for the solution of the eigenvalue problem of linear differential and integral operators*, *J. Res. Natl. Bur. Stand. B* **45** (1950) 255.

[232] J.-R. Soh, F. de Juan, M.G. Vergniory, N.B.M. Schröter, M.C. Rahn, D.Y. Yan et al., *Ideal weyl semimetal induced by magnetic exchange*, *Phys. Rev. B* **100** (2019) 201102(R).

[233] Y.-H. Lu, B.-Z. Wang and X.-J. Liu, *Ideal weyl semimetal with 3d spin-orbit coupled ultracold quantum gas*, *Science Bulletin* **65** (2020) 2080.

[234] D. Grassano, O. Pulci, E. Cannuccia and F. Bechstedt, *Influence of anisotropy, tilt and pairing of weyl nodes: the weyl semimetals taas, tap, nbas and nbp*, *Eur. Phys. J. B* **93** (2020) .

[235] G. Grosso and G.P. Parravicini, *Solid State Physics*, Academic Press (2000).

[236] F. Bassani and G.P. Parravicini, *Electronic States and Optical Transitions in Solids*, Pergamon Press, Oxford (1975).